Greece 2.0
NATIONAL RECOVERY AND RESILIENCE PLAN

GREENERGY

Resilient Vertical Forest Renovation of Reinforced Concrete Structures in Seismic Prone Areas
(H.F.R.I. Project Number 015376)

Assessment of the performance of tested renovated 3d VF structure.

Deliverable D2.6 Work package 2

Funding source

“Hellenic Foundation for Research & Innovation (H.F.R.I.)
Greece 2.0
Basic Research Financing Action”

Host Organization

ΔΗΜΟΚΡΙΤΕΙΟ ΠΑΝΕΠΙΣΤΗΜΙΟ ΘΡΑΚΗΣ | DEMOCRITUS UNIVERSITY OF THRACE

Democritus University of Thrace (DUTH)

Collaborating Organizations
Aristotle University of Thessaloniki (AUTH)

July 2025

H.F.R.I. Hellenic Foundation for Research & Innovation
Greece 2.0 NATIONAL RECOVERY AND RESILIENCE PLAN
Funded by the European Union NextGenerationEU

The research project is implemented in the framework of H.F.R.I call "Basic research Financing (Horizontal support of all Sciences)" under the National Recovery and Resilience Plan "Greece 2.0" funded by the European Union – NextGenerationEU (H.F.R.I. Project Number: 015376)

Version	Date	Comments-Modifications
1	July 2025	Final Version
2		

Suggested citation:

Rousakis T., Voutetaki M., Kellis S., Zapris A., Xynopoulos I., Sapidis G., Lappa M., Papadopoulos N., Mallinis G., Karabini M., Stefanidou M., Theodoridou I., Kytinou V., Chalioris C., 2025. Assessment of the performance of tested renovated 3d VF structure. Greenergy-Resilient Vertical Forest Renovation of Reinforced Concrete Structures in Seismic Prone Areas (H.F.R.I. Project Number 015376). Deliverable D2.6 Democritus University of Thrace, Xanthi.

Project Title	Resilient Vertical Forest Renovation of Reinforced Concrete Structures in Seismic Prone Areas
Acronym	GREENERGY
HFRI Project Number	015376
Call identifier	Basic Research Financing (Horizontal support for all Sciences), National Recovery and Resilience Plan (Greece 2.0) / Sub-action 2. Funding Projects in Leading-Edge Sectors – RRFQ: Basic Research Financing (Horizontal support for all Sciences)
Thematic area	ThA1. Physical Sciences, Engineering Sciences and Technology, Environment and Energy
Thematic Field	1.16 Smart Cities
Host Organization	Democritus University of Thrace
Collaborating Institutions	Aristotle University of Thessaloniki
Project starting date	13/3/2024
Project Principal Investigator	**Dr. Theodoros Rousakis**
Affiliation	**Democritus University of Thrace / Department of Civil Engineering**
Email	**trousak@civil.duth.gr**
Telephone	25410 79645, 461 / 6977421569
Deliverable number and title	*D2.6 Assessment of the performance of tested renovated 3d VF structure.*
Related work package	**WP2** – Experimental dynamic assessment of physical model structure towards holistic renovation
Authors	Theodoros Rousakis, Maristella Voutetaki, Stefanos Kellis, Adamantis Zapris, Ioannis Xynopoulos, Georgios Sapidis, Martha Lappa, Nikolaos Papadopoulos, (DUTh), Martha Karabini, Kytinou Violetta, Chalioris Constantine. Georgios Mallinis, Maria Stefanidou, Ifigeneia Theodoridou (AUTh)

Τίτλος Έργου	Ανθεκτική Αντισεισμική Ανακαίνιση Κατασκευών από Ωπλισμένο Σκυρόδεμα σε Κάθετο Δάσος
Ακρωνύμιο	GREENERGY
Αριθμός Έργου ΕΛΙΔΕΚ	015376
Δράση	Χρηματοδότηση Βασικής Έρευνας (Οριζόντια υποστήριξη όλων των Επιστημών), Εθνικό Σχέδιο Ανάκαμψης και Ανθεκτικότητας (Ελλάδα 2.0)
Θεματική Περιοχή	ΘΠ1. Φυσικές Επιστήμες, Επιστήμες Μηχανικού και Τεχνολογίας, Περιβάλλον και Ενέργεια
Θεματικό Πεδίο	1.16 Έξυπνες Πόλεις
Φορέας Υποδοχής	Δημοκρίτειο Πανεπιστήμιο Θράκης
Συνεργαζόμενος Φορέας	Αριστοτέλειο Πανεπιστήμιο Θεσσαλονίκης
Ημερομηνία έναρξης Έργου	13/3/2024
Επιστημονικά Υπεύθυνος Έργου	**Δρ. Θεόδωρος Ρουσάκης**
Ίδρυμα / Τμήμα	**Δημοκρίτειο Πανεπιστήμιο Θράκης / Πολιτικών Μηχανικών**
Email	**trousak@civil.duth.gr**
Τηλέφωνα	25410 79645, 461 / 6977421569
Αριθμός και Τίτλος Παραδοτέου	***Π2.6 Αποτίμηση της επιτελεστικότητας από πειραματικές δοκιμές στην ανακαινισμένη με ΚΔ κατασκευή***
Σχετική Ενότητα Εργασίας	**ΕΕ2** – Πειραματική δυναμική αποτίμηση του φυσικού προσομοιώματος της κατασκευής προς την ολιστική ανακαίνιση
Συγγραφείς	Θεόδωρος Ρουσάκης, Μαριστέλλα Βουτετάκη, Στέφανος Κέλλης, Αδαμάντης Ζάπρης, Ιωάννης Ξυνόπουλος, Γεώργιος Σαπίδης, Μάρθα Λάππα, Νικόλαος Παπαδόπουλος (ΔΠΘ), Μάρθα Καραμπίνη, Βιολέττα Κυτίνου, Κωνσταντίνος Χαλιορής Γιώργος Μαλλίνης, Μαρία Στεφανίδου, Ιφιγένεια Θεοδωρίδου (ΑΠΘ)

Acknowledgements

This project is carried out within the framework of the National Recovery and Resilience Plan Greece 2.0, funded by the European Union – NextGenerationEU (Implementation body: HFRI).

Περιεχόμενα

Acknowledgements .... *v*

LIST OF TABLES .... *vii*

LIST OF FIGURES .... *viii*

LIST OF ACRONYMS .... *xiii*

ABSTRACT .... *xiv*

ΠΕΡΙΛΗΨΗ .... *xv*

1 Test set up and instrumentation *1*

2 Position of smart PZT sensors for the vertical forest (VF) structure *12*

3 Assessment of the performance of tested renovated structure. *13*

3.1 Assessment of the recordings of tested renovated 3d VF structure. 14

3.2 Concluding assessment remarks 80

3.3 Damage assessment 81

3.4 Assessment of the performance of the tested as-built VF renovated structure using PZT sensors 122

4 Conclusions *132*

References *133*

LIST OF TABLES

Table 1.1: List of accelerometers, draw wire meters and strain gauges placed inside and on the structure ... 7
Table 3.1: List of all performed tests ... 13
Table 3.1.1a Summary of results... 31
Table 3.1.1b Summary of results (continued) ... 33
Table 3.1.1c Summary of results (continued) ... 35
Table 3.1.1d Summary of results (continued) ... 37
Table 3.1.1e Summary of results (continued) ... 39
Table 3.1.1f Summary of results (continued) ... 41
Table 3.1.1g Summary of results (continued) ... 43
Table 3.1.1h Summary of results (continued) ... 45
Table 3.1.1i Summary of results (continued) ... 47
Table 3.1.1j Summary of results (continued) ... 49
Table 3.1.1k Summary of results (continued) ... 51
Table 3.1.1l Summary of results (continued) ... 53
Table 3.1.1m Summary of results (continued) ... 55
Table 3.1.1n Summary of results (continued) ... 57
Table 3.1.1o Summary of results (continued) ... 59
Table 3.1.1p Summary of results (continued) ... 61
Table 3.1.1q Summary of results (continued) ... 63
Table 3.1.1r Summary of results (continued) ... 65
Table 3.1.1s Summary of results (continued) ... 67
Table 3.1.1t Summary of results (continued) ... 69
Table 3.1.1u Summary of results (continued) ... 71
Table 3.1.1v Summary of results (continued)... 73
Table 3.1.1w Summary of results (continued)... 75
Table 3.1.1x Summary of results (continued)... 78

LIST OF FIGURES

Figure 1.1 Position of accelerometers (specimen's view perpendicular to the direction of the seismic table movement) 1
Figure 1.2 Position of the draw wire sensors on the concrete structure slab and foundation beams (specimen's view perpendicular to the direction of the seismic table movement) 2
Figure 1.3 Floor plan with strain gauges at the bottom of the columns 3
Figure 1.4 Floor plan with strain gauges at the top of the columns 4
Figure 1.5 View of the structure with strain gauges in frame of Columns 2-3 5
Figure 1.6 View of the structure with strain gauges in frame of columns 1-4 5
Figure 1.7 View of the infill wall with strain gauges in frame 1-4 6
Figure 1.8 View of the infill wall with strain gauges in frame 2-3 6
Figure 1.9 Cross section of the structure with strain gauge SG21 in frame of columns 4-1 9
Figure 1.10 Cross section of the structure with strain gauge SG22 in frame of columns 2-3 10
Figure 1.11 Cross section of the structure with strain gauges SG23, DG24 in frame of columns 3-4.. 11
Figure 3.1.1 Bottom and slab acceleration time-histories for the two levels of earthquake intensity (a) 0.07g, (b) 0.1g 15
Figure 3.1.2 Bottom and slab acceleration time-histories for the two levels of earthquake intensity (a) 0.14g, (b) 0.20g 16
Figure 3.1.3 Bottom and slab acceleration time-histories for the two levels of earthquake intensity (a) 0.34g, (b) 0.50g 17
Figure 3.1.4 Bottom and slab acceleration time-histories for the two levels of earthquake intensity (a) 0.55g, (b) 0.74g 18
Figure 3.1.5 Bottom and slab acceleration time-histories for the two levels of earthquake intensity (a) 0.80g, (b) 1.10g 19
Figure 3.1.6 Bottom and slab acceleration time-histories for the two levels of earthquake intensity (a) 1.3g (2), (b) 1.4g 20
Figure 3.1.7 Bottom and slab acceleration time-histories for the level of earthquake intensity 0.20g. 21
Figure 3.1.8 Bottom and slab acceleration time-histories for the two levels of white noise before intensity (a) 0.07g (without bottom fixing of the vertical living walls), (b) 0.07g 23
Figure 3.1.9 Bottom and slab acceleration time-histories for the two levels of white noise before intensity (a) 0.14g, (b) 0.34g 24
Figure 3.1.10 Bottom and slab acceleration time-histories for the two levels of white noise before intensity (a) 0.5g, (b) 0.55g 25
Figure 3.1.11 Bottom and slab acceleration time-histories for the two levels of white noise before intensity (a) 0.74g, (b) 0.8g 26
Figure 3.1.12 Bottom and slab acceleration time-histories for the two levels of white noise before intensity (a) 1.1g, (b) 1.3g 27
Figure 3.1.13 Bottom and slab acceleration time-histories for the two levels of white noise before intensity (a) 1.4g, (b) 0.2g 28
Figure 3.1.14 Bottom and slab acceleration time-histories for the white noise after intensity 0.2g 29
Figure 3.3.1 Observed damage after Wnb0.07g(without), Wnb0.07g, EQ0.07g, EQ0.1g, Wnb0.14g tests:. Slight rocking of planter 5. 82
Figure 3.3.2 Observed damage after EQ0.14g, EQ0.2g, Wnb0.34g, Wnb0.5g, Wnb0.55g tests:. Slight rocking of planter 2 and 5. 83

Figure 3.3.3 Observed damage after EQ0.34 test: Planter 2 basalt rope loosening was observed, then it was tightened. Rocking of planter 2, 3, 4 and 5. 84
Figure 3.3.4 Observed damage after EQ0.5g test: Rocking of planter 2, 3, 4 and 5. Micro-displacement of planter 4. 85
Figure 3.3.5 Observed damage after Wnb0.55g, WNb0.74g, Wnb0.8g tests: Rocking of planter 2, 3, 4 and 5. Micro-displacement of planter 4. 86
Figure 3.3.6 Observed damage after EQ0.55 test: Planter 3 displacement of prestressing device was noticed and it was tightened again. Rocking of planter 2, 3, 4 and 5. Micro-displacement of planter 4 87
Figure 3.3.7 Observed damage after EQ0.74g test: Fracture of the basalt rope of planter 3. Basalt rope loosening of planters 2,5 and tightened again. Intense rocking of planter 2, 3, 4 and 5. Micro-displacement of planter 4. 88
Figure 3.3.8 Observed damage after EQ0.80g test: Intense rocking of planter 4 leading to micro displacement of the PM pads and of the planter itself. Planter 3 basalt rope was loosening. Intense rocking of planter 2, 3 and 5. 89
Figure 3.3.9 Observed damage after Wnb1.1g, Wnb1.3g, Wnb1.4 test: Rocking of planter 5, 4, 3 ,2... 90
Figure 3.3.10 Observed damage after EQ1.1g test: intense rocking of planter 4 leading to micro displacement of the PM pads and of the planter itself. Fracture of the one basalt rope of planter 3. Displacement of prestressing devices of planter 2 and 5 and loosening of basalt ropes. Intense rocking of planter 2, 3, 5 and rocking of planter 1. 91
Figure 3.3.11 Observed damage after EQ1.3g test: Intense rocking of planter 4 leading to displacement (+-3 cm) of the PM pads and of the planter itself. Planter 1 showed bottom microdisplacements because of slight loosening of the steel rod. Fracture of the one basalt rope of planter 2. Planters 2,3 and 5 showed bottom displacements. Intense rocking of all planters. 92
Figure 3.3.12 Observed damage after Wnb1.3g (2) test: Rocking of planter 4 and 5. 93
Figure 3.3.13 Observed damage after EQ1.3g(2) test: Intense rocking of planter 4 leading to displacement (+-3 cm) of the PM pads and of the planter itself. Fracture of basalt rope of planter 3. Fracture of both basalt ropes of planter 5. Displacement of prestressing device of planter 2. Intense rocking of all planters. 94
Figure 3.3.14 Observed damage after EQ1.3g(2) test : Intense rocking of planter 4 leading to displacement (+-4 cm) of the PM pads and of the planter itself. Planter 1 showed bottom micro displacements because of slight loosening of the steel rod. Fracture of the one basalt rope of planter 3. Planter 5 and 2 showed bottom micro displacements. Intense rocking of all planters. 95
Figure 3.3.15 Observed damage after Wnb0.2g, EQ0.2g, Wna0.2g tests: Rocking of all planters. 96
Figure 3.3.16 Observed damage after 1.1g test: Left living wall LW1-4L, showed basalt rope loosening without detachment of PU pads allowing micromovements for high direct horizontal loads (severe wind) but no living wall collapse was observed. 98
Figure 3.3.17 Observed damage after 1.1g test: Left vertical living wall LW3-2L showed basalt rope loosening without detachment of PU pads allowing micromovements for high direct horizontal loads (severe wind) but no living wall collapse was observed. 99
Figure 3.3.18 Observed damage after 1.3g test: Left living wall LW1-4L, showed basalt rope loosening without detachment of PU pads allowing micromovements for low direct horizontal loads (frequent wind) but no living wall collapse was observed. 100
Figure 3.3.19 Observed damage after 1.3g test: Left vertical living wall LW3-2L showed basalt rope loosening without detachment of PU pads allowing micromovements for low direct horizontal loads (frequent wind) but no living wall collapse was observed. 101

Figure 3.3.20 Observed damage after 1.3g(2) test: Left living wall LW1-4L, showed basalt rope loosening leading to detachment of PU pads allowing micromovements for low direct horizontal loads (frequent wind) but no living wall collapse was observed. 102
Figure 3.3.21 Anchoring details and PU pads dimensions (under the top slab), left living wall LW1-4L: detachment of PU pads after EQ1.3g (2) 103
Figure 3.3.22 Observed damage after 1.3g(2) test: Left vertical living wall LW3-2L showed basalt rope loosening leading to detachment of PU pads allowing micromovements for low direct horizontal 104
Figure 3.3.23 Anchoring details and PU pads dimensions (under the top slab), left living wall LW3-2L: detachment of PU pads after EQ1.3g (2) 105
Figure 3.3.24 Observed damage after 1.3g(2) test: Steel rod (hemlock) slight loosening at the top of living wall LW3-4R allowing micromovements for low direct horizontal loads (frequent wind) but no living wall collapse was observed. 106
Figure 3.3.25 Observed damage after 1.4g test: Left living wall LW1-4L, showed basalt rope loosening leading to detachment of PU pads allowing micromovements for low direct horizontal loads (frequent wind) but no living wall collapse was observed. LW1-4R showed slight basalt rope loosening allowing 107
Figure 3.3.26 Anchoring details and PU pads dimensions (under the top slab), left living wall LW1-4L: detachment of PU pads after EQ1.4g 108
Figure 3.3.27 Observed damage after 1.4g test: Living walls LW2-3R showed slight basalt rope loosening allowing micromovements for high direct horizontal loads (severe wind), but no living wall collapse was observed. Left vertical living wall LW2-3L showed basalt rope loosening leading to detachment of PU pads allowing micromovements for low direct horizontal loads (frequent wind) but no living wall collapse was observed. 109
Figure 3.3.28 Anchoring details and PU pads dimensions (under the top slab), left living wall LW3-2L: detachment of PU pads after EQ1.4g 110
Figure 3.3.29 Observed damage after 1.4g test: Living walls LW1-2Lshowed slight basalt rope loosening allowing micromovements for high direct horizontal loads (severe wind), but no living wall collapse was observed. Living wall LW1-2R showed basalt rope loosening allowing micromovements for medium direct horizontal loads (intense wind), but no living wall collapse was observed. 111
Figure 3.3.30 Observed damage after 1.4g test: Steel rod (hemlock) slight loosening at the top of living wall LW4-3R allowing micromovements for low direct horizontal loads (frequent wind) but no living wall collapse was observed. 112
Figure 3.3.31 Observed damage after EQ1.3g test: The columns entered yielding strain of their longitudinal steel reinforcements at the bottom. Damage with crushing of bottom brick at partial infill wall 2-3 114
Figure 3.3.32 Observed damage after EQ1.3g(2) test: Damage with crushing of bottom brick at partial infill wall occurred. The columns entered yielding strain of their longitudinal steel reinforcements at the bottom and at the top critical regions (columns 1, 4). 115
Figure 3.3.33 Observed damage after EQ1.3g(2) test: Damage with crushing of bottom brick at partial infill wall occurred. The columns entered yielding strain of their longitudinal steel reinforcements at the bottom and at the top critical regions (columns 2, 3). 116
Figure 3.3.34 Observed damage after EQ1.4g test: Damage with crushing of bottom brick at both partial infill walls occurred at very high displacement drift levels (2,62%). Local fracture of the FRPU jacket at the boundary between the crushed brick and the bottom foundation beam. Additional cracks at some mortar joints between bricks of the partial infill walls at their internal face (side with no FRPU jacket). The columns entered yielding strain of their longitudinal steel reinforcements at the bottom and at the top critical regions (columns 1, 2, 3, 4). 117

Figure 3.3.35 Observed damage after EQ1.4g test: Observed damage after 1.4g test: Damage with crushing of bottom brick at both partial infill walls occurred at very high displacement drift levels (2,62%). Local fracture of the FRPU jacket at the boundary between the crushed brick and the bottom foundation beam. Additional cracks at some mortar joints between bricks of the partial infill walls at their internal face (side with no FRPU jacket). The columns entered yielding strain of their longitudinal steel reinforcements at the bottom and at the top critical regions (columns 1, 2, 3, 4). 118
Figure 3.3.36 Observed damage after EQ1.4g test: Observed damage after 1.4g test: Damage with crushing of bottom brick at both partial infill walls occurred at very high displacement drift levels (2,62%). Local fracture of the FRPU jacket at the boundary between the crushed brick and the bottom foundation beam. Additional cracks at some mortar joints between bricks of the partial infill walls at their internal face (side with no FRPU jacket). The columns entered yielding strain of their longitudinal steel reinforcements at the bottom and at the top critical regions (columns 1, 2, 3, 4). 119
Figure 3.3.37 Observed damage after EQ1.4g test: Observed damage after 1.4g test: Damage with crushing of bottom brick at both partial infill walls occurred at very high displacement drift levels (2,62%). Local fracture of the FRPU jacket at the boundary between the crushed brick and the bottom foundation beam. Additional cracks at some mortar joints between bricks of the partial infill walls at their internal face (side with no FRPU jacket). The columns entered yielding strain of their longitudinal steel reinforcements at the bottom and at the top critical regions (columns 1, 2, 3, 4). 120
Figure 3.3.38 Characteristic observed damage after all seismic tests: (a) interior side of wall infill 1-4 parallel to the direction of movement of seismic table (b) wall infill 2-3 parallel to the direction of movement of seismic table (c) Interior top side of wall infill 1-4, parallel to the direction of movement of the seismic table (d) detachment of PU pads 121
Figure 3.4.1: Voltage frequency responses of the PZT sensors inside beam B14..... 123
Figure 3.4.2: Voltage frequency responses of the PZT sensors inside beam B12..... 123
Figure 3.4.3: Voltage frequency responses of the PZT sensors inside the slab 124
Figure 3.4.4: Voltage frequency responses of the PZT sensors inside column 1 (Top, Middle, Bottom) 124
Figure 3.4.5: Voltage frequency responses of the PZT sensors inside column 2 (Top, Middle)..... 125
Figure 3.4.6: Voltage frequency responses of the PZT sensors inside column 3 (Top, Middle,) 125
Figure 3.4.7: Voltage frequency responses of the PZT sensors inside column 4 (Top, Middle, Bottom) 126
Figure 3.4.8: Voltage frequency responses of the PZT sensors on partially infilled walls (Upper, Middle, Bottom) 126
Figure 3.4.9: Voltage frequency responses of the PZT sensors on full Infill wall between columns 1 127
Figure 3.4.10: Voltage frequency responses of the PZT sensors placed on top of column 1 : MORJPuT at the infill wall and MI1JPuT at the partial infill wall 128
Figure 3.4.11: Voltage frequency responses of the PZT sensors (column 2: VFAnBF, LW2-3R, column 4: VFAnBS, LW1-4R anchoring metal structure for living wall as well as anchoring metal structures for planter 1, VFZnS) 128
Figure 3.4.12: Voltage frequency responses of the PZT sensors externally attached (Y4ERB and Y1ERB – columns 3 and 4 bottom) on the basalt rope..... 129
Figure 3.4.13: Voltage frequency responses of the PZT sensors inside column 1 (Top, Middle) at all excitations 130
Figure 3.4.14: Voltage frequency responses of the PZT sensors inside column 2 (Top, Middle) at all excitations 130

Figure 3.4.15: Voltage frequency responses of the PZT sensors inside column 3 (Top, Middle) at all excitations 131
Figure 3.4.16: Voltage frequency responses of the PZT sensors inside column 4 (Top, Middle) at all excitations 131

LIST OF ACRONYMS

VF	Vertical Forest
RC	Reinforced Concrete
PZT	Piezoelectric sensors or piezoelectric transducers
3D	3 Dimensions
etc	et cetera
D26	Deliverable 26
PUFJ	Polyurethane Flexible Joints
FRPU	Fiber Reinforced Polyurethane
SHM	Structural Health Monitoring
EMI	Electromechanical Impedance
DUTH	Democritus University of Thrace
e.g.	for example
SG	Strain gauges
AUTH	Aristotle University of Thessaloniki

ABSTRACT

GREENERGY aims to assess the dynamic performance of old type deficient structures after receiving innovative, lightweight, non-corrosive, minimally invasive, natural, recyclable, reusable, replaceable, flexible Vertical Forest renovation related retrofits. The second phase included the replication of seismic excitations during the first phase for a direct comparative assessment of the renovated structure. Further, additional number of suitable seismic table excitations was performed to provide equivalent levels of induced seismic intensity, considering the increased top mass of the structure because of VF renovations. Before and after each earthquake shaking, the structure was excited through the whole range of frequencies of the structure under suitable designed low acceleration intensity in order to investigate changes in eigen periods of the structure. The assessment provides the results from characteristic peak acceleration, drifts, strain, structural health monitoring recordings with PZTs and observations that validate the resilient performance of the structural green and forestry renovations. Minimally invasive retrofits resulted in a renovated structure with higher global stiffness despite the increased top mass of the structure. Interesting structural damage redistribution and structural damage barrier mechanisms are revealed. Five different cases of simulated planters' (with trees) anchoring are assessed as well as eight different cases of top attachment of simulated vertical living walls. The assessment concludes an excellent human life protection up to advanced Ultimate Limit State (ULS) performance levels, against undesirable brick infill disintegration, RC structure damage, planter overturning or damage as well as against vertical living wall collapse. Experimental results reveal a high potential on the vision of high-density urban forestation in existing buildings through suitable vertical forest renovation. Suitably renovated existing structures can safely resist upper boundary load per square meter (of building floor plan, top and balconies) of forestry through planters or upper boundary load per square meter (of available elevations) of vertical living walls for severe seismic excitations.

Keywords: experiment, seismic table, reinforced concrete, brick wall infills, seismic excitation, intervention, Vertical Forest, resilience, renovation, structural, structural health monitoring, PZT, polyurethane, basalt, planters, vertical living walls, glass fiber grid jacket, greenery, human safety, life protection

ΠΕΡΙΛΗΨΗ

Το έργο GREENERGY στοχεύει να αξιολογήσει την δυναμική συμπεριφορά και επιτελεστικότητα παλαιού τύπου ανεπαρκών κατασκευών μετά την καινοτόμο, ελαφριά, αντιδιαβρωτική, ελάχιστα επεμβατική, φυσική, ανακυκλώσιμη, επαναχρησιμοποιούμενη, αντικαταστάσιμη, εύκαμπτη ενίσχυση, σχετιζόμενη με ανακαίνιση Κάθετου Δάσους. Η δεύτερη φάση περιλαμβάνει την αναπαραγωγή των σεισμικών διεγέρσεων της πρώτης φάσης για μια άμεση συγκριτική αποτίμηση της ανακαινισμένης κατασκευής με την αρχική. Επιπλέον, πρόσθετος αριθμός κατάλληλων σεισμικών διεγέρσεων εκτελέστηκε ώστε να παρασχεθούν ισοδύναμα επίπεδα εισαγόμενης σεισμικής έντασης, λαμβάνοντας υπόψην την αυξημένη ωφέλιμη μάζα της πλάκας της κατασκευής εξαιτίας της ανακίνησης Κάθετου Δάσους. Πριν και μετά από κάθε σεισμική διέγερση η κατασκευή διεγέρθηκε σε όλο το εύρος συχνοτήτων, με κατάλληλα σχεδιασμένη χαμηλή ένταση, προκειμένου να διερευνηθούν οι αλλαγές στις ιδιοπεριόδους της κατασκευής. Η αποτίμηση παρέχει τα αποτελέσματα χαρακτηριστικών μέγιστων επιταγχύνσεων, σχετικών μετακινήσεων, ανηγμένων παραμορφώσεων, καταγραφών δομικής υγείας με PZTs και παρατηρήσεων που τεκμηριώνουν ανθεκτική (ανανηπτική) επίδοση πράσινων δομοστατικών και δασικών ανακαινίσεων. Οι ελάχιστα επεμβατικές ενισχύσεις οδήγησαν σε ανακαινισμένη κατασκευή με αυξημένη δυσκαμψία παρά την αυξημένη μάζα της πλάκας της κατασκευής. Αποκαλύπτονται ενδιαφέροντες μηχανισμοί ανακατανομής δομοστατικής βλάβης και φράγματος δομοστατικής βλάβης. Αποτιμώνται πέντε διαφορετικές περιπτώσεις αγκυρώσεων προσομοιωμένων γλαστρών (με δέντρα) καθώς και οκτώ διαφορετικές περιπτώσεις άνω στήριξης προσομοιωμένων κάθετων ζωντανών τοίχων. Συμπεραίνεται εξαιρετική προστασία ανθρώπινης ζωής έως προχωρημένα επίπεδα επιτελεστικότητας Οριακής Κατάστασης Αστοχίας (ΟΚΑ), έναντι ανεπιθύμητης αποδιοργάνωσης τοιχοπλήρωσης ή βλάβης φέροντα οργανισμού ΩΣ ή ανατροπής/βλάβης γλάστρας ή αστοχίας κάθετων ζωντανών τοίχων. Τα πειραματικά αποτελέσματα αποκαλύπτουν υψηλή δυναμική του οράματος της πυκνής αστικής αναδάσωσης σε υφιστάμενα κτήρια, μέσω κατάλληλης ανακαίνισης με κάθετα δάση. Κατάλληλα ανακαινισμένα υφιστάμενα κτήρια μπορούν με ασφάλεια να αναλάβουν υψηλά φορτία ανά τετραγωνικό μέτρο (κάτοψης κτηρίου σε δώμα και μπαλκόνια) κάθετου δάσους μέσω γλαστρών ή υψηλά φορτία ανά τετραγωνικό μέτρο (διαθέσιμων εξωτερικών όψεων) κάθετων ζωντανών τοίχων για καταστρεπτικές σεισμικές διεγέρσεις.

Λέξεις κλειδιά: πείραμα, σεισμική τράπεζα, οπλισμένο σκυρόδεμα, τοιχοπληρώσεις, τούβλα, σεισμική διέγερση, ενίσχυση, Κάθετα δάση, ανθεκτικότητα, ανανηπτικότητα, ανακαίνιση, δομικός, δομοστατικός, παρακολούθηση δομικής υγείας SHM, PZT, πολυουρεθάνη, μανδύας υαλοπλέγματος, βασάλτης, γλάστρες, κάθετοι ζωντανοί τοίχοι, φύτευση, ανθρώπινη ασφάλεια, προστασία ζωής

1 Test set up and instrumentation

Below are the diagrams with the location of the measuring instruments (for more details see D2.3), as well as the relevant table.

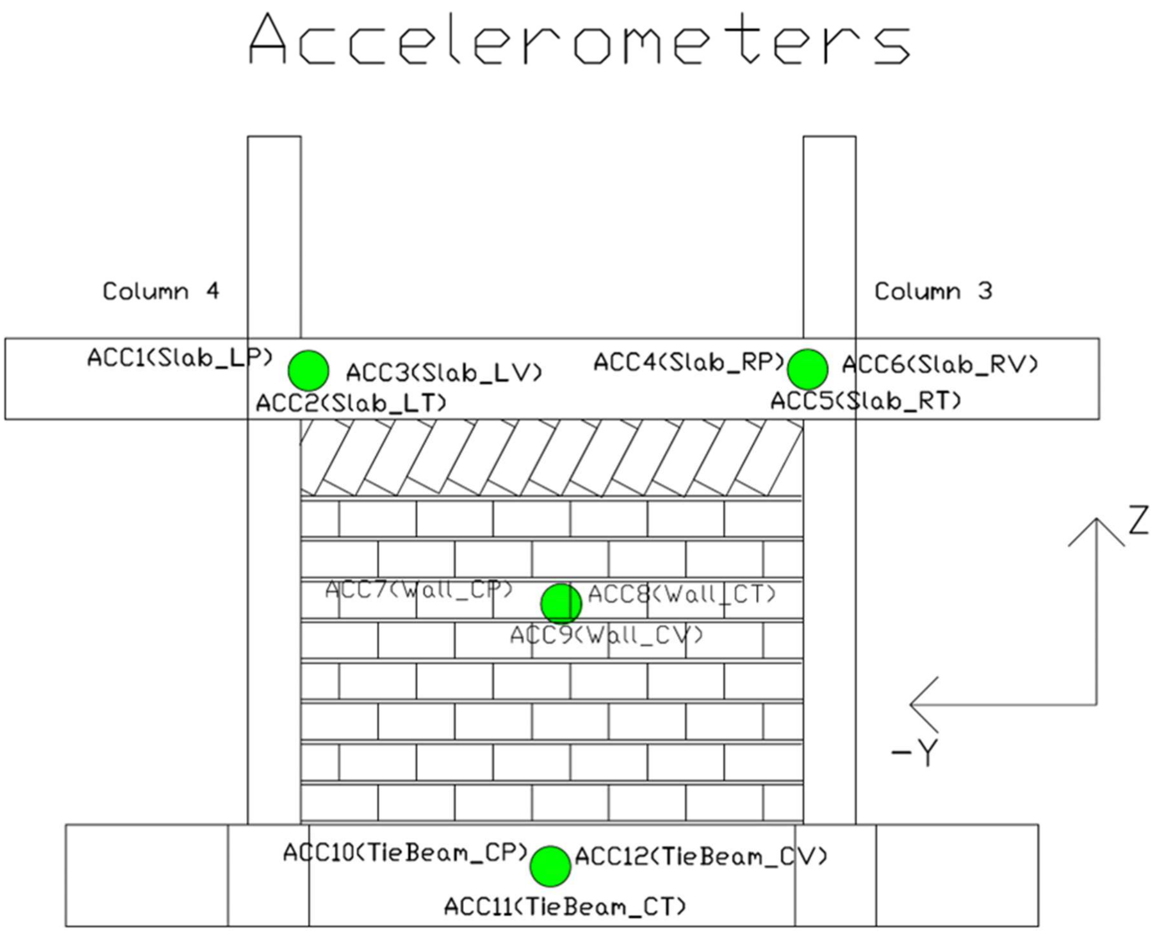

Figure 1.1 Position of accelerometers (specimen's view perpendicular to the direction of the seismic table movement)

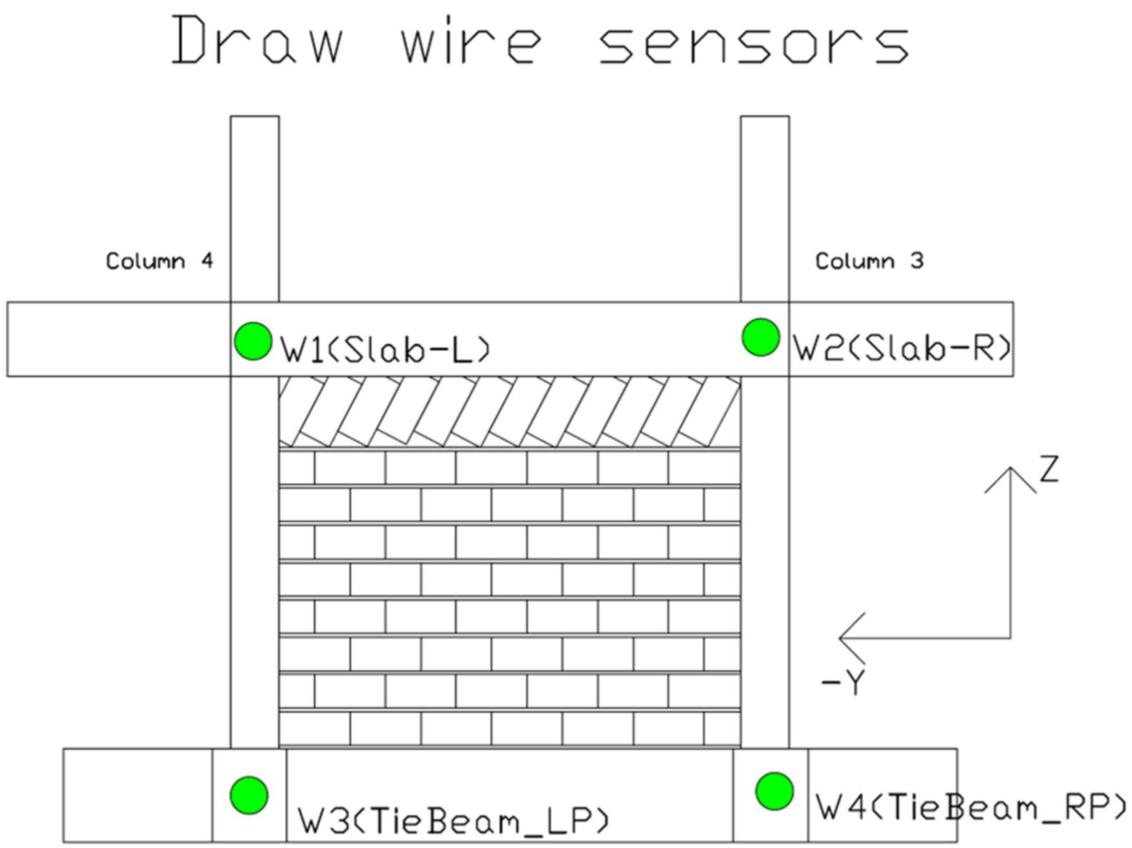

Figure 1.2 Position of the draw wire sensors on the concrete structure slab and foundation beams (specimen's view perpendicular to the direction of the seismic table movement)

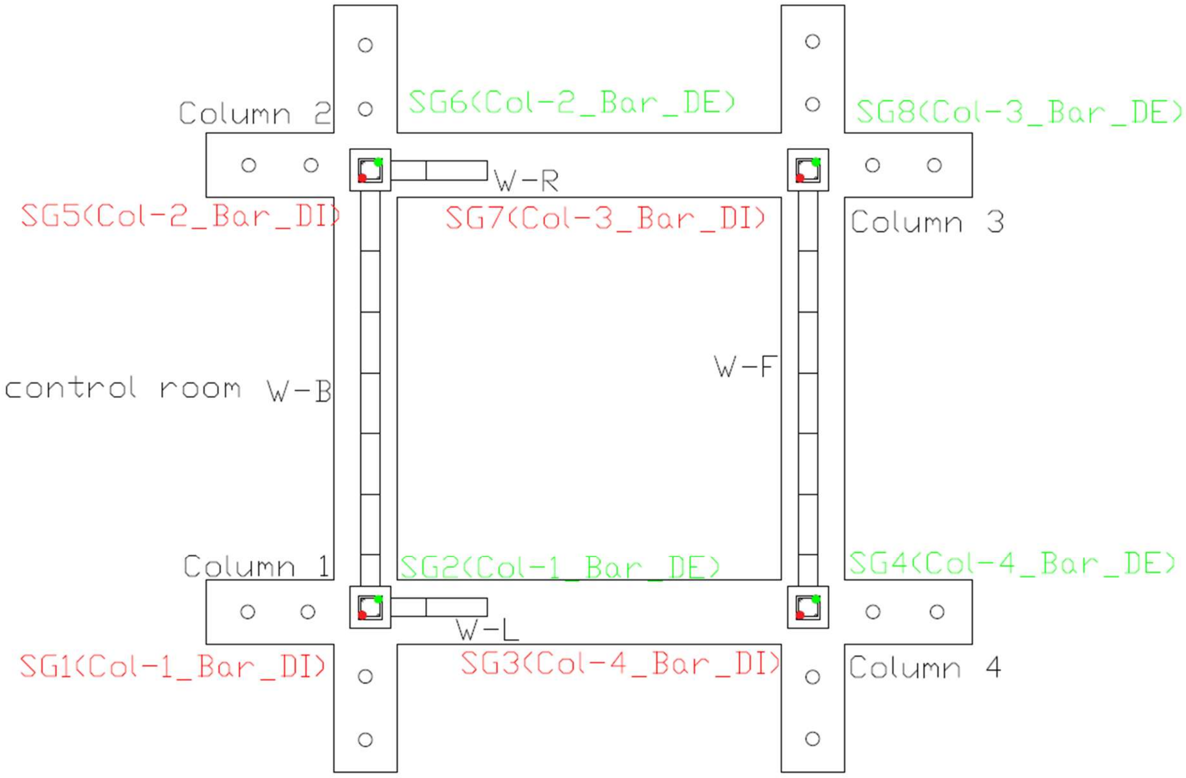

Figure 1.3 Floor plan with strain gauges at the bottom of the columns

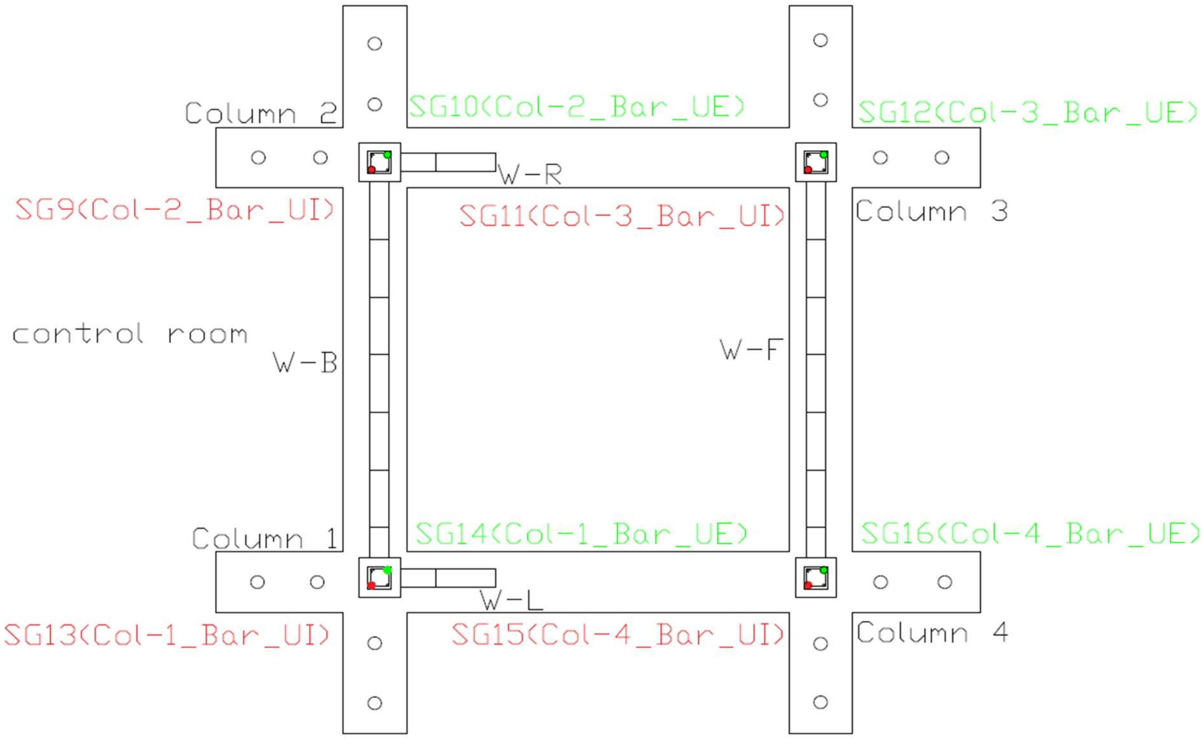

Figure 1.4 Floor plan with strain gauges at the top of the columns

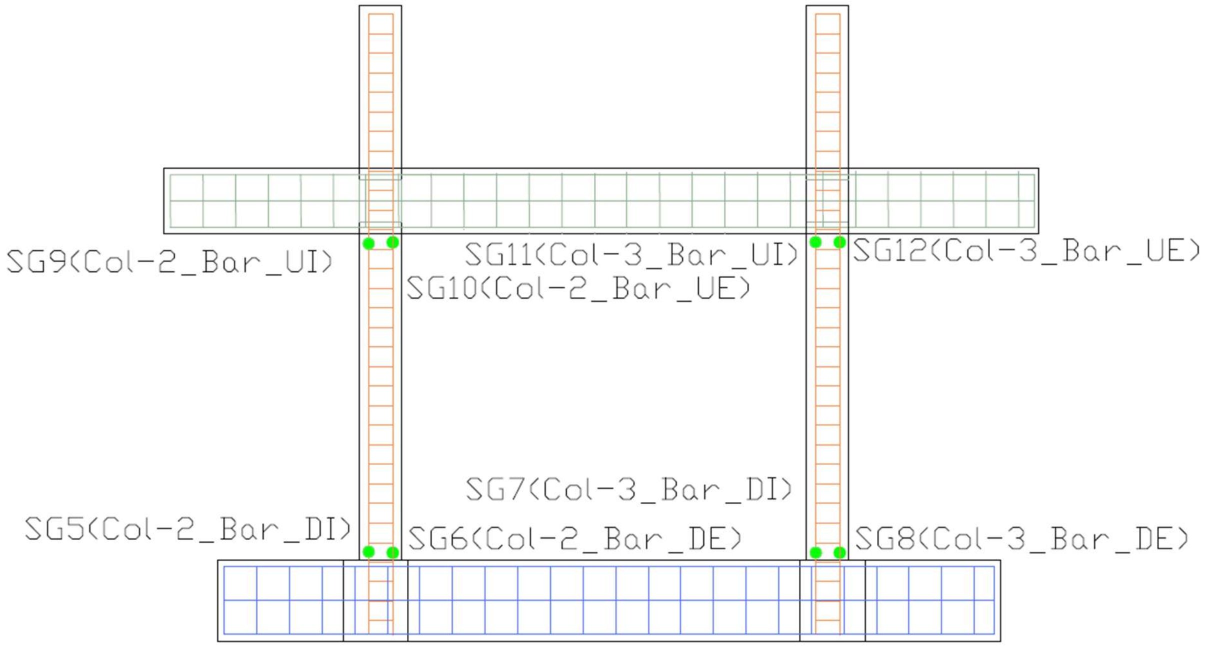

Figure 1.5 View of the structure with strain gauges in frame of Columns 2-3

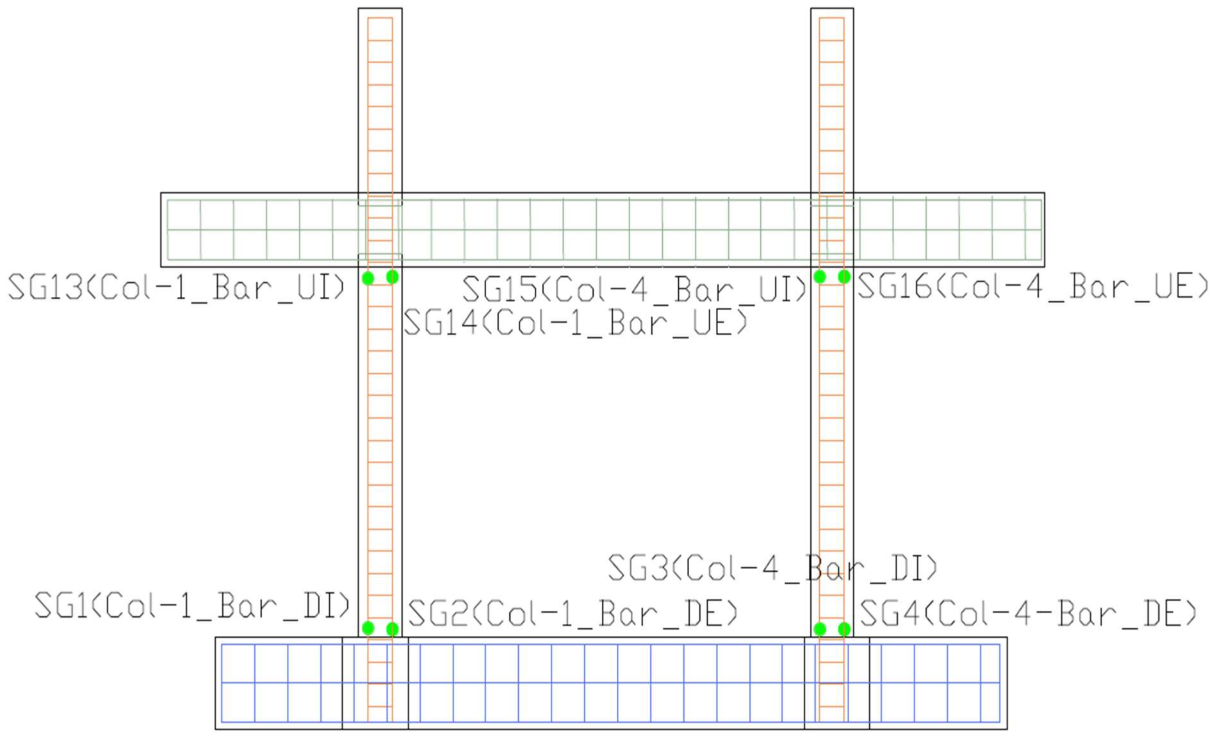

Figure 1.6 View of the structure with strain gauges in frame of columns 1-4

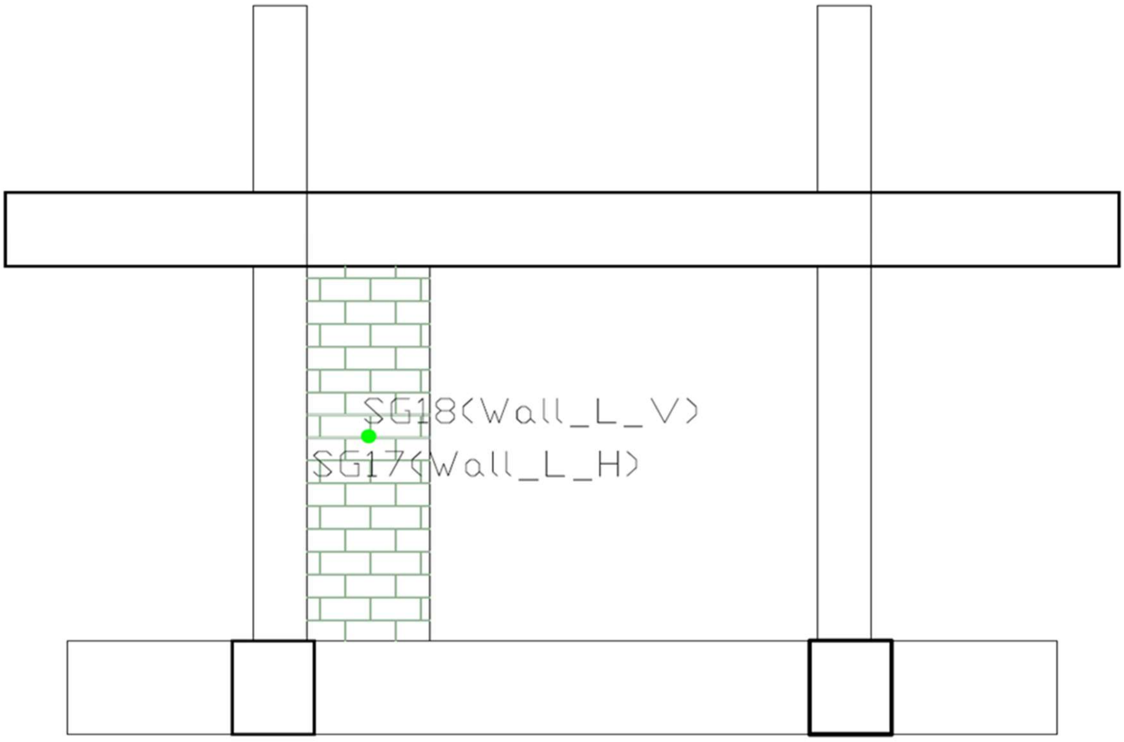

Figure 1.7 View of the infill wall with strain gauges in frame 1-4

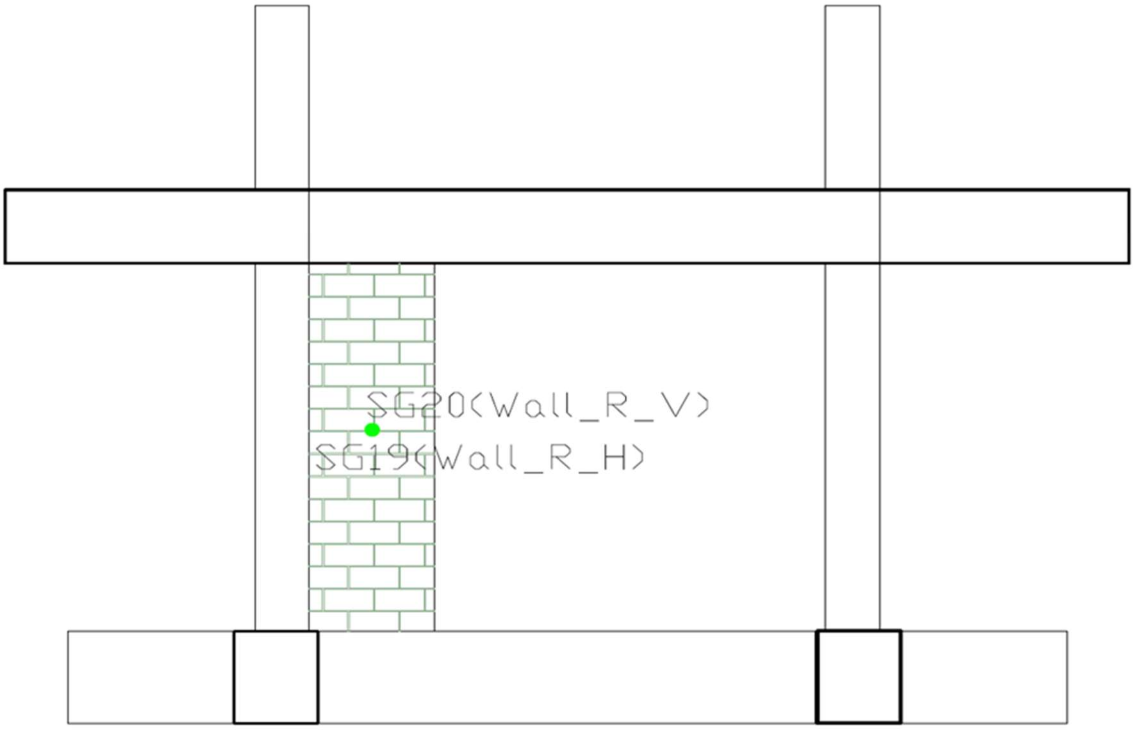

Figure 1.8 View of the infill wall with strain gauges in frame 2-3

Table 1.1: List of accelerometers, draw wire meters and strain gauges placed inside and on the structure

Ch No.	Channel name	Type of instrument	Measured quantity (units)	Position
1	ACC 1	Accelerometer	Acceleration (g)	On the slab, on the left corner, dir. (x)
2	ACC 2			On the slab, on the left corner, dir. (y)
3	ACC 3			On the slab, on the left corner, dir. (z)
4	ACC 4			On the slab, on the right corner, dir. (x)
5	ACC 5			On the slab, on the right corner, dir. (y)
6	ACC 6			On the slab, on the right corner, dir. (z)
7	ACC 7			On the infill, on the center, dir (x)
8	ACC 8			On the infill, on the center, dir (y)
9	ACC 9			On the infill, on the center, dir (x)
10	ACC 10			On the foundation, on the center, dir (x)
11	ACC 11			On the foundation, on the center, dir (y)
12	ACC 12			On the foundation, on the center, dir (z)
13	W 1	Draw wire sensors	Length (mm)	On the slab, on the left side
14	W 2			On the slab, on the right side
15	W 3			On the foundation, on the left side
16	W 4			On the foundation, on the right side
17	W 5			along the partial masonry infill diagonal
18	W 6			along the partial masonry infill diagonal
19	W 7			along the partial masonry infill diagonal
20	W 8			along the partial masonry infill diagonal
21	S1	Strain gauges	Strain	In the longitudinal reinforcement, on the underside
22	S2			
23	S3			
24	S4			
25	S5			
26	S6			
27	S7			
28	S8			
29	S9			In the longitudinal reinforcement, on the upper side
30	S10			
31	S11			
32	S12			

33	S13			
34	S14			
35	S15			
36	S16			
37	S17	Strain gauges	Strain	On the centre of partial masonry 1 along direction x
38	S18			On the centre of partial masonry 1 along direction z
39	S19			On the centre of partial masonry 2 along direction x
40	S20			On the centre of partial masonry 2 along direction z
41	S21			On the polyurethane (PM) at the joint between column 1 and the partial masonry, 5cm under the slab along direction x
42	S22			On the polyurethane (PM) at the joint between column 2 and the partial masonry, 5 cm under the slab along direction x
43	S23			On the rope, column 3
44	S24			On the rope, column 4

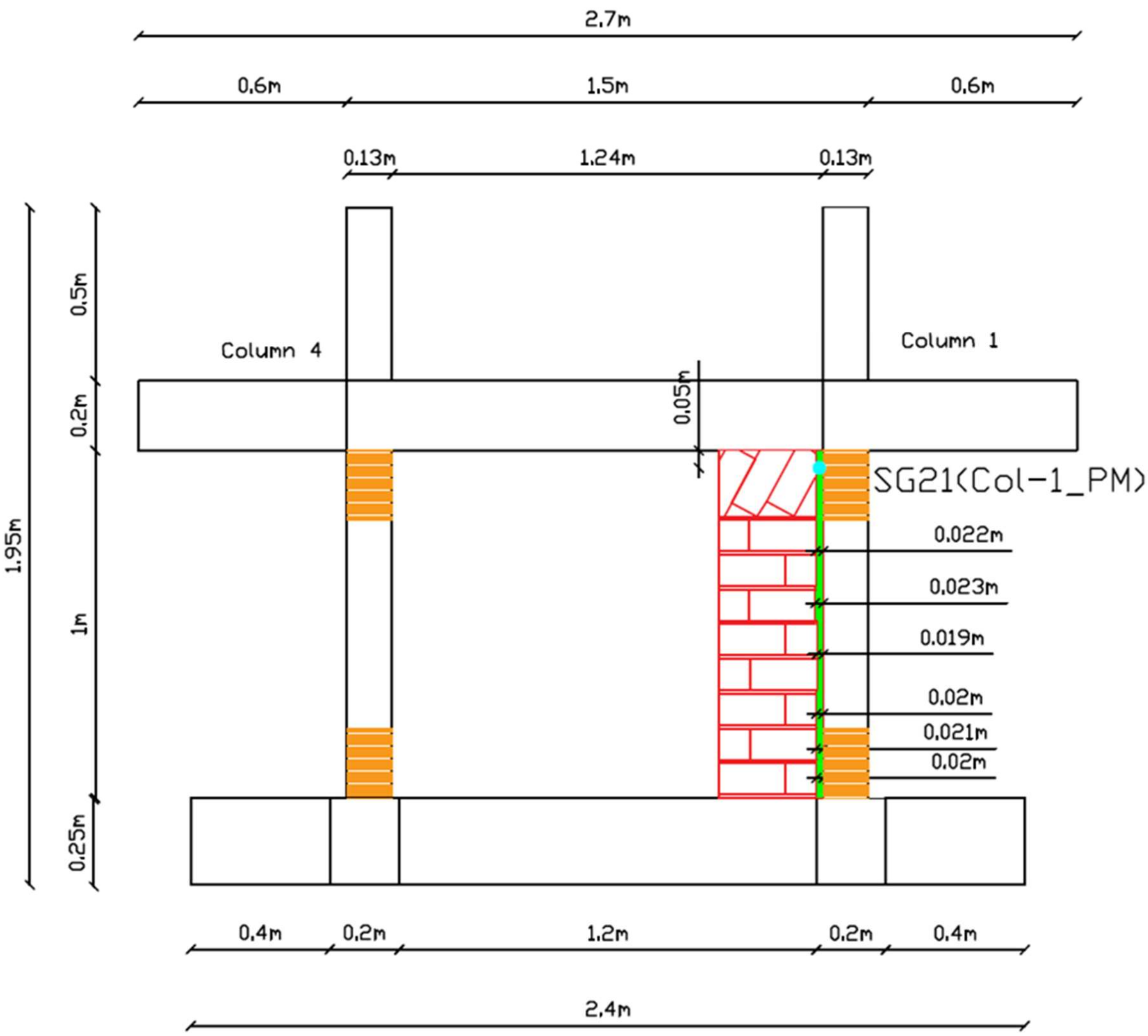

Figure 1.9 Cross section of the structure with strain gauge SG21 in frame of columns 4-1

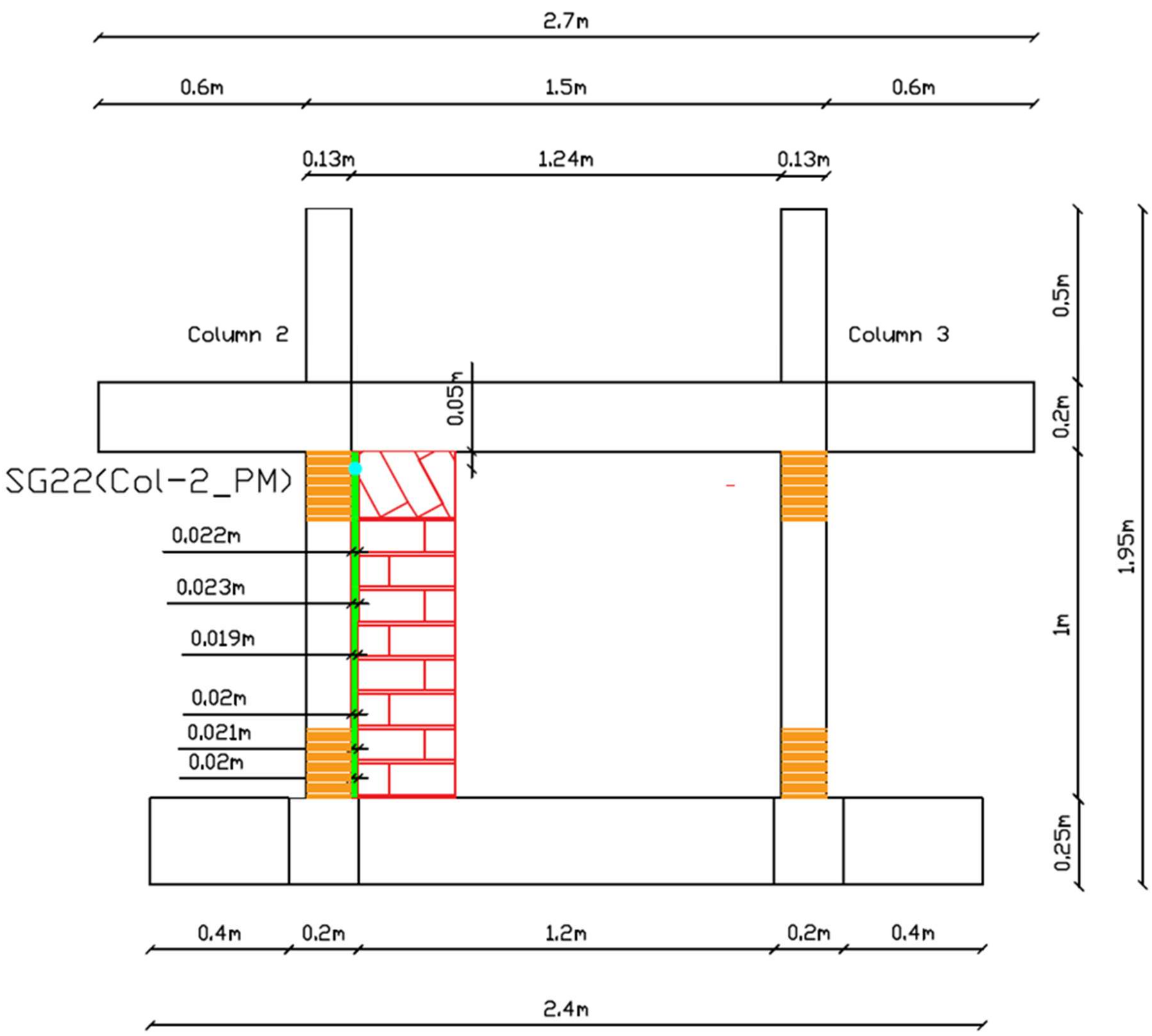

Figure 1.10 Cross section of the structure with strain gauge SG22 in frame of columns 2-3

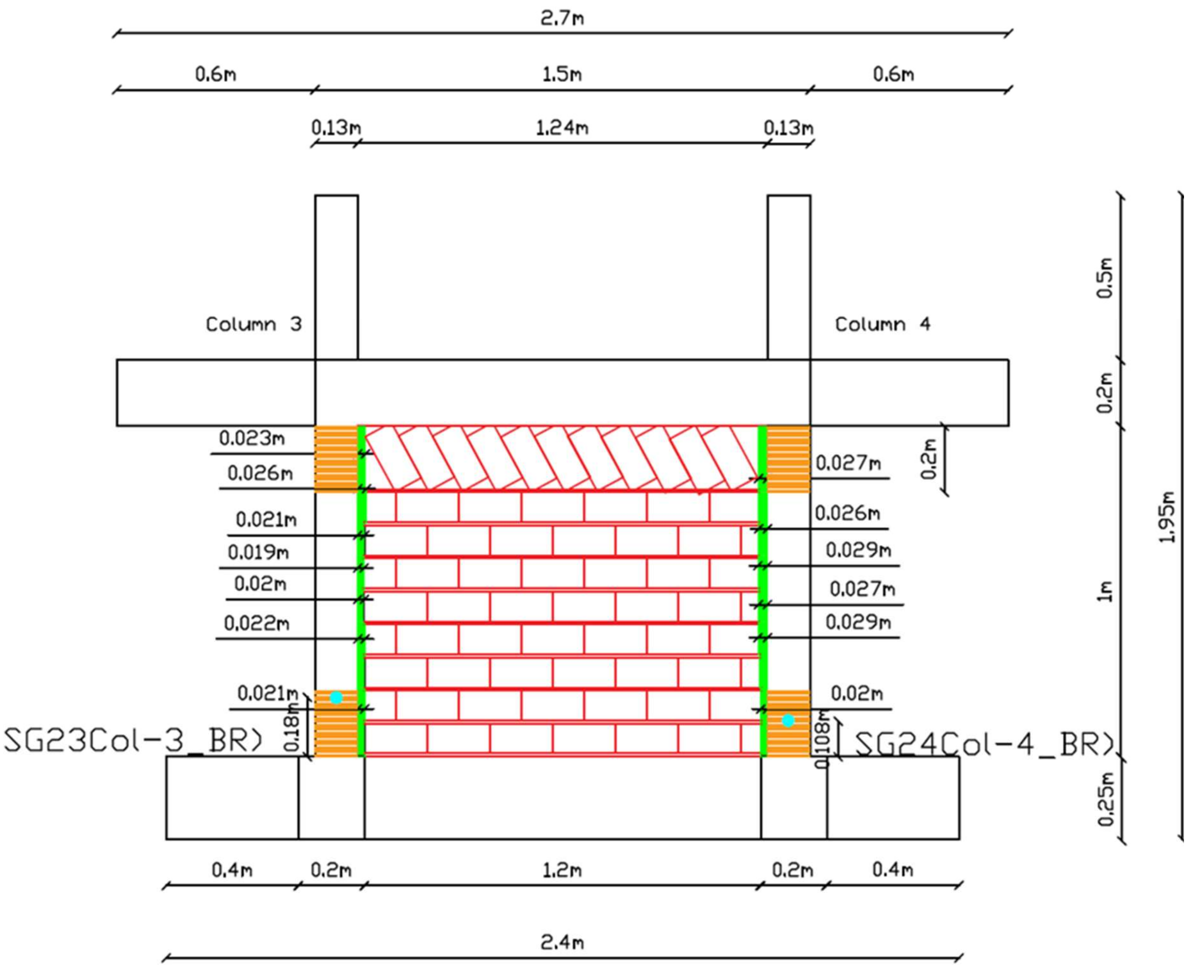

Figure 1.11 Cross section of the structure with strain gauges SG23, DG24 in frame of columns 3-4

2 Position of smart PZT sensors for the vertical forest (VF) structure

The PZT instrumentation for the renovated structure is presented in deliverables D22, D24 and D25.

3 Assessment of the performance of tested renovated structure.

Below are the excitations applied to the seismic table, as shown in table 3.1. (for more details see D2.4)

Table 3.1: List of all performed tests

Performed tests			
Test No.	**Name**	**Type of excitation**	**Intensity (g)**
Phase B			
ST1	WNb0,07g (without)	White noise	0,05g
ST2	WNb0,07g	White noise	0,05g
ST3	EQ0,07g	Earthquake	0,07g
ST4	EQ0,1g	Earthquake	0,1g
ST5	WNb0,14g	White noise	0.08g
ST6	EQ0,14g	Earthquake	0,14g
ST7	EQ0,2g	Earthquake	0.2g
ST8	WNb0,34g	White noise	0,08g
ST9	EQ0,34g	Earthquake	0,34g
ST10	WNb0,5g	White noise	0,08g
ST11	EQ0,5g	Earthquake	0,5g
ST12	WNb0,55g	White noise	0,08g
ST13	EQ0,55g	Earthquake	0,55g
ST14	WNb0,74g	White noise	0,08g
ST15	EQ0,74g	Earthquake	0,74g
ST16	WNb0,8g	White noise	0,08g
ST17	EQ0,8g	Earthquake	1,1g
ST18	WNb1,1g	White noise	0,08g
ST19	EQ1,1g	Earthquake	1,3g
ST20	WNb1,3g	White noise	0,08g
ST21	EQ1,3g	Earthquake	1,3g
ST22	WNb1,3g(2)	White noise	0,08g
ST23	EQ1,3g(2)	Earthquake	1,3g
ST24	WNb1,4g	White noise	0,08g
ST25	EQ1,4g	Earthquake	1,4g
ST26	WNb0,2g	White noise	0,08
ST27	EQ0,2g	Earthquake	0,2g
ST28	WNa0,2g	White noise	0,08g

3.1 Assessment of the recordings of tested renovated 3d VF structure.

Figure 3.1.1-3.1.7 displays the acceleration time histories for the one-storey rc building at twelve different levels of earthquake intensity. That is the dynamic shake table tests comprised of gradually increasing maximum input intensity level (peak acceleration of the excitation of the seismic table) from 0,07g to 1,4g (0,07g, 0,1g, 0,14g, 0,2g, 0,34g, 0,5g, 0,55g, 0,74g, 0,8g, 1,1g, 1,3g, 1,3g, 1,4g, 0,2g) based on the adopted earthquake Thessaloniki 1978. Before and after each earthquake excitation, the structure was excited through the whole range of frequencies of the structure (white noise excitation, Figure 3.1.8 – 3.1.14) under low acceleration intensity in order to investigate changes in eigen periods of the structure. The peak acceleration of each one of the fourteen white noise excitations of the seismic table was 0,05g and 0,08g. The direction of excitation was parallel to partial infills (W-L, W-R in plane) and vertical to full infills plane (W-B, W-F out of plane).

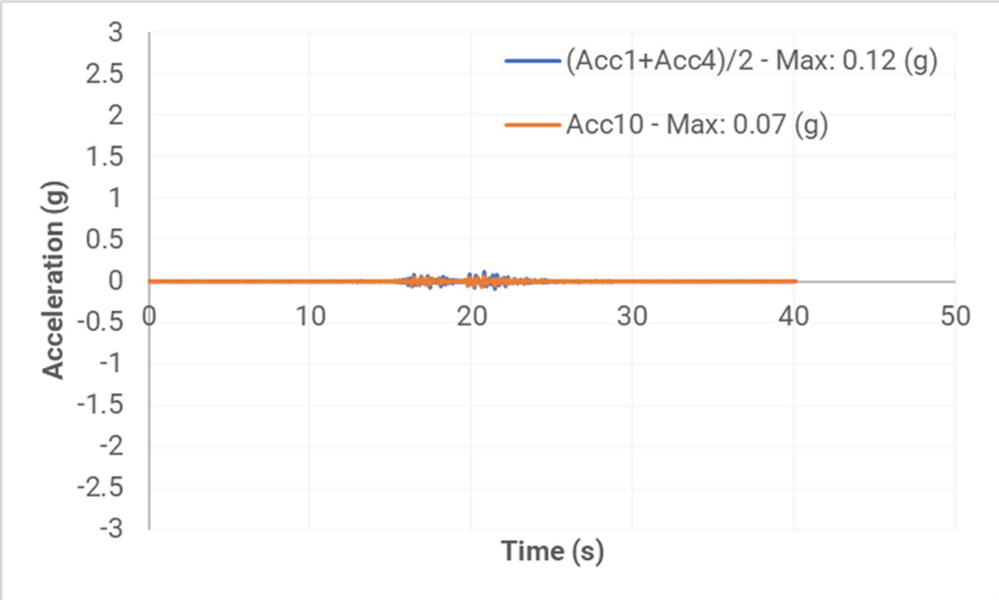

(a)

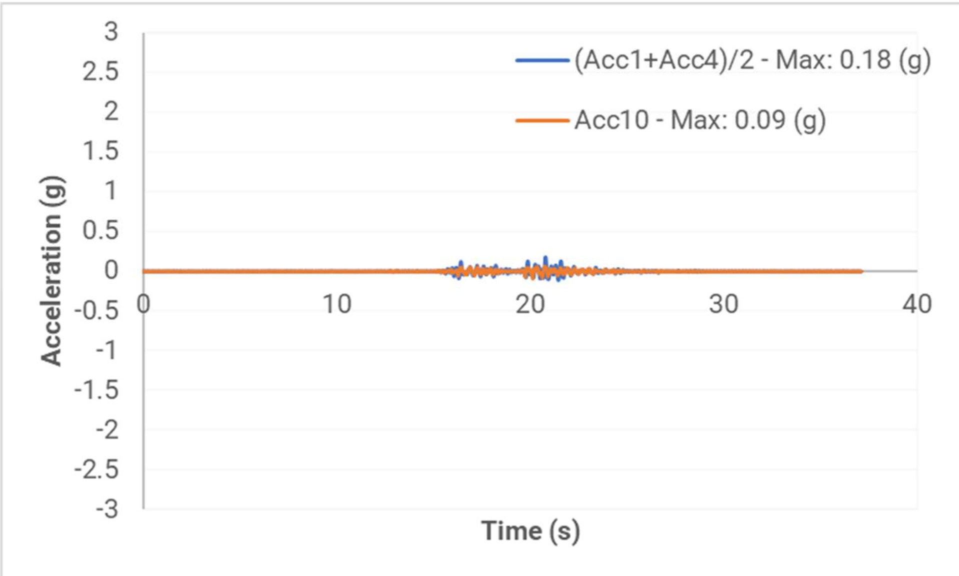

(b)

Figure 3.1.1 Bottom and slab acceleration time-histories for the two levels of earthquake intensity (a) 0.07g, (b) 0.1g

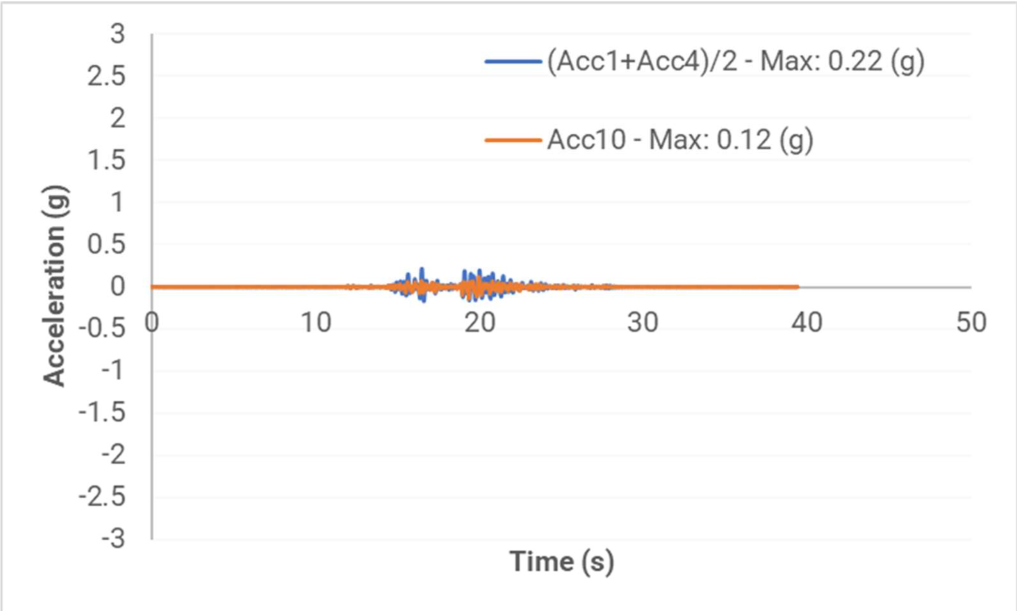

(a)

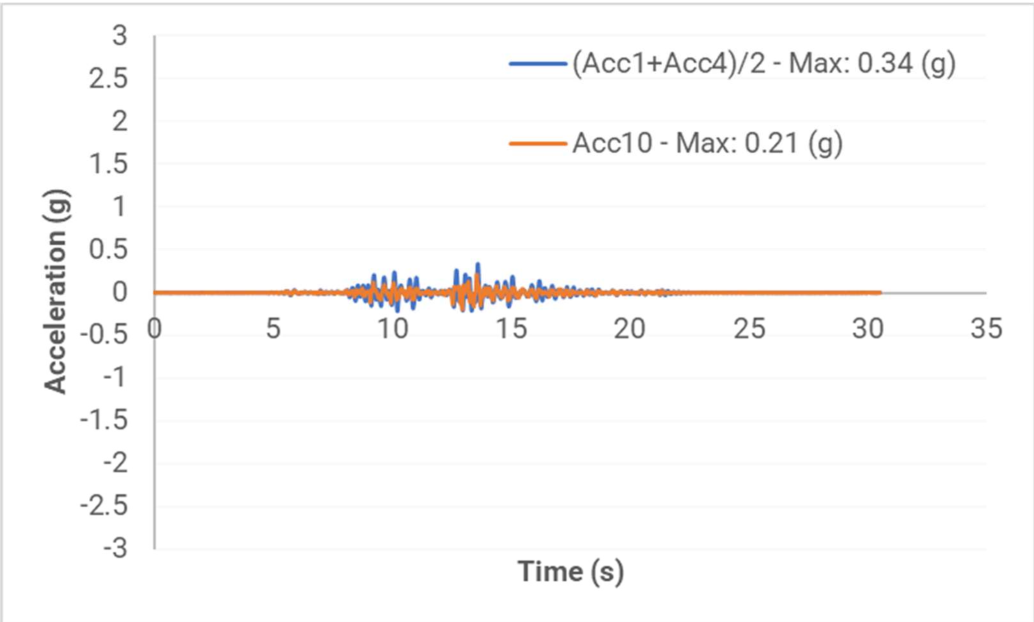

(b)

Figure 3.1.2 Bottom and slab acceleration time-histories for the two levels of earthquake intensity (a) 0.14g, (b) 0.20g

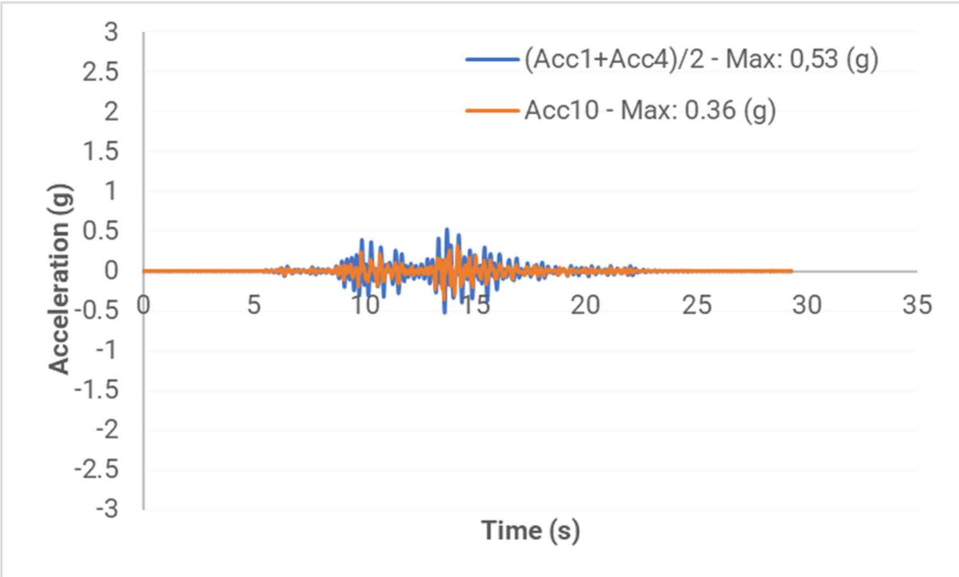

(a)

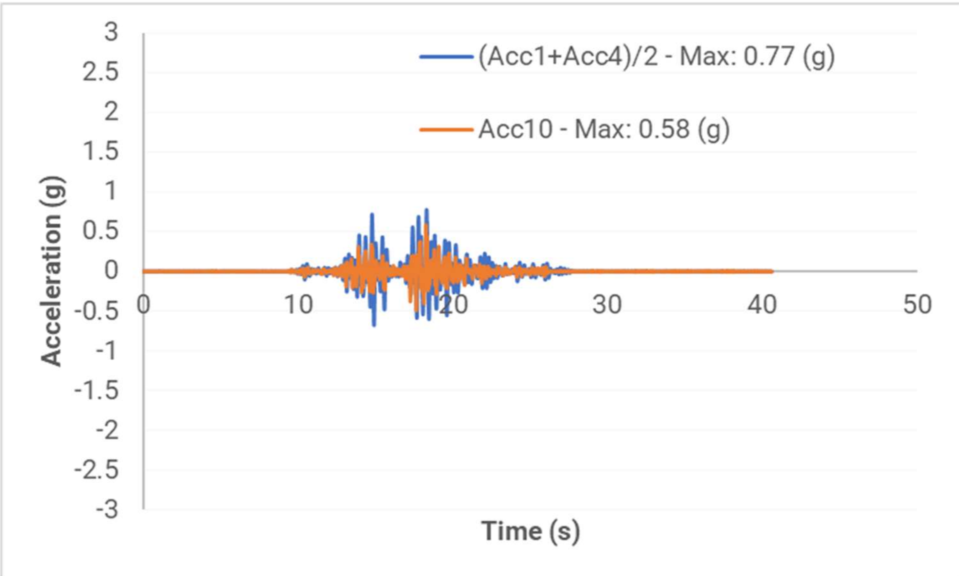

(b)

Figure 3.1.3 Bottom and slab acceleration time-histories for the two levels of earthquake intensity (a) 0.34g, (b) 0.50g

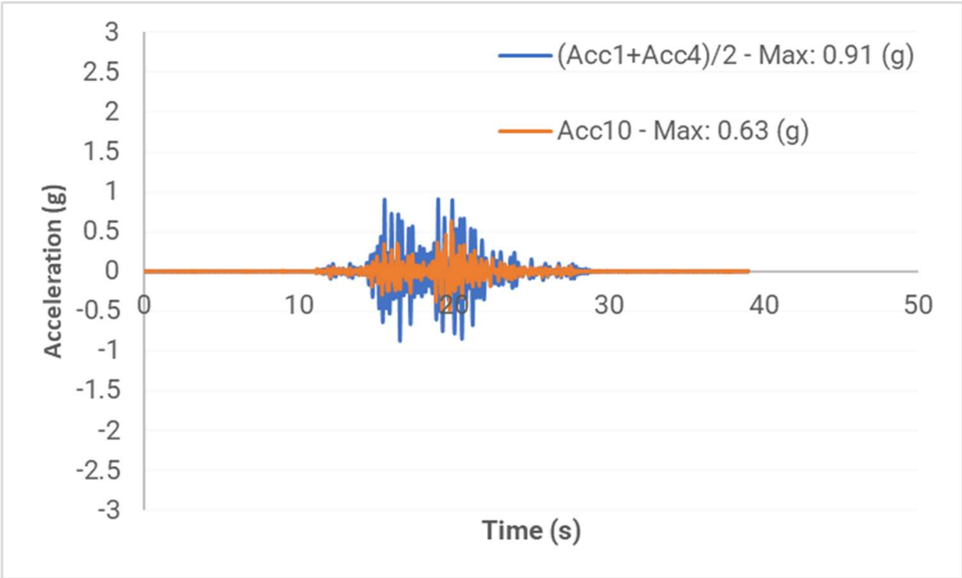

(a)

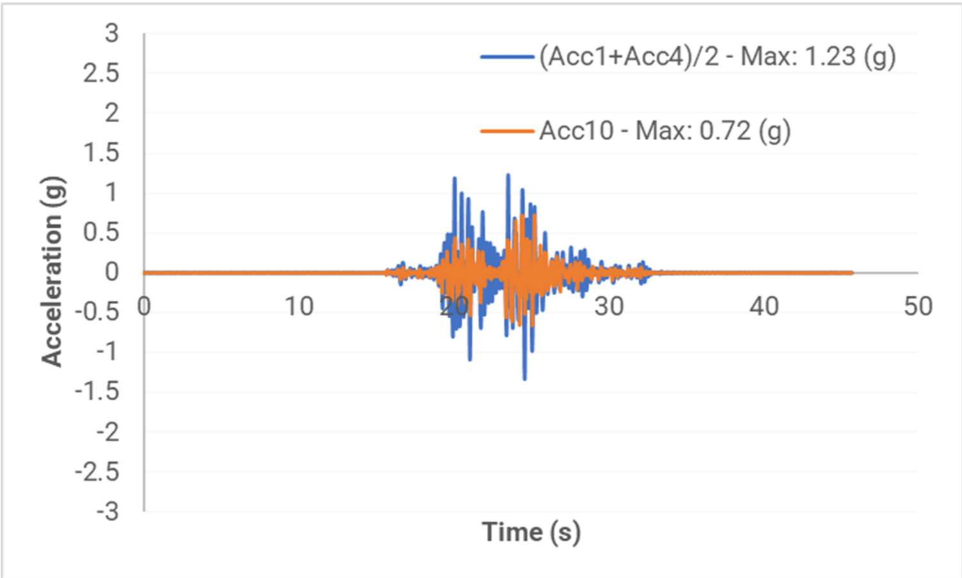

(b)

Figure 3.1.4 Bottom and slab acceleration time-histories for the two levels of earthquake intensity (a) 0.55g, (b) 0.74g

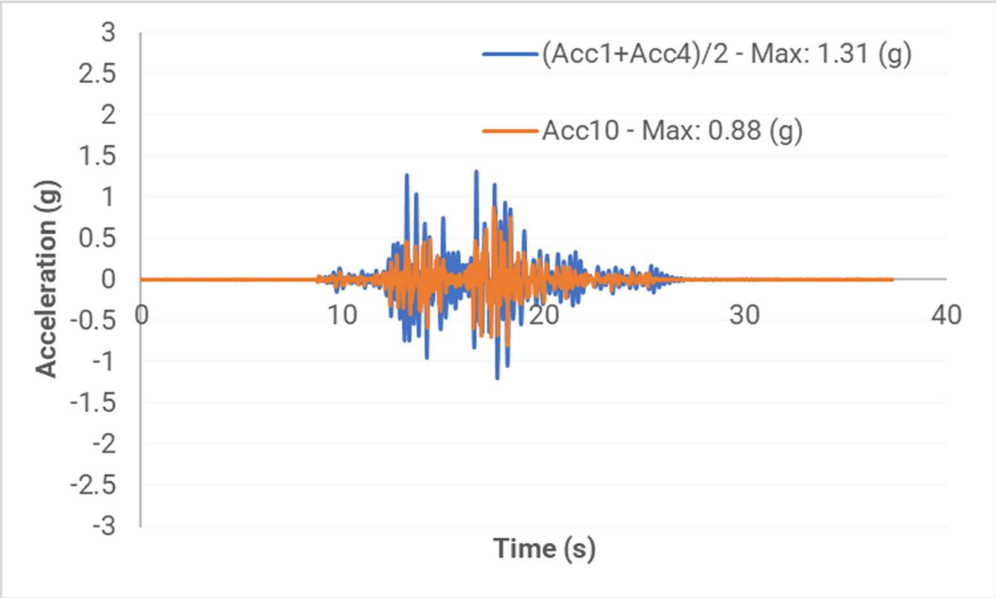

(a)

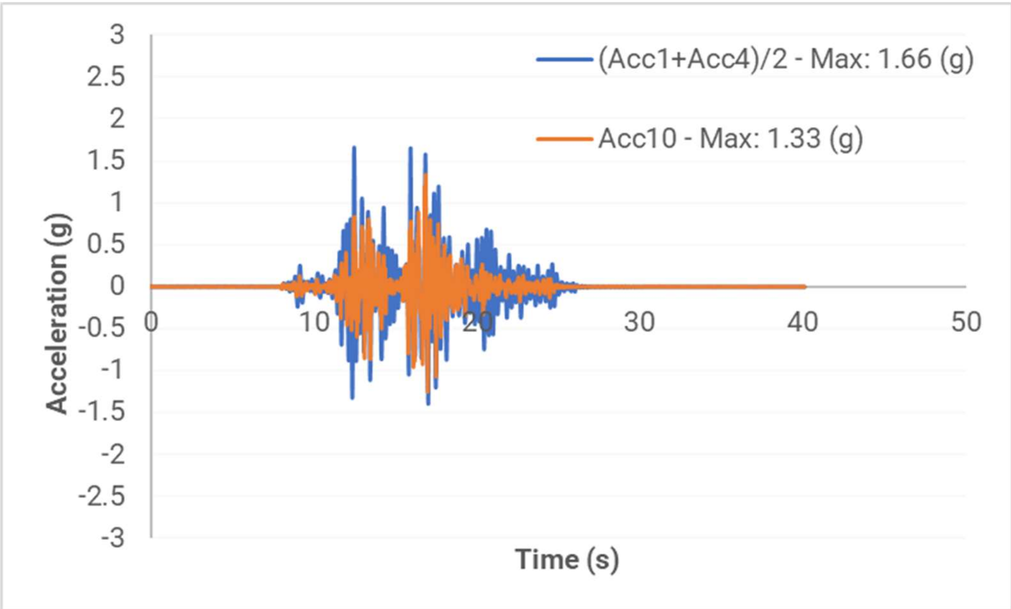

(b)

Figure 3.1.5 Bottom and slab acceleration time-histories for the two levels of earthquake intensity (a) 0.80g, (b) 1.10g

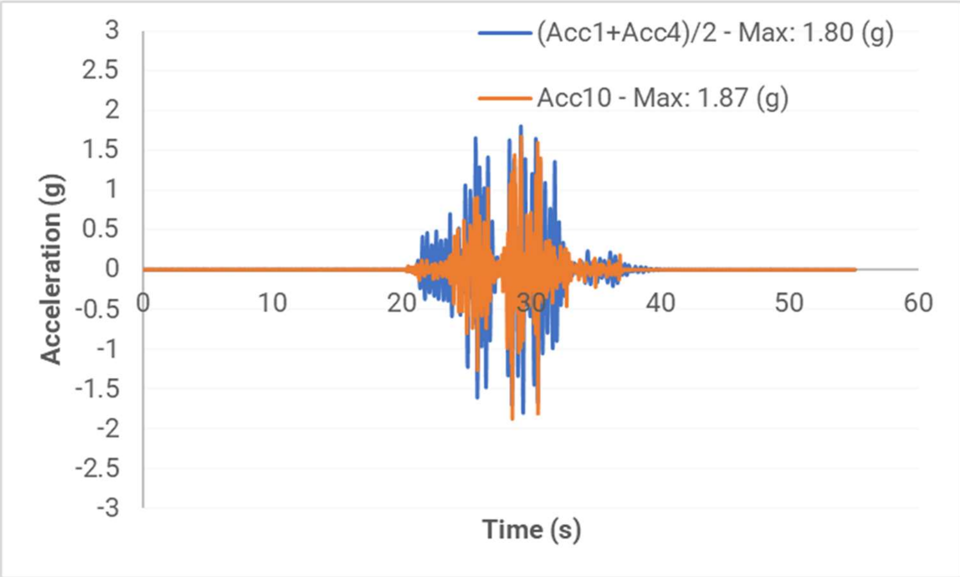

(a)

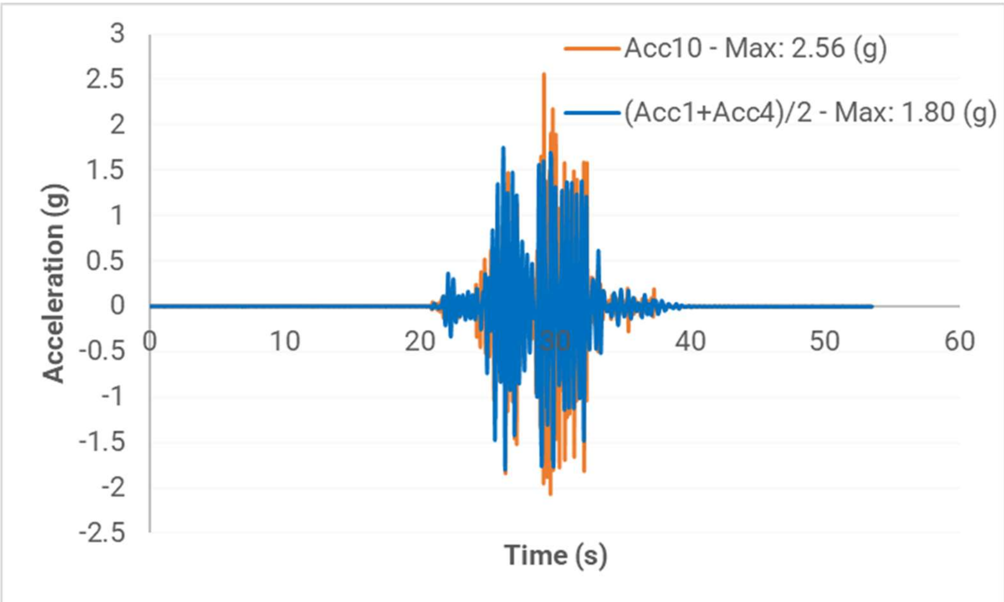

(b)

Figure 3.1.6 Bottom and slab acceleration time-histories for the two levels of earthquake intensity (a) 1.3g (2), (b) 1.4g

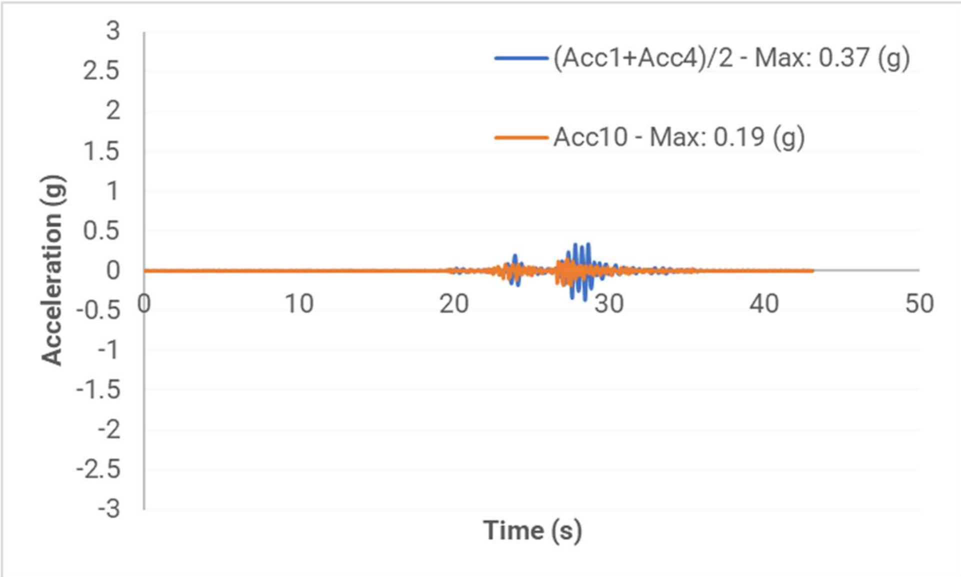

Figure 3.1.7 Bottom and slab acceleration time-histories for the level of earthquake intensity 0.20g

Regarding excitation EQ0.07g, the peak acceleration at the bottom (PGA) level was 0.07g and the peak acceleration at the top (PFA) level was 0.12g. At 0.1g excitation, the top slab acceleration is 2 times the ground acceleration. Peak top acceleration of 0.18g occurred 0.656 sec after peak shake table acceleration. During excitation EQ0.14g the peak acceleration at the ground (PGA) level was 0.12g and the peak acceleration at the slab (PFA) level was 0.22g. During EQ0.2g, the peak top acceleration of 0.34g occurred 0.044 sec after peak shake table acceleration of 0.21g. For EQ0.2g, the slab acceleration is 1.62 times the bottom acceleration. At excitation with intensity EQ0.34g the peak acceleration at the bottom (PGA) level was 0.36g and the peak acceleration at the floor (PFA) level was 0.53g. At 0.34g, the floor acceleration is 1.47 times the ground acceleration. The peak top acceleration of 0.53g occurred 0.13 sec after peak shake table acceleration. Regarding excitation EQ0.5g, the peak acceleration at the ground (PGA) level was 0.58g and the peak acceleration at the floor (PFA) level was 0.77g. Regarding excitation EQ0.55g, the peak acceleration at the ground (PGA) level was 0.63g and the peak acceleration at the floor (PFA) level was 0.91g. At EQ0.74g excitation, the floor acceleration is 1.71 times the ground acceleration. Peak top acceleration of 1.23 g occurred 0.624 sec before peak shake table acceleration. Regarding excitation 0.8g, the peak acceleration at the ground (PGA) level was 0.88g and the peak acceleration at the top (PFA) level was 1.31g. At EQ1.1g excitation, the floor acceleration is 1.25 as much as the ground acceleration. Peak top acceleration of 1.66 g occurred 4.39 sec before peak shake table acceleration. Regarding excitation EQ1.3g (2), the peak acceleration at the bottom (PGA) level was 1.87g and the peak acceleration at the top (PFA) level was 1.8g. At 1.4g excitation, the top slab acceleration is 0.7 times the ground acceleration. Peak top acceleration of 1.8g occurred 2.884 sec before peak shake table acceleration. At excitation with intensity 0.2g the peak acceleration at the ground (PGA) level was 0.19g and the peak acceleration at the floor (PFA) level was 0.37g.

Below are the comparative acceleration-time diagrams at the top and bottom of the structure, for the six white noise excitations.

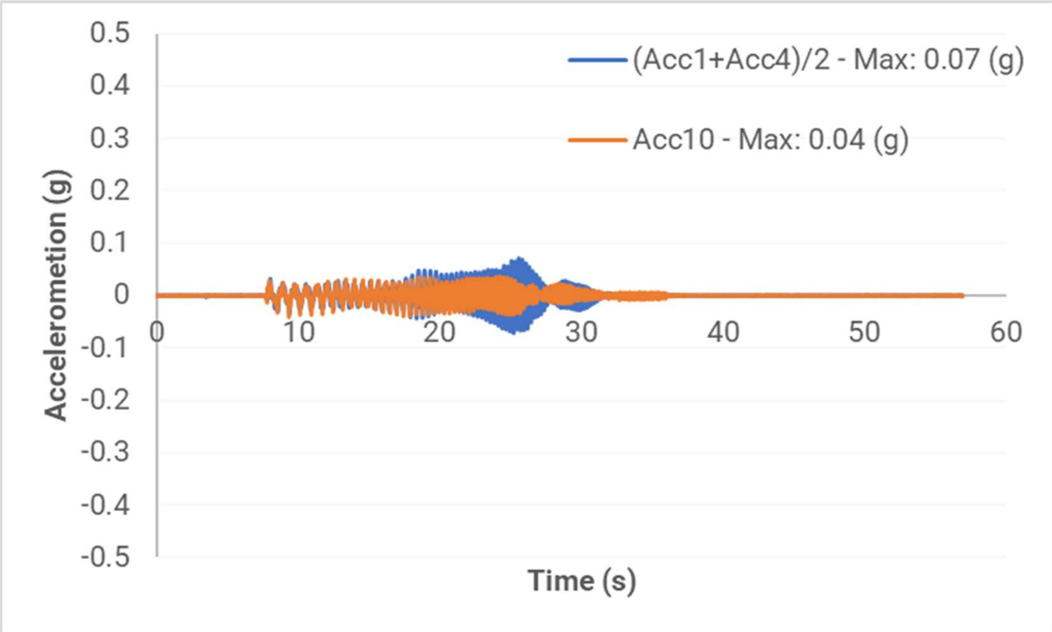

(a)

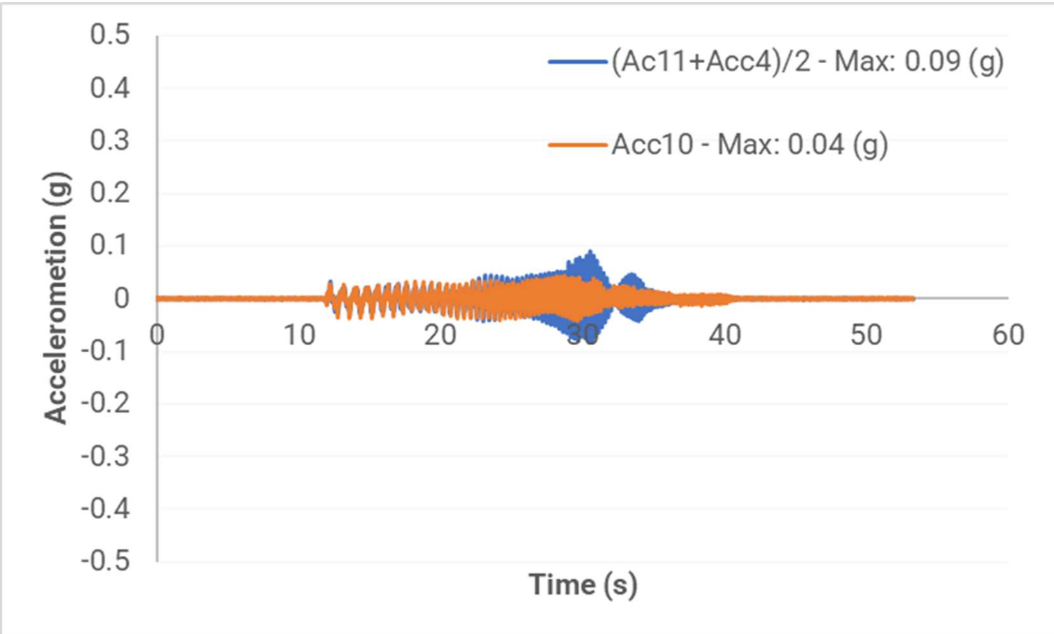

(b)

Figure 3.1.8 Bottom and slab acceleration time-histories for the two levels of white noise before intensity (a) 0.07g (without bottom fixing of the vertical living walls), (b) 0.07g

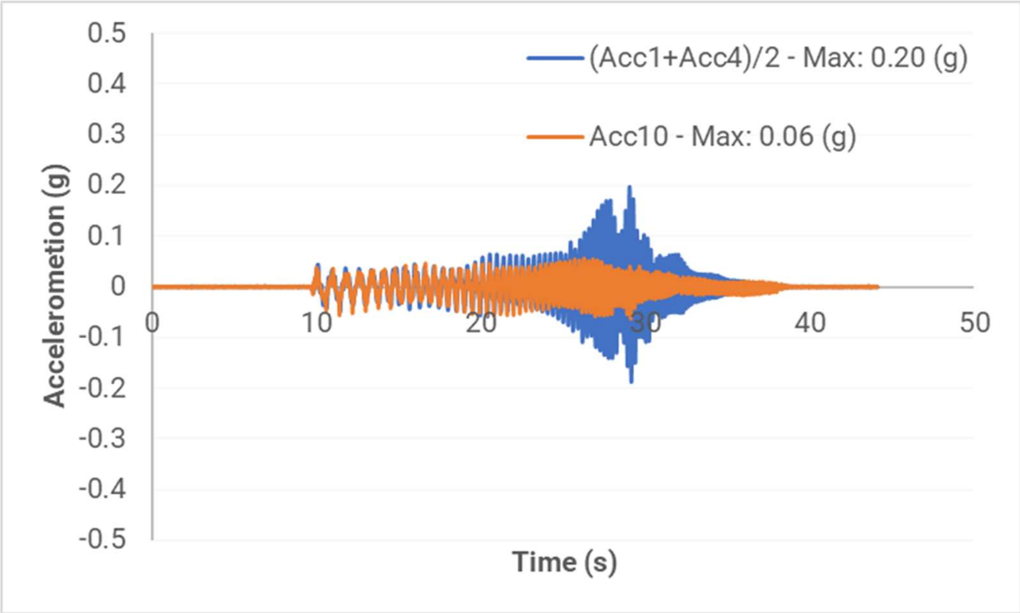

(a)

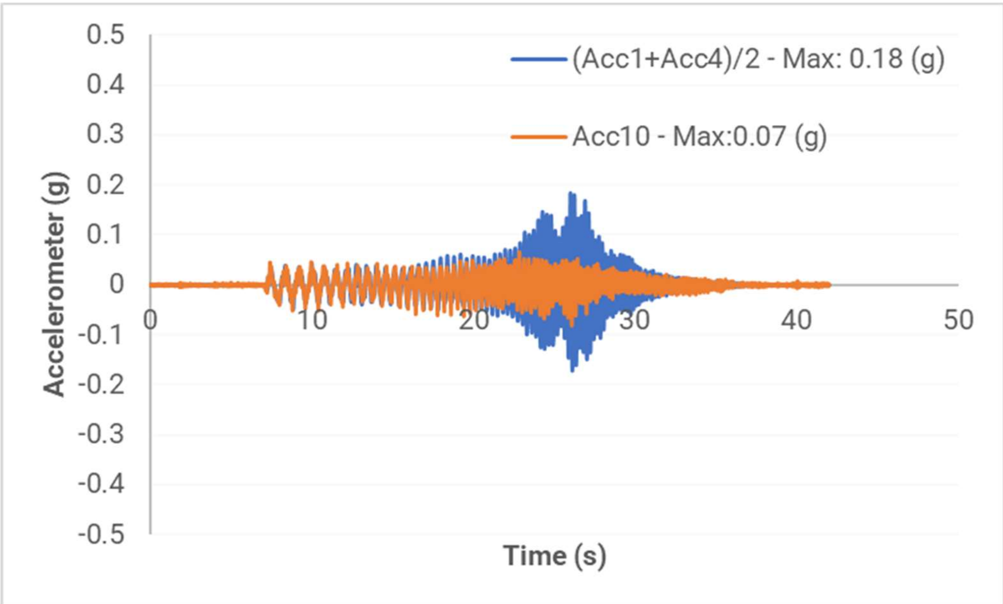

(b)

Figure 3.1.9 Bottom and slab acceleration time-histories for the two levels of white noise before intensity (a) 0.14g, (b) 0.34g

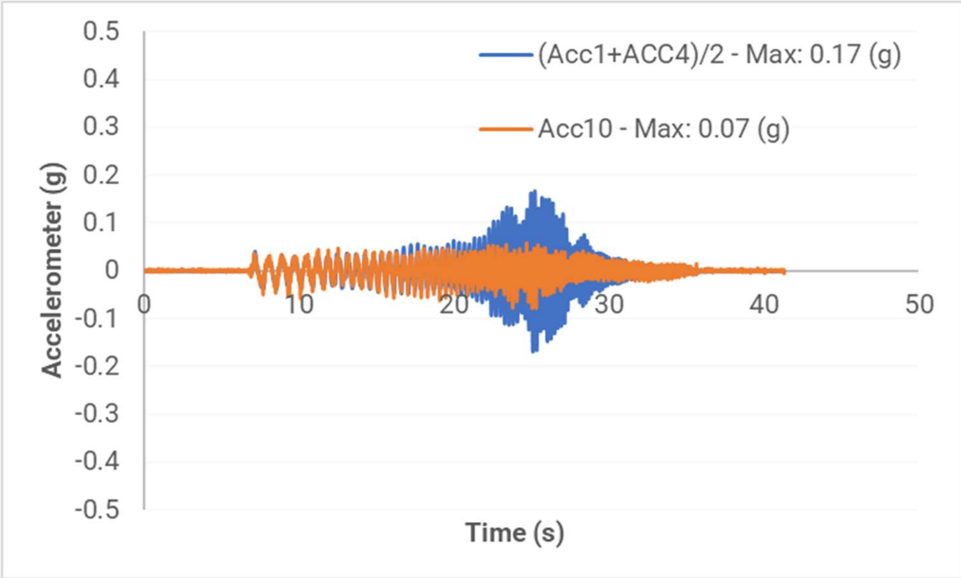

(a)

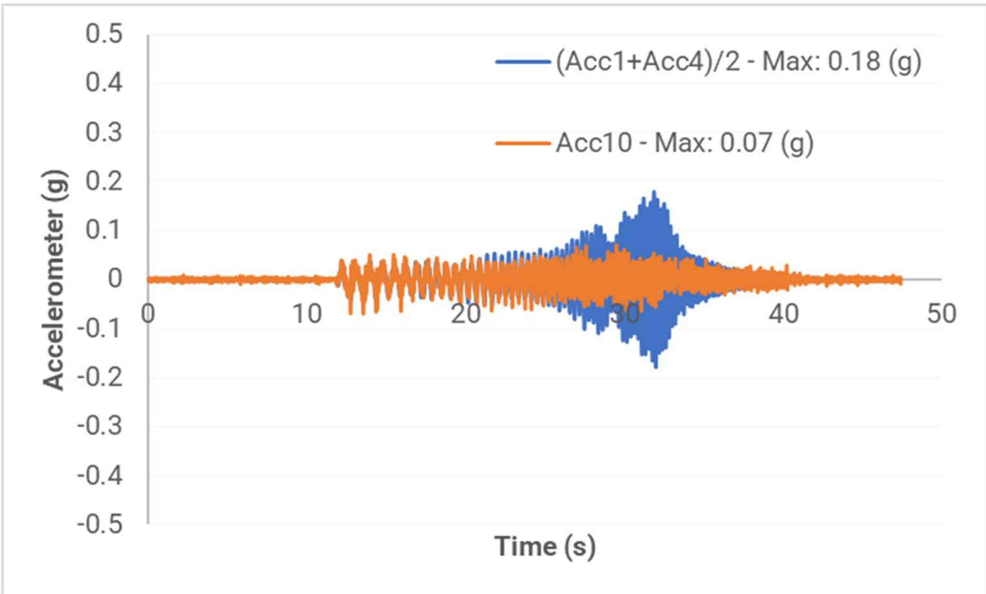

(b)

Figure 3.1.10 Bottom and slab acceleration time-histories for the two levels of white noise before intensity (a) 0.5g, (b) 0.55g

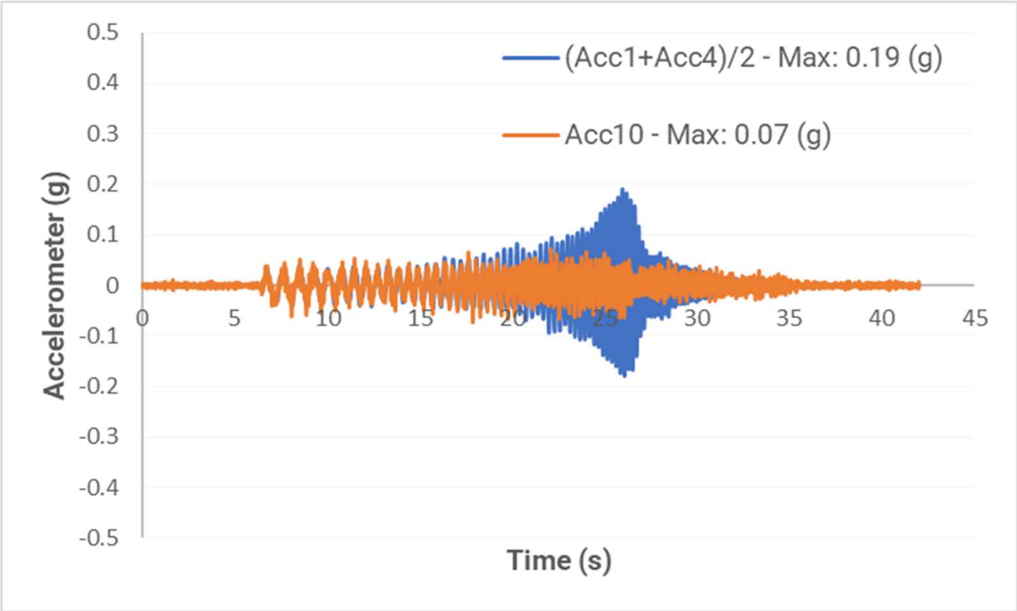

(a)

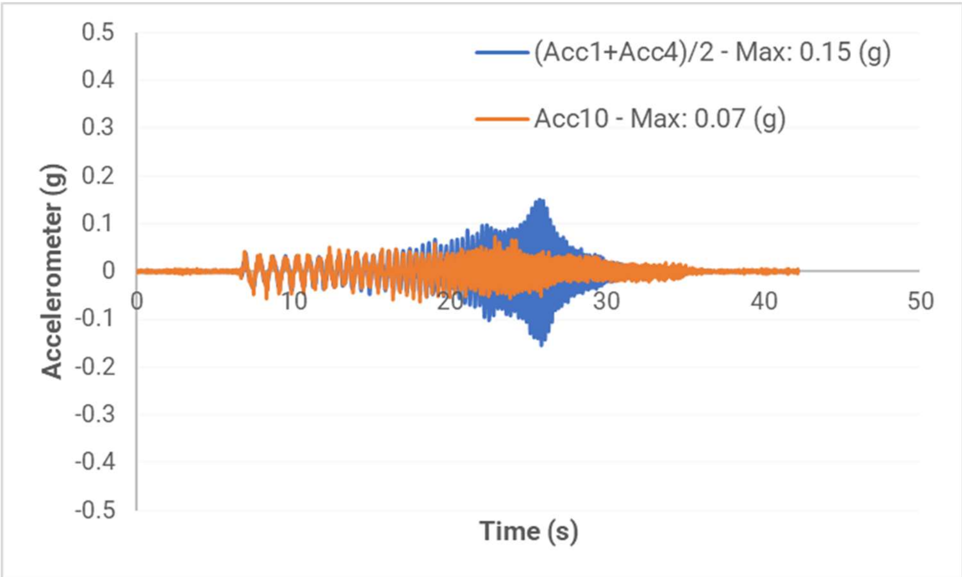

(b)

Figure 3.1.11 Bottom and slab acceleration time-histories for the two levels of white noise before intensity (a) 0.74g, (b) 0.8g

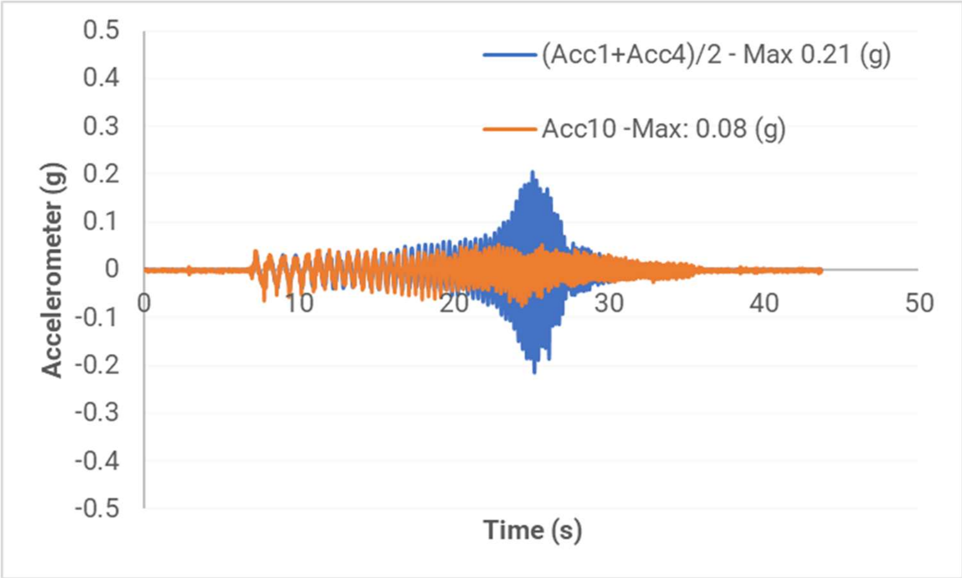

(a)

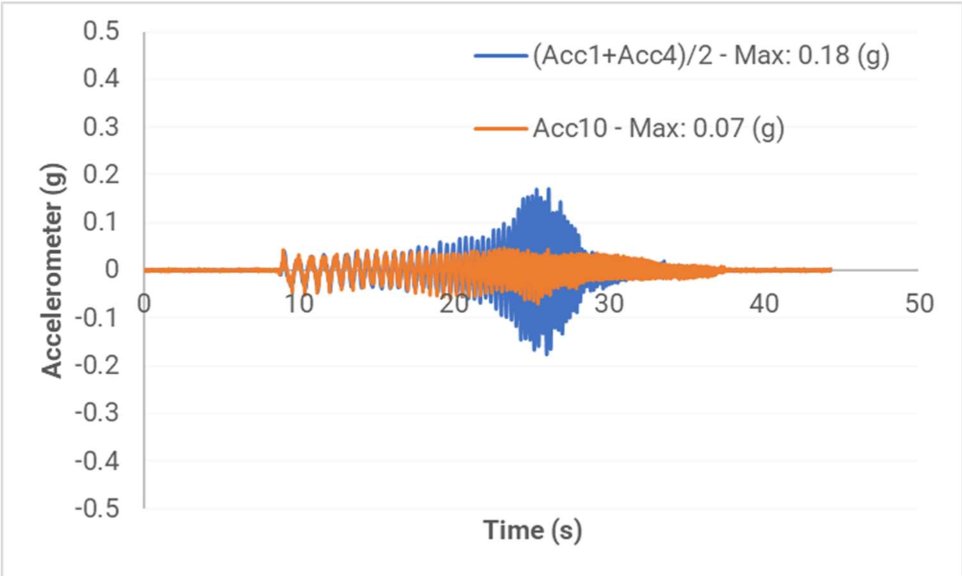

(b)

Figure 3.1.12 Bottom and slab acceleration time-histories for the two levels of white noise before intensity (a) 1.1g, (b) 1.3g

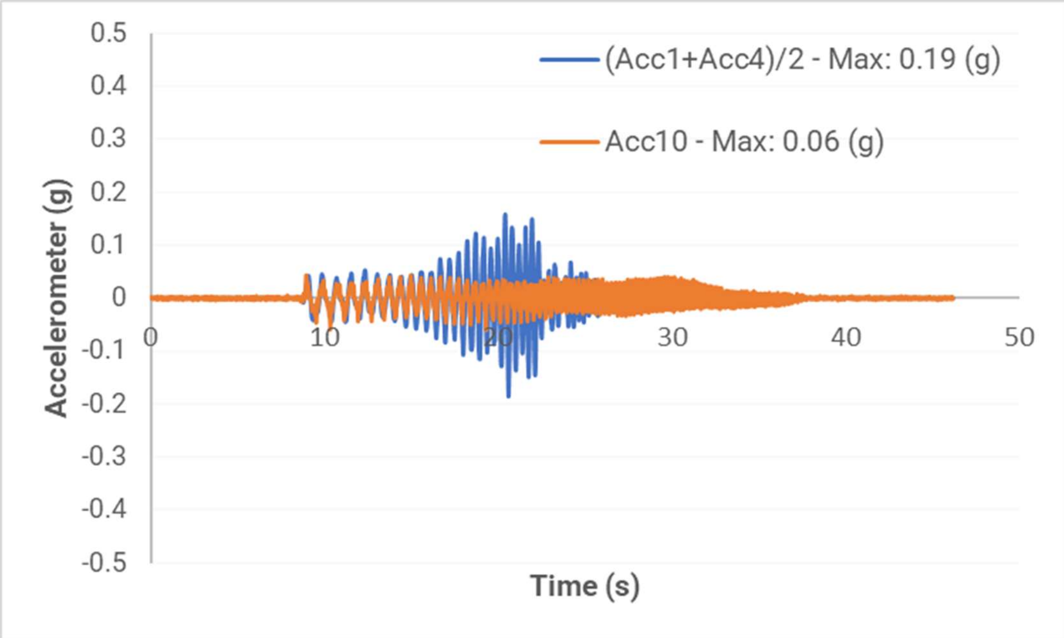

(a)

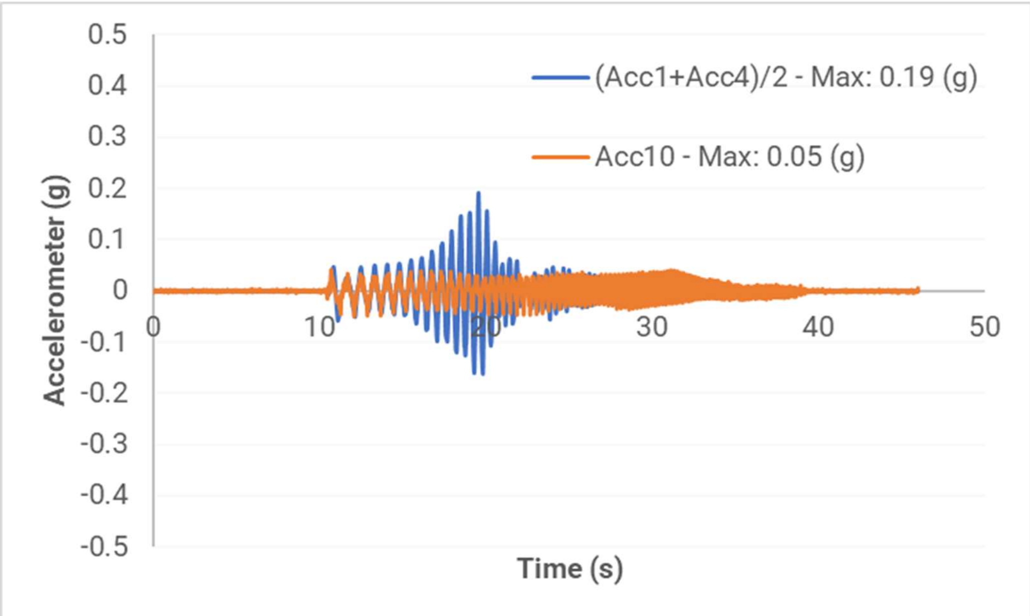

(b)

Figure 3.1.13 Bottom and slab acceleration time-histories for the two levels of white noise before intensity (a) 1.4g, (b) 0.2g

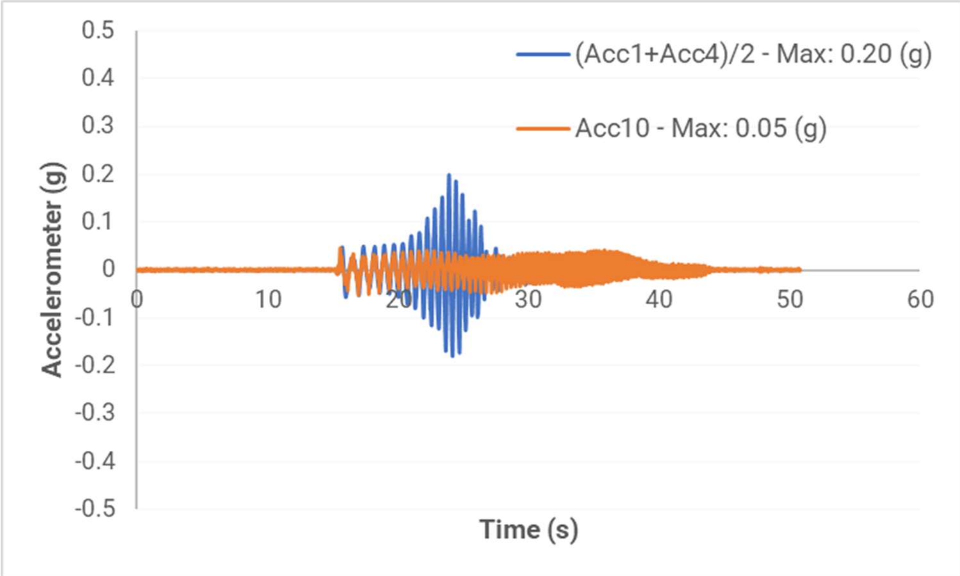

Figure 3.1.14 Bottom and slab acceleration time-histories for the white noise after intensity 0.2g

Regarding excitation white noise before EQ0.07g (without bottom fixing of the vertical living walls), that is WNb0.07g, the peak acceleration at the bottom (PGA) level was 0.04g and the top acceleration at the floor (PFA) level was 0.07g. Peak top acceleration of 0.07g occurred 15.854 sec after peak shake table acceleration. At excitation white noise before EQ0.07g with intensity 0.05g the peak acceleration at the bottom (PGA) level was 0.04g and the peak acceleration at the floor (PFA) level was 0.09g. Peak top acceleration of 0.09g occurred 1.819 sec after peak shake table acceleration. At WNb0.14g excitation, the floor acceleration is 3.33 times the ground acceleration. At excitation white noise before EQ0.34g the peak acceleration at the ground (PGA) level was 0.07g and the peak acceleration at the floor (PFA) level was 0.18g. At WNb0.5g, the floor acceleration is 2.43 times the ground acceleration. Peak top acceleration of 0.17 g occurred 0.036 sec after peak shake table acceleration. Regarding excitation white noise before EQ0.55g, the peak acceleration at the ground (PGA) level was 0.07g and the peak acceleration at the floor (PFA) level was 0.18g. At WNb0.74g, the floor acceleration is 2.71 times the ground acceleration. Peak top acceleration of 0.19g occurred 8.082 sec after peak shake table acceleration. Regarding excitation white noise before WNb0.8g, the peak acceleration at the bottom (PGA) level was 0.07g and the peak acceleration at the top (PFA) level was 0.15g. At WNb1.1g excitation, the floor acceleration is 2.63 times the ground acceleration. Peak top acceleration of 0.21g occurred 0.806 sec after peak shake table acceleration. Regarding excitation white noise after 1.3g, the peak acceleration at the ground (PGA) level was 0.07g and the peak acceleration at the floor (PFA) level was 0.18g. At WNb1.4g excitation, the floor acceleration is 3.17 times the ground acceleration. Peak top acceleration of 0.19g occurred 1.294 sec after peak shake table acceleration. At WNb0.2g excitation, the floor acceleration is 3.80 times the ground acceleration. Peak top acceleration of 0.19g occurred 7.486 sec after peak shake table acceleration. Regarding excitation white noise after 0.2g, the peak acceleration at the ground (PGA) level was 0.05g and the peak acceleration at the floor (PFA) level was 0.2g. At WNa0.2g excitation, the floor acceleration is 4 times the ground acceleration. Peak top acceleration of 0.2g occurred 6.95 sec after peak shake table acceleration.

Below are the tables with the summary of results for accelerometers, draw wires and strain gauges.

Table 3.1.1a Summary of results

		max Acc1 (g)	min Acc1 (g)	max Acc2 (g)	min Acc2(g)	max Acc3 (g)	min Acc3 (g)
ST1	**Wnb0,07g (without)**	0.07	-0.06	0.05	-0.06	0.02	-0.02
ST2	**Wnb0,07g**	0.08	-0.07	0.06	-0.06	0.04	-0.05
ST3	**EQ0,07g**	0.09	-0.1	0.05	-0.06	0.06	-0.06
ST4	**EQ0,1g**	0.1	-0.17	0.06	-0.07	0.02	-0.04
ST5	**Wnb0,14g**	0.19	-0.18	0.09	-0.1	0.09	-0.18
ST6	**EQ0,14g**	0.17	-0.21	0.08	-0.08	0.15	-0.08
ST7	**EQ0,2g**	0.21	-0.32	0.12	-0.12	0.28	-0.86
ST8	**Wnb0,34g**	0.17	-0.19	0.1	-0.14	0.15	-0.16
ST9	**EQ0,34g**	0.55	-0.54	0.17	-0.26	0.51	-0.52
ST10	**Wnb0,5g**	0.17	-0.18	0.09	-0.1	0.31	-0.59
ST11	**EQ0,5g**	0.65	-0.75	0.25	-0.29	0.85	-0.87
ST12	**Wnb0,55g**	0.18	-0.18	0.07	-0.08	0.16	-0.23
ST13	**EQ0,55g**	0.85	-0.89	0.21	-0.22	0.96	-0.91
ST14	**Wnb0,74g**	0.18	-0.18	0.08	-0.09	0.19	-0.11
ST15	**EQ0,74g**	1.37	-1.21	0.41	-0.51	1	-1.21
ST16	**Wnb0,8g**	0.17	-0.13	0.07	-0.11	0.36	-0.44
ST17	**EQ0,8g**	1.23	-1.3	0.45	-1.17	1.11	-1.86
ST18	**Wnb1,1g**	0.21	-0.2	0.06	-0.05	0.12	-0.09
ST19	**EQ1,1g**	1.39	-1.75	0.71	-0.76	0.69	-1.22

ST20	**Wnb1,3g**	0.17	-0.17	0.06	-0.07	0.09	-0.11
ST21	**EQ1,3g**	0	0	0	0	0	0
ST22	**Wnb1,3g(2)**	0	0	0	0	0	0
ST23	**EQ1,3g(2)**	1.91	-1.8	0.49	-0.67	1.37	-1.96
ST24	**Wnb 1,4g**	0.18	-0.16	0.06	-0.07	0.12	-0.12
ST25	**EQ1,4g**	2.05	-1.81	0.49	-0.69	1.42	-2.47
ST26	**Wnb0,2g (2)**	0.16	-0.19	0.06	-0.06	0.11	-0.07
ST27	**EQ0,2g (2)**	0.36	-0.36	0.12	-0.09	0.29	-0.17
ST28	**Wna0,2g**	0.19	-0.19	0.06	-0.07	0.14	-0.13

Table 3.1.1b Summary of results (continued)

		max Acc4 (g)	min Acc4 (g)	max Acc5 (g)	min Acc5 (g)	max Acc6 (g)	min Acc6 (g)
ST1	**Wnb0,07g (without)**	0.08	-0.09	0.05	-0.05	0.01	-0.01
ST2	**Wnb0,07g**	0.09	-0.11	0.06	-0.06	0.03	-0.05
ST3	**EQ0,07g**	0.1	-0.13	0.05	-0.05	-0.04	0.04
ST4	**EQ0,1g**	0.12	-0.19	0.06	-0.06	0.03	-0.02
ST5	**Wnb0,14g**	0.18	-0.21	0.09	-0.1	0.17	-0.25
ST6	**EQ0,14g**	0.18	-0.23	0.09	-0.08	0.2	-0.25
ST7	**EQ0,2g**	0.24	-0.35	0.15	-0.12	0.51	-1.21
ST8	**Wnb0,34g**	0.18	-0.19	0.1	-0.13	0.18	-0.14
ST9	**EQ0,34g**	0.5	-0.53	0.18	-0.24	0.7	-0.77
ST10	**Wnb0,5g**	0.17	-0.17	0.08	-0.1	0.33	-0.61
ST11	**EQ0,5g**	0.7	-0.8	0.25	-0.49	1.58	-1.12
ST12	**Wnb0,55g**	0.18	-0.18	0.06	-0.07	0.14	-0.29
ST13	**EQ0,55g**	0.89	-0.93	0.2	-0.2	0.61	-1.95
ST14	**Wnb0,74g**	0.18	-0.2	0.08	-0.08	0.21	-0.27
ST15	**EQ0,74g**	1.37	-1.24	0.4	-0.49	1.17	-0.89
ST16	**Wnb0,8g**	0.15	-0.17	0.07	-0.1	0.4	-0.45
ST17	**EQ0,8g**	1.44	-1.33	0.71	-0.52	0.76	-0.09
ST18	**Wnb1,1g**	0.22	-0.21	0.06	-0.05	0.06	-0.09
ST19	**EQ1,1g**	1.55	-1.66	0.69	-0.73	0.99	-0.91
ST20	**Wnb1,3g**	0.19	-0.18	0.06	-0.07	0.12	-0.1
ST21	**EQ1,3g**	0	0	0	0	0	0
ST22	**Wnb1,3g(2)**	0	0	0	0	0	0

ST23	**EQ1,3g(2)**	1.82	-1.82	1.04	-0.67	0.84	-1.23
ST24	**Wnb 1,4g**	0.19	-0.15	0.07	-0.07	0.1	-0.1
ST25	**EQ1,4g**	1.78	-1.86	0.64	-0.69	1.13	-3.51
ST26	**Wnb0,2g (2)**	0.17	-0.2	0.06	-0.06	0.15	-0.09
ST27	**EQ0,2g (2)**	0.37	-0.34	0.13	-0.1	0.19	-0.56
ST28	**Wna0,2g**	0.18	-0.21	0.06	-0.06	0.31	-0.16

Table 3.1.1c Summary of results (continued)

		max Acc7 (g)	min Acc7 (g)	max Acc8 (g)	min Acc8 (g)	max Acc9 (g)	min Acc9 (g)
ST1	**Wnb0,07g (without)**	0.05	-0.04	0.02	-0.02	0.01	-0.01
ST2	**Wnb0,07g**	0.09	-0.1	0.03	-0.02	0.02	-0.02
ST3	**EQ0,07g**	0.09	-0.15	0.03	-0.02	0.02	-0.02
ST4	**EQ0,1g**	0.09	-0.1	0.03	-0.03	0.01	-0.02
ST5	**Wnb0,14g**	0.1	-0.1	0.05	-0.03	0.05	-0.06
ST6	**EQ0,14g**	0.14	-0.12	0.04	-0.03	0.05	-0.07
ST7	**EQ0,2g**	0.19	-0.2	0.08	-0.08	0.12	-0.19
ST8	**Wnb0,34g**	0.11	-0.12	0.05	-0.04	0.05	-0.05
ST9	**EQ0,34g**	0.45	-0.36	0.13	-0.17	0.14	-0.13
ST10	**Wnb0,5g**	0.11	-0.11	0.01	-0.03	0.07	-0.09
ST11	**EQ0,5g**	0.55	-0.64	0.15	-0.16	0.24	-0.27
ST12	**Wnb0,55g**	0.11	-0.12	0.04	-0.04	0.03	-0.04
ST13	**EQ0,55g**	0.72	-0.65	0.12	-0.18	0.21	-0.19
ST14	**Wnb0,74g**	0.11	-0.11	0.04	-0.04	0.04	-0.04
ST15	**EQ0,74g**	1.19	-1.01	0.25	-0.22	0.26	-0.28
ST16	**Wnb0,8g**	0.1	-0.11	0.04	-0.06	0.06	-0.05
ST17	**EQ0,8g**	1.21	-1.05	0.32	-0.31	0.26	-0.24
ST18	**Wnb1,1g**	0.11	-0.11	0.03	-0.03	0.04	-0.04
ST19	**EQ1,1g**	1.5	-1.75	0.32	-0.38	0.28	-0.32
ST20	**Wnb1,3g**	0.12	-0.1	0.03	-0.04	0.03	-0.03
ST21	**EQ1,3g**						
ST22	**Wnb1,3g(2)**						

ST23	**EQ1,3g(2)**	2.08	-2.17	0.57	-0.53	0.32	-0.42
ST24	**Wnb 1,4g**	0.15	-0.11	0.03	-0.03	0.05	-0.04
ST25	**EQ1,4g**	2.31	-2	0.68	-0.77	0.81	-1.03
ST26	**Wnb0,2g (2)**	0.11	-0.11	0.03	-0.03	0.04	-0.04
ST27	**EQ0,2g (2)**	0.27	-0.26	0.11	-0.06	0.09	-0.08
ST28	**Wna0,2g**	0.16	-0.15	0.03	-0.09	0.05	-0.05

Table 3.1.1d Summary of results (continued)

		max Acc10 (g)	min Acc10 (g)	max Acc11 (g)	min Acc11 (g)	max Acc12 (g)	min Acc12 (g)	FAF
ST1	Wnb0,07g (without)	0.04	-0.04	0.02	-0.02	0.02	0	1.75
ST2	Wnb0,07g	0.04	-0.04	0.02	-0.03	0.01	-0.01	2.25
ST3	EQ0,07g	0.07	-0.06	0.03	-0.02	0.02	-0.02	1.71
ST4	EQ0,1g	0.09	-0.06	0.03	-0.03	0.01	-0.01	2.00
ST5	Wnb0,14g	0.06	-0.06	0.03	-0.04	0.03	-0.02	3.33
ST6	EQ0,14g	0.14	-0.12	0.04	-0.03	0.02	-0.02	1.57
ST7	EQ0,2g	0.19	-0.21	0.05	-0.05	0.02	-0.11	1.79
ST8	Wnb0,34g	0.08	-0.07	0.04	-0.05	0.03	-0.04	2.25
ST9	EQ0,34g	0.36	-0.32	0.14	-0.11	0.1	-0.09	1.47
ST10	Wnb0,5g	0.08	-0.06	0.06	-0.05	0.05	-0.04	2.13
ST11	EQ0,5g	0.49	-0.58	0.14	-0.12	0.24	-0.19	1.57
ST12	Wnb0,55g	0.07	-0.07	0.05	-0.04	0.03	-0.03	2.57
ST13	EQ0,55g	0.49	-0.63	0.12	-0.09	0.13	-0.22	1.86
ST14	Wnb0,74g	0.07	-0.07	0.05	-0.04	0.03	-0.03	2.71
ST15	EQ0,74g	0.66	-0.72	0.39	-0.33	0.18	-0.16	1.86
ST16	Wnb0,8g	0.06	-0.07	0.05	-0.04	0.03	-0.04	2.50
ST17	EQ0,8g	0.8	-0.88	0.47	-0.38	0.23	-0.21	1.64
ST18	Wnb1,1g	0.08	-0.05	0.04	-0.03	0.03	-0.03	2.50
ST19	EQ1,1g	1.25	-1.33	0.64	-0.65	0.21	-0.19	1.33
ST20	Wnb1,3g	0.07	-0.05	0.04	-0.03	0.02	-0.03	2.43
ST21	EQ1,3g							
ST22	Wnb1,3g(2)							

ST23	**EQ1,3g(2)**	1.87	-1.67	0.68	-0.71	0.85	-0.99	0.96
ST24	**Wnb 1,4g**	0.06	-0.04	0.02	-0.02	0.02	-0.03	2.67
ST25	**EQ1,4g**	2.07	-2.56	0.7	-0.87	1.17	-0.89	0.85
ST26	**Wnb0,2g (2)**	0.05	-0.04	0.03	-0.02	0.02	-0.03	3.80
ST27	**EQ0,2g (2)**	0.19	-0.15	0.05	-0.05	0.06	-0.05	1.74
ST28	**Wna0,2g**	0.05	-0.05	0.02	-0.02	0.03	-0.03	4.00

Table 3.1.1e Summary of results (continued)

		Intensity (g)	max W1 (mm)	min W1 (mm)	max W2 (mm)	min W2 (mm)
ST1	**Wnb0,07g (without)**	0.05	13.41	-10.79	13.7	-10.67
ST2	**Wnb0,07g**	0.05	13.53	-10.65	13.76	-10.59
ST3	**EQ0,07g**	0.07	2.06	-1.89	2.38	-1.81
ST4	**EQ0,1g**	0.1	3.28	-2.82	3.58	-2.78
ST5	**Wnb0,14g**	0.08	20.91	-16.33	21.18	-16.32
ST6	**EQ0,14g**	0.14	4.05	-4.38	4.5	-4.46
ST7	**EQ0,2g**	0.2	6.38	-5.88	6.88	-5.88
ST8	**Wnb0,34g**	0.08	20.95	-16.36	21.18	-16.45
ST9	**EQ0,34g**	0.34	10.66	-11.39	10.95	-11.07
ST10	**Wnb0,5g**	0.08	21.03	-16.31	21.24	-16.42
ST11	**EQ0,5g**	0.5	20.99	-16.35	21.2	-16.48
ST12	**Wnb0,55g**	0.08	15.68	-16.01	15.99	-15.8
ST13	**EQ0,55g**	0.55	17.28	-15.13	17.96	-15.68
ST14	**Wnb0,74g**	0.08	21.02	-16.39	21.24	-16.43
ST15	**EQ0,74g**	0.74	21.66	-20.24	23.21	-20.3
ST16	**Wnb0,8g**	0.08	21.09	-16.35	21.31	-16.52
ST17	**EQ0,8g**	0.8	23.65	-22.18	24.54	-23.54
ST18	**Wnb1,1g**	0.08	21.19	-16.3	21.28	-16.47
ST19	**EQ1,1g**	1.1	32.92	-31.36	34.41	-31.04
ST20	**Wnb1,3g**	0.08	21.28	-16.41	21.32	-16.59
ST21	**EQ1,3g**	1.3	41.66	-38.62	44.14	-36.64
ST22	**Wnb1,3g(2)**	0.08	21.57	-16.66	21.74	-16.86

ST23	**EQ1,3g(2)**	1.3	43.47	-46.53	42.95	-46.48
ST24	**Wnb 1,4g**	0.08	22.38	-16.91	22.52	-16.85
ST25	**EQ1,4g**	1.4	55.95	-58.84	55.35	-59.73
ST26	**Wnb0,2g (2)**	0.08	23.43	-21.52	23.74	-21.2
ST27	**EQ0,2g (2)**	0.2	12.44	-11.22	12.09	-10.94
ST28	**Wna0,2g**	0.08	23.55	-22.26	23.84	-22.02

Table 3.1.1f Summary of results (continued)

		Intensity (g)	max W3 (mm)	min W3 (mm)	max W4 (mm)	min W4 (mm)
ST1	**Wnb0,07g (without)**	0.05	13.56	-10.61	13.84	-10.73
ST2	**Wnb0,07g**	0.05	13.58	-10.55	13.95	-10.64
ST3	**EQ0,07g**	0.07	1.48	-1.42	1.72	-1.46
ST4	**EQ0,1g**	0.1	2.18	-2.11	2.37	-2.15
ST5	**Wnb0,14g**	0.08	21.14	-16.33	4.68	-16.28
ST6	**EQ0,14g**	0.14	2.96	-2.91	3.23	-3.09
ST7	**EQ0,2g**	0.2	4.3	-4.13	4.68	-4.39
ST8	**Wnb0,34g**	0.08	21.16	-16.35	21.21	-16.32
ST9	**EQ0,34g**	0.34	7.45	-7.22	7.78	-7.48
ST10	**Wnb0,5g**	0.08	21.05	-16.33	21.16	-16.28
ST11	**EQ0,5g**	0.5	21.24	-16.3	21.34	-16.26
ST12	**Wnb0,55g**	0.08	11.15	-10.49	11.49	-10.73
ST13	**EQ0,55g**	0.55	12.39	-11.32	12.71	-11.63
ST14	**Wnb0,74g**	0.08	21.13	-16.27	21.29	-16.24
ST15	**EQ0,74g**	0.74	16.69	-15.4	17.97	-14.62
ST16	**Wnb0,8g**	0.08	21.11	-16.28	21.13	-16.3
ST17	**EQ0,8g**	0.8	18.04	-16.45	18.51	-16.4
ST18	**Wnb1,1g**	0.08	21.07	-16.33	21.16	-16.39
ST19	**EQ1,1g**	1.1	24.51	-22.82	25.66	-22.16
ST20	**Wnb1,3g**	0.08	21.13	-16.25	21.19	-16.32
ST21	**EQ1,3g**	1.3	29.76	-27.24	31.92	-24.75
ST22	**Wnb1,3g(2)**	0.08	20.97	-16.28	21.18	-16.42

ST23	**EQ1,3g(2)**	1.3	28.79	-28.11	27.7	-29.52
ST24	**Wnb 1,4g**	0.08	21.91	-15.4	21.19	-16.32
ST25	**EQ1,4g**	1.4	34.28	-33.79	34.58	-37.61
ST26	**Wnb0,2g (2)**	0.08	21.07	-16.46	21.11	-16.43
ST27	**EQ0,2g (2)**	0.2	4.34	-4.05	4.54	-4.21
ST28	**Wna0,2g**	0.08	21	-16.44	21.07	-16.48

Table 3.1.1g Summary of results (continued)

		Intensity (g)	max (W1+W2)/2 (mm)	min (W1+W2)/2 (mm)	max (W3+W4)/2 (mm)	min (W3+W4)/2 (mm)
ST1	Wnb0,07g (without)	0.05	13.55	-10.73	13.7	-10.67
ST2	Wnb0,07g	0.05	13.65	-10.62	13.76	-10.6
ST3	EQ0,07g	0.07	2.22	-1.85	1.6	-1.44
ST4	EQ0,1g	0.1	3.43	-2.8	2.28	-2.13
ST5	Wnb0,14g	0.08	21.04	-16.32	21.16	-16.3
ST6	EQ0,14g	0.14	4.27	-4.42	3.09	-3
ST7	EQ0,2g	0.2	6.63	-5.88	4.49	-4.26
ST8	Wnb0,34g	0.08	21.06	-16.4	21.18	-16.34
ST9	EQ0,34g	0.34	10.79	-11.22	7.62	-7.35
ST10	Wnb0,5g	0.08	21.14	-16.36	21.1	-16.3
ST11	EQ0,5g	0.5	15.83	-15.9	11.32	-10.61
ST12	Wnb0,55g	0.08	21.09	-16.42	21.29	-16.27
ST13	EQ0,55g	0.55	17.61	-15.41	12.55	-11.47
ST14	Wnb0,74g	0.08	21.13	-16.4	21.21	-16.25
ST15	EQ0,74g	0.74	20.41	-20.27	17.32	-15.01
ST16	Wnb0,8g	0.08	21.2	-16.43	21.12	-16.29
ST17	EQ0,8g	0.8	24.08	-22.84	18.27	-16.42
ST18	Wnb1,1g	0.08	21.23	-16.38	21.11	-16.36
ST19	EQ1,1g	1.1	33.63	-31.2	25.08	-22.49
ST20	Wnb1,3g	0.08	21.2	-16.5	21.16	-16.28
ST21	EQ1,3g	1.3	42.86	-37.63	30.58	-25.99

ST22	**Wnb1,3g(2)**	0.08	21.66	-16.76	21.08	-16.34
ST23	**EQ1,3g(2)**	1.3	43.19	-46.5	28.24	-28.77
ST24	**Wnb 1,4g**	0.08	22.45	-16.88	21.54	-15.82
ST25	**EQ1,4g**	1.4	55.62	-59.12	34.42	-35.7
ST26	**Wnb0,2g (2)**	0.08	23.58	-21.36	21.09	-16.44
ST27	**EQ0,2g (2)**	0.2	12.25	-11.08	4.44	-4.13
ST28	**Wna0,2g**	0.08	23.7	-22.14	21.03	-16.46

Table 3.1.1h Summary of results (continued)

		Intensity (g)	max(mean (W1,W2) - mean (W3,W4)) (mm)	min(mean (W1,W2) - mean (W3,W4)) (mm)
ST1	**Wnb0,07g (without)**	0.05	0.62	-0.75
ST2	**Wnb0,07g**	0.05	0.8	-0.84
ST3	**EQ0,07g**	0.07	0.81	-0.96
ST4	**EQ0,1g**	0.1	1.53	-1.21
ST5	**Wnb0,14g**	0.08	1.69	-1.77
ST6	**EQ0,14g**	0.14	1.85	-1.73
ST7	**EQ0,2g**	0.2	2.83	-2.08
ST8	**Wnb0,34g**	0.08	1.63	-1.72
ST9	**EQ0,34g**	0.34	4.46	-5.63
ST10	**Wnb0,5g**	0.08	1.67	-1.71
ST11	**EQ0,5g**	0.5	6.83	-6.48
ST12	**Wnb0,55g**	0.08	1.59	-1.74
ST13	**EQ0,55g**	0.55	7.61	-8.43
ST14	**Wnb0,74g**	0.08	1.73	-1.92
ST15	**EQ0,74g**	0.74	10.27	-10.48
ST16	**Wnb0,8g**	0.08	1.61	-1.71
ST17	**EQ0,8g**	0.8	11.23	-10.98
ST18	**Wnb1,1g**	0.08	2.39	-2.57
ST19	**EQ1,1g**	1.1	14.08	-13.92
ST20	**Wnb1,3g**	0.08	2.35	-2.44
ST21	**EQ1,3g**	1.3	19.76	-20.18

ST22	**Wnb1,3g(2)**	0.08	3.56	-3.94
ST23	**EQ1,3g(2)**	1.3	21.34	-24.64
ST24	**Wnb 1,4g**	0.08	4.66	-6.56
ST25	**EQ1,4g**	1.4	26.56	-32.1
ST26	**Wnb0,2g (2)**	0.08	9.52	-8.25
ST27	**EQ0,2g (2)**	0.2	12.5	-12.01
ST28	**Wna0,2g**	0.08	9.64	-8.71

Table 3.1.1i Summary of results (continued)

		Intensity (g)	max drift (%o)	min drift (%o)	Residual drift (mm)	Residual drift (%o)
ST1	Wnb0,07g (without)	0.05	0.51	-0.61	-0.02	-0.02
ST2	Wnb0,07g	0.05	0.65	-0.69	0.00	0.00
ST3	EQ0,07g	0.07	0.66	-0.78	0.03	0.02
ST4	EQ0,1g	0.1	1.25	-0.99	0.01	0.01
ST5	Wnb0,14g	0.08	1.38	-1.44	-0.01	-0.01
ST6	EQ0,14g	0.14	1.51	-1.41	0.01	0.01
ST7	EQ0,2g	0.2	2.31	-1.70	0.02	0.02
ST8	Wnb0,34g	0.08	1.33	-1.40	-0.02	-0.02
ST9	EQ0,34g	0.34	3.64	-4.60	-0.05	-0.04
ST10	Wnb0,5g	0.08	1.36	-1.40	-0.02	-0.02
ST11	EQ0,5g	0.5	5.58	-5.29	-0.01	-0.01
ST12	Wnb0,55g	0.08	1.30	-1.42	0.02	0.02
ST13	EQ0,55g	0.55	6.21	-6.88	-0.08	-0.07
ST14	Wnb0,74g	0.08	1.41	-1.57	-0.01	-0.01
ST15	EQ0,74g	0.74	8.38	-8.56	-0.18	-0.15
ST16	Wnb0,8g	0.08	1.31	-1.40	0.02	0.02
ST17	EQ0,8g	0.8	9.17	-8.96	-0.06	-0.05
ST18	Wnb1,1g	0.08	1.95	-2.10	-0.03	-0.02
ST19	EQ1,1g	1.1	11.49	-11.36	-0.02	-0.02
ST20	Wnb1,3g	0.08	1.92	-1.99	0.02	0.02
ST21	EQ1,3g	1.3	16.13	-16.47	0.25	0.20
ST22	Wnb1,3g(2)	0.08	2.91	-3.22	-0.15	-0.12

ST23	**EQ1,3g(2)**	1.3	17.42	-20.11	-1.10	-0.90
ST24	**Wnb 1,4g**	0.08	3.80	-5.36	-0.80	-0.65
ST25	**EQ1,4g**	1.4	21.68	-26.20	-2.37	-1.93
ST26	**Wnb0,2g (2)**	0.08	7.77	-6.73	0.00	0.00
ST27	**EQ0,2g (2)**	0.2	10.20	-9.80	-0.16	-0.13
ST28	**Wna0,2g**	0.08	7.87	-7.11	-0.02	-0.02

Table 3.1.1j Summary of results (continued)

		Intensity (g)	max SG1 (ustrain)	min SG1 (ustrain)	Residual SG1	max SG2 (ustrain)	min SG2 (ustrain)	Residual SG2
ST1	**Wnb0,07g (without)**	0.05	58	-48	2	19	-30	-5
ST2	**Wnb0,07g**	0.05	57	-57	0	21	-15	3
ST3	**EQ0,07g**	0.07	64	-53	5	16	-26	-5
ST4	**EQ0,1g**	0.1	81	-90	4	19	-24	-6
ST5	**Wnb0,14g**	0.08	118	-94	-1	26	-25	-2
ST6	**EQ0,14g**	0.14	116	-105	-1	27	-26	-1
ST7	**EQ0,2g**	0.2	140	-146	1	32	-20	-3
ST8	**Wnb0,34g**	0.08	116	-91	0	27	-23	-3
ST9	**EQ0,34g**	0.34	391	-195	-2	72	-23	-5
ST10	**Wnb0,5g**	0.08	108	-103	-7	31	-29	1
ST11	**EQ0,5g**	0.5	473	-197	3	206	-24	-7
ST12	**Wnb0,55g**	0.08	110	-105	-6	32	-26	3
ST13	**EQ0,55g**	0.55	648	-207	8	263	-22	-2
ST14	**Wnb0,74g**	0.08	116	-106	-6	35	-27	-4
ST15	**EQ0,74g**	0.74	866	-249	-7	431	-31	-5
ST16	**Wnb0,8g**	0.08	114	-91	1	30	-20	2
ST17	**EQ0,8g**	0.8	962	-242	1	510	-21	0
ST18	**Wnb1,1g**	0.08	167	-131	1	41	-21	4
ST19	**EQ1,1g**	1.1	1218	-287	15	781	-43	-6
ST20	**Wnb1,3g**	0.08	178	-144	2	37	-27	-4
ST21	**EQ1,3g**	1.3	1280	-749	-254	1242	-40	44

ST22	**Wnb1,3g(2)**	0.08	214	-193	-7	88	-15	1
ST23	**EQ1,3g(2)**	1.3	1466	-615	-43	1334	-22	24
ST24	**Wnb 1,4g**	0.08	255	-205	-8	161	-32	3
ST25	**EQ1,4g**	1.4	1739	-640	436	1336	-142	2
ST26	**Wnb0,2g (2)**	0.08	105	-166	-22	265	-113	3
ST27	**EQ0,2g (2)**	0.2	202	-150	54	430	-149	-2
ST28	**Wna0,2g**	0.08	152	-150	12	276	-137	1

Table 3.1.1k Summary of results (continued)

		Intensity (g)	max SG3 (ustrain)	min SG3 (ustrain)	Residual SG3	max SG4 (ustrain)	min SG4 (ustrain)	Residual SG4
ST1	**Wnb0,07g (without)**	0.05	28	-18	5	48	-48	3
ST2	**Wnb0,07g**	0.05	25	-19	1	66	-59	0
ST3	**EQ0,07g**	0.07	29	-19	-2	71	-56	-5
ST4	**EQ0,1g**	0.1	18	-22	2	127	-66	6
ST5	**Wnb0,14g**	0.08	23	-23	0	128	-108	-7
ST6	**EQ0,14g**	0.14	30	-19	0	142	-96	-1
ST7	**EQ0,2g**	0.2	37	-24	-2	223	-121	2
ST8	**Wnb0,34g**	0.08	35	-20	-3	123	-95	2
ST9	**EQ0,34g**	0.34	63	-29	-7	365	-238	-4
ST10	**Wnb0,5g**	0.08	21	-22	-4	133	-94	3
ST11	**EQ0,5g**	0.5	109	-32	-2	532	-247	-3
ST12	**Wnb0,55g**	0.08	24	-24	-1	125	-89	3
ST13	**EQ0,55g**	0.55	178	-20	2	575	-286	-9
ST14	**Wnb0,74g**	0.08	30	-18	2	130	-97	2
ST15	**EQ0,74g**	0.74	301	-54	-11	819	-321	-5
ST16	**Wnb0,8g**	0.08	34	-30	2	94	-99	-10
ST17	**EQ0,8g**	0.8	378	-54	-11	880	-321	-3
ST18	**Wnb1,1g**	0.08	23	-26	0	162	-125	3
ST19	**EQ1,1g**	1.1	554	-46	5	1217	-399	-37
ST20	**Wnb1,3g**	0.08	22	-24	-4	144	-108	-9
ST21	**EQ1,3g**	1.3	1140	-54	42	1399	-553	-37

ST22	**Wnb1,3g(2)**	0.08	84	-17	4	177	-133	2
ST23	**EQ1,3g(2)**	1.3	1567	-53	156	1592	-454	138
ST24	**Wnb 1,4g**	0.08	198	-82	-3	196	-183	0
ST25	**EQ1,4g**	1.4	1532	-373	14	1908	-408	279
ST26	**Wnb0,2g (2)**	0.08	253	-237	4	342	-249	5
ST27	**EQ0,2g (2)**	0.2	374	-300	-4	482	-297	-9
ST28	**Wna0,2g**	0.08	274	-178	5	309	-226	-2

Table 3.1.1l Summary of results (continued)

		Intensity (g)	max SG5 (ustrain)	min SG5 (ustrain)	Residual SG5	max SG6 (ustrain)	min SG6 (ustrain)	Residual SG6
ST1	**Wnb0,07g (without)**	0.05	120	-119	2	55	-45	2
ST2	**Wnb0,07g**	0.05	128	-121	2	42	-38	1
ST3	**EQ0,07g**	0.07	103	-134	-1	42	-49	0
ST4	**EQ0,1g**	0.1	165	-205	-1	56	-70	1
ST5	**Wnb0,14g**	0.08	254	-229	5	86	-72	2
ST6	**EQ0,14g**	0.14	248	-257	-2	79	-76	0
ST7	**EQ0,2g**	0.2	318	-343	-6	95	-77	1
ST8	**Wnb0,34g**	0.08	235	-215	1	81	-74	0
ST9	**EQ0,34g**	0.34	857	-481	3	263	-77	34
ST10	**Wnb0,5g**	0.08	242	-223	1	76	-68	-2
ST11	**EQ0,5g**	0.5	1026	-503	1	545	-68	24
ST12	**Wnb0,55g**	0.08	232	-213	0	75	-57	1
ST13	**EQ0,55g**	0.55	1507	-556	10	716	-77	-16
ST14	**Wnb0,74g**	0.08	267	-242	1	80	-59	0
ST15	**EQ0,74g**	0.74	1773	-639	24	991	-69	7
ST16	**Wnb0,8g**	0.08	249	-235	-1	71	-53	1
ST17	**EQ0,8g**	0.8	1997	-675	6	1120	-66	8
ST18	**Wnb1,1g**	0.08	395	-327	1	90	-61	-2
ST19	**EQ1,1g**	1.1	2656	-735	-29	13832	-48	8637
ST20	**Wnb1,3g**	0.08	343	-287	-1	68	-32	-4
ST21	**EQ1,3g**	1.3	2693	-1539	-534	523	-11803	-8535

ST22	**Wnb1,3g(2)**	0.08	393	-249	2	150	-28	22
ST23	**EQ1,3g(2)**	1.3	3511	-1222	58	10919	-8657	-7139
ST24	**Wnb 1,4g**	0.08	564	-481	2	301	-40	-6
ST25	**EQ1,4g**	1.4	3887	-1302	195	11843	-7802	-4448
ST26	**Wnb0,2g (2)**	0.08	764	-775	3	588	-200	6
ST27	**EQ0,2g (2)**	0.2	1074	-926	-14	743	-259	-29
ST28	**Wna0,2g**	0.08	753	-709	2	586	-214	-7

Table 3.1.1m Summary of results (continued)

		Intensity (g)	max SG7 (ustrain)	min SG7 (ustrain)	Residual SG7	max SG8 (ustrain)	min SG8 (ustrain)	Residual SG8
ST1	**Wnb0,07g (without)**	0.05	23	-27	-3	64	-55	-2
ST2	**Wnb0,07g**	0.05	23	-23	-2	58	-79	-3
ST3	**EQ0,07g**	0.07	25	-29	1	64	-58	1
ST4	**EQ0,1g**	0.1	26	-21	-1	117	-73	2
ST5	**Wnb0,14g**	0.08	25	-25	-4	128	-118	-3
ST6	**EQ0,14g**	0.14	30	-25	-3	147	-111	-5
ST7	**EQ0,2g**	0.2	32	-24	-1	211	-139	-3
ST8	**Wnb0,34g**	0.08	27	-22	2	120	-113	0
ST9	**EQ0,34g**	0.34	65	-37	-12	370	-265	-10
ST10	**Wnb0,5g**	0.08	31	-21	-1	125	-111	0
ST11	**EQ0,5g**	0.5	139	-28	-10	542	-256	0
ST12	**Wnb0,55g**	0.08	27	-20	0	112	-102	6
ST13	**EQ0,55g**	0.55	253	-31	-5	618	-267	-6
ST14	**Wnb0,74g**	0.08	32	-25	-6	121	-109	-10
ST15	**EQ0,74g**	0.74	346	-50	-4	841	-304	-21
ST16	**Wnb0,8g**	0.08	33	-17	1	116	-101	5
ST17	**EQ0,8g**	0.8	404	-46	0	938	-298	-12
ST18	**Wnb1,1g**	0.08	24	-20	-2	161	-140	-3
ST19	**EQ1,1g**	1.1	601	-45	-12	1159	-292	4
ST20	**Wnb1,3g**	0.08	34	-23	3	164	-130	6
ST21	**EQ1,3g**	1.3	1230	-33	66	1393	-504	-117

ST22	**Wnb1,3g(2)**	0.08	114	-43	-10	181	-185	7
ST23	**EQ1,3g(2)**	1.3	1430	-111	124	1458	-390	-17
ST24	**Wnb 1,4g**	0.08	132	-135	-11	182	-193	-6
ST25	**EQ1,4g**	1.4	1260	-500	-240	1454	-430	31
ST26	**Wnb0,2g (2)**	0.08	132	-198	-21	304	-228	0
ST27	**EQ0,2g (2)**	0.2	268	-190	36	444	-305	-6
ST28	**Wna0,2g**	0.08	158	-196	5	306	-282	-1

Table 3.1.1n Summary of results (continued)

		Intensity (g)	max SG9 (ustrain)	min SG9 (ustrain)	Residual SG9	max SG11 (ustrain)	min SG11 (ustrain)	Residual SG11
ST1	**Wnb0,07g (without)**	0.05	86	-47	0	48	-45	7
ST2	**Wnb0,07g**	0.05	42	-26	-3	52	-51	2
ST3	**EQ0,07g**	0.07	52	-25	-2	51	-52	1
ST4	**EQ0,1g**	0.1	135	-26	-2	88	-67	-6
ST5	**Wnb0,14g**	0.08	150	-32	-4	101	-97	-6
ST6	**EQ0,14g**	0.14	182	-30	-3	106	-94	2
ST7	**EQ0,2g**	0.2	307	-35	-4	170	-105	-4
ST8	**Wnb0,34g**	0.08	132	-26	1	87	-92	-3
ST9	**EQ0,34g**	0.34	552	-44	-13	300	-163	-2
ST10	**Wnb0,5g**	0.08	139	-20	0	84	-85	9
ST11	**EQ0,5g**	0.5	884	-56	-15	434	-160	-2
ST12	**Wnb0,55g**	0.08	133	-18	1	76	-86	0
ST13	**EQ0,55g**	0.55	1073	-33	-10	516	-161	-6
ST14	**Wnb0,74g**	0.08	160	-20	0	91	-89	5
ST15	**EQ0,74g**	0.74	1333	-75	-62	711	-157	-10
ST16	**Wnb0,8g**	0.08	119	-6	1	73	-93	-5
ST17	**EQ0,8g**	0.8	1513	-20	-13	789	-153	0
ST18	**Wnb1,1g**	0.08	195	-7	0	107	-113	-5
ST19	**EQ1,1g**	1.1	1906	-78	-22	995	-157	20

ST20	**Wnb1,3g**	0.08	214	-36	0	113	-118	-3
ST21	**EQ1,3g**	1.3	2251	-742	-164	1203	-453	-153
ST22	**Wnb1,3g(2)**	0.08	245	-189	0	217	-202	1
ST23	**EQ1,3g(2)**	1.3	2673	-350	4	1341	-292	32
ST24	**Wnb 1,4g**	0.08	338	-232	-2	214	-227	-1
ST25	**EQ1,4g**	1.4	3042	-483	-98	1275	-463	-53
ST26	**Wnb0,2g (2)**	0.08	624	-383	-1	317	-289	4
ST27	**EQ0,2g (2)**	0.2	752	-419	-18	486	-408	-3
ST28	**Wna0,2g**	0.08	560	-403	-3	367	-354	2

Table 3.1.1o Summary of results (continued)

		Intensity (g)	max SG12 (ustrain)	min SG12 (ustrain)	Residual SG12	max SG13 (ustrain)	min SG13 (ustrain)	Residual SG13
ST1	**Wnb0,07g (without)**	0.05	19	-34	-11	23	-18	1
ST2	**Wnb0,07g**	0.05	29	-24	-1	29	-19	2
ST3	**EQ0,07g**	0.07	29	-28	-5	35	-22	-2
ST4	**EQ0,1g**	0.1	44	-30	-3	69	-21	-3
ST5	**Wnb0,14g**	0.08	48	-28	1	81	-23	-1
ST6	**EQ0,14g**	0.14	43	-34	-7	87	-23	-3
ST7	**EQ0,2g**	0.2	67	-34	1	153	-28	0
ST8	**Wnb0,34g**	0.08	47	-31	-3	82	-19	0
ST9	**EQ0,34g**	0.34	122	-31	-3	282	-35	-1
ST10	**Wnb0,5g**	0.08	46	-24	-3	74	-17	6
ST11	**EQ0,5g**	0.5	187	-36	-6	448	-44	-3
ST12	**Wnb0,55g**	0.08	44	-24	1	75	-19	2
ST13	**EQ0,55g**	0.55	310	-28	-4	502	-34	-3
ST14	**Wnb0,74g**	0.08	52	-29	0	77	-22	1
ST15	**EQ0,74g**	0.74	409	-27	-9	717	-45	0
ST16	**Wnb0,8g**	0.08	43	-19	-1	61	-21	4
ST17	**EQ0,8g**	0.8	486	-29	3	799	-37	7
ST18	**Wnb1,1g**	0.08	58	-18	-1	105	-22	-5
ST19	**EQ1,1g**	1.1	100	-37	-19	1107	-50	-14
ST20	**Wnb1,3g**	0.08	60	-20	2	87	-20	0
ST21	**EQ1,3g**	1.3	1267	-38	73	1313	-334	-42

ST22	**Wnb1,3g(2)**	0.08	136	-32	1	147	-133	-7
ST23	**EQ1,3g(2)**	1.3	1290	-269	-72	1331	-252	-16
ST24	**Wnb 1,4g**	0.08	177	-132	-6	156	-137	-3
ST25	**EQ1,4g**	1.4	1330	-445	0	1229	-294	-50
ST26	**Wnb0,2g (2)**	0.08	234	-201	-3	240	-142	-3
ST27	**EQ0,2g (2)**	0.2	413	-334	0	384	-266	1
ST28	**Wna0,2g**	0.08	284	-255	-7	280	-206	0

Table 3.1.1p Summary of results (continued)

		Intensity (g)	max SG14 (ustrain)	min SG14 (ustrain)	Residual SG14	max SG15 (ustrain)	min SG15 (ustrain)	Residual SG15
ST1	**Wnb0,07g (without)**	0.05	45	-47	-6	46	-43	1
ST2	**Wnb0,07g**	0.05	54	-53	-12	61	-48	5
ST3	**EQ0,07g**	0.07	65	-45	-7	61	-56	-1
ST4	**EQ0,1g**	0.1	67	-56	-3	107	-69	1
ST5	**Wnb0,14g**	0.08	101	-70	-6	119	-108	-5
ST6	**EQ0,14g**	0.14	100	-63	3	119	-92	3
ST7	**EQ0,2g**	0.2	119	-71	-3	192	-113	-6
ST8	**Wnb0,34g**	0.08	95	-74	-2	108	-90	-1
ST9	**EQ0,34g**	0.34	342	-92	-6	329	-201	1
ST10	**Wnb0,5g**	0.08	101	-69	-1	100	-96	-3
ST11	**EQ0,5g**	0.5	419	-85	9	500	-199	-3
ST12	**Wnb0,55g**	0.08	106	-69	1	91	-94	-4
ST13	**EQ0,55g**	0.55	570	-92	0	538	-210	-7
ST14	**Wnb0,74g**	0.08	109	-82	-4	100	-96	-1
ST15	**EQ0,74g**	0.74	773	-110	-3	788	-255	-10
ST16	**Wnb0,8g**	0.08	106	-60	8	90	-78	3
ST17	**EQ0,8g**	0.8	859	-104	1	879	-244	0
ST18	**Wnb1,1g**	0.08	141	-100	-7	135	-105	3
ST19	**EQ1,1g**	1.1	1072	-126	20	1501	-237	340
ST20	**Wnb1,3g**	0.08	137	-101	2	109	-123	1
ST21	**EQ1,3g**	1.3	1374	-300	-81	3230	-296	1083

ST22	**Wnb1,3g(2)**	0.08	180	-143	6	128	-147	-6
ST23	**EQ1,3g(2)**	1.3	1398	-471	12	1406	-361	174
ST24	**Wnb 1,4g**	0.08	220	-194	-2	137	-204	-17
ST25	**EQ1,4g**	1.4	1299	-767	-14	1279	-283	105
ST26	**Wnb0,2g (2)**	0.08	292	-288	-2	164	-226	-21
ST27	**EQ0,2g (2)**	0.2	420	-460	5	206	-257	-30
ST28	**Wna0,2g**	0.08	301	-356	-2	164	-216	-15

Table 3.1.1q Summary of results (continued)

		Intensity (g)	max SG16 (ustrain)	min SG16 (ustrain)	Residual SG16	max SG17 (ustrain)	min SG17 (ustrain)	Residual SG17
ST1	**Wnb0,07g (without)**	0.05	28	-17	5	23	-21	1
ST2	**Wnb0,07g**	0.05	22	-21	5	25	-20	3
ST3	**EQ0,07g**	0.07	22	-25	-3	22	-19	-2
ST4	**EQ0,1g**	0.1	28	-23	-4	20	-22	3
ST5	**Wnb0,14g**	0.08	45	-21	4	20	-25	-8
ST6	**EQ0,14g**	0.14	46	-18	4	20	-19	4
ST7	**EQ0,2g**	0.2	48	-23	-2	18	-27	-2
ST8	**Wnb0,34g**	0.08	40	-22	-1	17	-20	-3
ST9	**EQ0,34g**	0.34	241	-28	-3	15	-23	-5
ST10	**Wnb0,5g**	0.08	48	-26	-5	23	-21	2
ST11	**EQ0,5g**	0.5	280	-58	-4	19	-21	2
ST12	**Wnb0,55g**	0.08	48	-23	-3	22	-16	3
ST13	**EQ0,55g**	0.55	352	-51	-9	23	-27	4
ST14	**Wnb0,74g**	0.08	54	-26	1	20	-17	-4
ST15	**EQ0,74g**	0.74	493	-48	-1	23	-29	0
ST16	**Wnb0,8g**	0.08	47	-29	-1	16	-26	-4
ST17	**EQ0,8g**	0.8	557	-47	0	24	-29	-3
ST18	**Wnb1,1g**	0.08	78	-27	-2	16	-24	-6
ST19	**EQ1,1g**	1.1	687	-48	22	33	-35	0
ST20	**Wnb1,3g**	0.08	105	-39	-5	33	-22	0
ST21	**EQ1,3g**	1.3	1317	-77	112	21	-33	-1

ST22	**Wnb1,3g(2)**	0.08	151	-121	9	28	-25	0
ST23	**EQ1,3g(2)**	1.3	1498	-306	19	38	-21	6
ST24	**Wnb 1,4g**	0.08	210	-211	1	18	-26	-6
ST25	**EQ1,4g**	1.4	2605	-500	1415	28	-17	6
ST26	**Wnb0,2g (2)**	0.08	196	-182	-5	21	-37	-2
ST27	**EQ0,2g (2)**	0.2	280	-213	0	24	-19	-4
ST28	**Wna0,2g**	0.08	213	-156	13	21	-20	1

Table 3.1.1r Summary of results (continued)

		Intensity (g)	max SG18 (ustrain)	min SG18 (ustrain)	Residual SG18	max SG20 (ustrain)	min SG20 (ustrain)	Residual SG20
ST1	**Wnb0,07g (without)**	0.05	19	-19	0	31	-35	2
ST2	**Wnb0,07g**	0.05	22	-15	2	20	-17	1
ST3	**EQ0,07g**	0.07	16	-23	-4	20	-20	0
ST4	**EQ0,1g**	0.1	25	-20	2	36	-30	1
ST5	**Wnb0,14g**	0.08	21	-22	-4	40	-44	1
ST6	**EQ0,14g**	0.14	22	-17	0	44	-43	1
ST7	**EQ0,2g**	0.2	16	-28	-2	60	-55	2
ST8	**Wnb0,34g**	0.08	22	-21	2	37	-40	0
ST9	**EQ0,34g**	0.34	24	-34	-2	81	-121	6
ST10	**Wnb0,5g**	0.08	23	-28	0	36	-37	0
ST11	**EQ0,5g**	0.5	27	-41	-2	76	-128	2
ST12	**Wnb0,55g**	0.08	20	-23	1	34	-33	0
ST13	**EQ0,55g**	0.55	29	-53	1	78	-149	12
ST14	**Wnb0,74g**	0.08	20	-23	-2	30	-31	0
ST15	**EQ0,74g**	0.74	28	-57	5	62	-125	29
ST16	**Wnb0,8g**	0.08	21	-24	-3	9	-11	0
ST17	**EQ0,8g**	0.8	28	-56	6	35	-62	5
ST18	**Wnb1,1g**	0.08	24	-18	2	9	-14	1
ST19	**EQ1,1g**	1.1	32	-55	8	28	-75	26
ST20	**Wnb1,3g**	0.08	24	-17	5	2	-6	0
ST21	**EQ1,3g**	1.3	21	-68	3	37	-73	33

ST22	**Wnb1,3g(2)**	0.08	17	-19	1	7	-20	0
ST23	**EQ1,3g(2)**	1.3	18	-58	-4	11	-82	0
ST24	**Wnb 1,4g**	0.08	16	-24	-1	11	-32	0
ST25	**EQ1,4g**	1.4	27	-62	1	15	-75	5
ST26	**Wnb0,2g (2)**	0.08	23	-23	6	9	-33	1
ST27	**EQ0,2g (2)**	0.2	30	-15	6	11	-46	1
ST28	**Wna0,2g**	0.08	24	-22	7	15	-39	0

Table 3.1.1s Summary of results (continued)

		Intensity (g)	max SG21 (ustrain)	min SG21 (ustrain)	Residual SG21	max SG22 (ustrain)	min SG22 (ustrain)	Residual SG22
ST1	**Wnb0,07g (without)**	0.05	49	-39	12	56	-48	0
ST2	**Wnb0,07g**	0.05	24	-18	0	36	-38	0
ST3	**EQ0,07g**	0.07	29	-27	-1	45	-51	1
ST4	**EQ0,1g**	0.1	40	-69	0	80	-63	1
ST5	**Wnb0,14g**	0.08	66	-84	2	89	-97	0
ST6	**EQ0,14g**	0.14	64	-97	-2	101	-96	-1
ST7	**EQ0,2g**	0.2	77	-151	-2	147	-121	-2
ST8	**Wnb0,34g**	0.08	60	-82	-1	81	-90	0
ST9	**EQ0,34g**	0.34	133	-227	-18	245	-276	-5
ST10	**Wnb0,5g**	0.08	58	-65	-2	84	-86	0
ST11	**EQ0,5g**	0.5	122	-255	-3	318	-301	-4
ST12	**Wnb0,55g**	0.08	52	-48	0	83	-84	1
ST13	**EQ0,55g**	0.55	201	-265	-10	355	-375	0
ST14	**Wnb0,74g**	0.08	55	-50	-1	92	-92	-1
ST15	**EQ0,74g**	0.74	212	-336	-22	447	-384	-1
ST16	**Wnb0,8g**	0.08	39	-42	-2	73	-83	0
ST17	**EQ0,8g**	0.8	296	-261	18	461	388	-2
ST18	**Wnb1,1g**	0.08	55	-52	-1	105	-119	1
ST19	**EQ1,1g**	1.1	304	-358	9	563	-414	7
ST20	**Wnb1,3g**	0.08	60	-73	0	101	-86	0
ST21	**EQ1,3g**	1.3	677	-444	-2	735	-218	-10
ST22	**Wnb1,3g(2)**	0.08	116	-103	-1	117	-89	-2
ST23	**EQ1,3g(2)**	1.3	868	-339	22	670	-175	-53

ST24	**Wnb 1,4g**	0.08	158	-148	1	81	-117	2
ST25	**EQ1,4g**	1.4	1173	-485	36	803	-126	49
ST26	**Wnb0,2g (2)**	0.08	246	-219	0	19	-90	3
ST27	**EQ0,2g (2)**	0.2	348	-292	-2	23	-71	-14
ST28	**Wna0,2g**	0.08	239	-216	-2	20	-67	-2

Table 3.1.1t Summary of results (continued)

		Intensity (g)	max SG23 (ustrain)	min SG23 (ustrain)	Residual SG23	max SG24 (ustrain)	min SG24 (ustrain)	Residual SG24
ST1	**Wnb0,07g (without)**	0.05						
ST2	**Wnb0,07g**	0.05						
ST3	**EQ0,07g**	0.07						
ST4	**EQ0,1g**	0.1						
ST5	**Wnb0,14g**	0.08						
ST6	**EQ0,14g**	0.14						
ST7	**EQ0,2g**	0.2						
ST8	**Wnb0,34g**	0.08						
ST9	**EQ0,34g**	0.34						
ST10	**Wnb0,5g**	0.08						
ST11	**EQ0,5g**	0.5	23	-23	-5	24	-16	1
ST12	**Wnb0,55g**	0.08	24	-28	-2	13	-18	-3
ST13	**EQ0,55g**	0.55	32	-15	1	17	-29	-7
ST14	**Wnb0,74g**	0.08	13	-24	-5	17	-17	-2
ST15	**EQ0,74g**	0.74	33	-20	-6	30	-27	7
ST16	**Wnb0,8g**	0.08	26	-16	3	15	-15	-1
ST17	**EQ0,8g**	0.8	34	-23	2	37	-24	11
ST18	**Wnb1,1g**	0.08	23	-14	7	20	-11	9
ST19	**EQ1,1g**	1.1	46	-21	-5	31	-40	-3
ST20	**Wnb1,3g**	0.08	11	-25	-5	19	-13	0
ST21	**EQ1,3g**	1.3	57	-18	-5	39	-32	2
ST22	**Wnb1,3g(2)**	0.08	16	-22	-1	19	-13	5
ST23	**EQ1,3g(2)**	1.3	54	-19	-1	44	-24	15

ST24	**Wnb 1,4g**	0.08	17	-23	-5	16	-16	0
ST25	**EQ1,4g**	1.4	58	-20	-1	32	-40	6
ST26	**Wnb0,2g (2)**	0.08	7	-33	-4	22	-11	-3
ST27	**EQ0,2g (2)**	0.2	10	-26	-1	12	-24	-6
ST28	**Wna0,2g**	0.08	21	-15	4	19	-24	-2

Table 3.1.1u Summary of results (continued)

			max(Acc1+Acc4)/2	min(Acc1+Acc4)/2	max((Acc1+Acc4)/2-Acc10) (g)	min((Acc1+Acc4)/2-Acc10) (g)	Δt (14-10) (sec)
		Intensity (g)					
ST1	**Wnb0,07g (without)**	0.05	0.07	-0.07	0.07	-0.08	15.85
ST2	**Wnb0,07g**	0.05	0.09	-0.08	0.08	-0.08	1.82
ST3	**EQ0,07g**	0.07	0.12	-0.09	0.1	-0.09	0.15
ST4	**EQ0,1g**	0.1	0.18	-0.11	0.15	-0.11	0.66
ST5	**Wnb0,14g**	0.08	0.2	-0.19	0.19	-0.18	-0.08
ST6	**EQ0,14g**	0.14	0.22	-0.17	0.18	-0.2	-3.64
ST7	**EQ0,2g**	0.2	0.34	-0.22	0.3	-0.27	0.04
ST8	**Wnb0,34g**	0.08	0.18	-0.17	0.17	-0.71	-0.08
ST9	**EQ0,34g**	0.34	0.53	-0.52	0.51	-0.64	0.13
ST10	**Wnb0,5g**	0.08	0.17	-0.17	0.17	-0.17	0.04
ST11	**EQ0,5g**	0.5	0.77	-0.68	0.8	-0.72	0.05
ST12	**Wnb0,55g**	0.08	0.18	-0.18	0.15	-0.21	2.38
ST13	**EQ0,55g**	0.55	0.91	-0.87	0.91	-0.87	-0.86
ST14	**Wnb0,74g**	0.08	0.19	-0.18	0.18	-0.2	8.08
ST15	**EQ0,74g**	0.74	1.23	-1.33	1.21	-1.2	-0.62
ST16	**Wnb0,8g**	0.08	0.15	-0.15	0.16	-0.19	2.96
ST17	**EQ0,8g**	0.8	1.31	-1.2	1.29	-1.29	-0.86
ST18	**Wnb1,1g**	0.08	0.2	-0.21	0.2	-0.22	0.81
ST19	**EQ1,1g**	1.1	1.66	-1.4	2.12	-1.71	-4.39
ST20	**Wnb1,3g**	0.08	0.17	-0.18	0.15	-0.17	0.56
ST21	**EQ1,3g**	1.3					
ST22	**Wnb1,3g(2)**	0.08					

ST23	**EQ1,3g(2)**	1.3	1.8	-1.8	2.65	-3.25	0.66
ST24	**Wnb 1,4g**	0.08	0.16	-0.19	0.17	-0.2	1.29
ST25	**EQ1,4g**	1.4	1.75	-1.8	3.74	-3.79	-2.88
ST26	**Wnb0,2g (2)**	0.08	0.19	-0.16	0.2	-0.18	7.49
ST27	**EQ0,2g (2)**	0.2	0.33	-0.37	0.43	-0.42	0.91
ST28	**Wna0,2g**	0.08	0.2	-0.18	0.2	-0.19	6.95

Table 3.1.1v Summary of results (continued)

		Intensity (g)	Planters
ST1	**Wnb0,07g (without)**	0.05	Slight rocking of planter 5.
ST2	**Wnb0,07g**	0.05	Slight rocking of planter 5.
ST3	**EQ0,07g**	0.07	Slight rocking of planter 5.
ST4	**EQ0,1g**	0.1	Slight rocking of planter 5.
ST5	**Wnb0,14g**	0.08	Slight rocking of planter 5.
ST6	**EQ0,14g**	0.14	Slight rocking of planter 2 and 5.
ST7	**EQ0,2g**	0.2	Slight rocking of planter 2 and 5.
ST8	**Wnb0,34g**	0.08	Slight rocking of planter 2 and 5.
ST9	**EQ0,34g**	0.34	Planter 2 basalt rope loosening were observed, then it was tightened. Rocking of planter 2, 3, 4 and 5.
ST10	**Wnb0,5g**	0.08	Slight rocking of planter 2 and 5.
ST11	**EQ0,5g**	0.5	Rocking of planter 2, 3, 4 and 5. Micro-displacement of planter 4.
ST12	**Wnb0,55g**	0.08	Slight rocking of planter 2, 5 and 4.
ST13	**EQ0,55g**	0.55	Planter 3 displacement of prestressing device was noticed and it was tightened again. Rocking of planter 2, 3, 4 and 5. Micro-displacement of planter 4.
ST14	**Wnb0,74g**	0.08	Slight rocking of planter 2, 5 and 4.
ST15	**EQ0,74g**	0.74	Fracture of the basalt rope of planter 3. Basalt rope loosening of planters 2,5 and tightened again. Intense rocking of planter 2, 3, 4 and 5. Micro-displacement of planter 4.
ST16	**Wnb0,8g**	0.08	Slight rocking of planter 2,4, 5.
ST17	**EQ0,8g**	0.8	Rocking of planter 4 leading to micro displacement of the PM pads and of the planter itself. Planter 3 basalt rope was loosening. Intense rocking of planter 2, 3, 4 and 5.
ST18	**Wnb1,1g**	0.08	Rocking of planter 5, 4, 3 ,2.
ST19	**EQ1,1g**	1.1	Rocking of planter 4 leading to micro displacement of the PM pads and of the planter itself. Fracture of the one basalt rope of planter 3. Displacement of

			prestressing devices of planter 2 and 5 and loosening of basalt ropes. Intense rocking of planter 2, 3, 4, 5 and rocking of planter 1.
ST20	**Wnb1,3g**	0.08	Rocking of planter 5,4,3,2.
ST21	**EQ1,3g**	1.3	Rocking of planter 4 leading to displacement (+-3 cm) of the PM pads and of the planter itself. Planter 1 showed bottom micro displacements because of slight loosening of the steel rod. Fracture of the one basalt rope of planter 2. Planters 2,3 and 5 showed bottom displacements. Intense rocking of all planters.
ST22	**Wnb1,3g(2)**	0.08	Rocking of planter 4 and 5.
ST23	**EQ1,3g(2)**	1.3	Rocking of planter 4 leading to displacement (+-3 cm) of the PM pads and of the planter itself. Fracture of basalt rope of planter 3. Fracture of both basalt ropes of planter 5. Displacement of prestressing device of planter 2. Intense rocking of all planters.
ST24	**Wnb 1,4g**	0.08	Rocking of planter 4,5,2,3.
ST25	**EQ1,4g**	1.4	Rocking of planter 4 leading to displacement (+-4 cm) of the PM pads and of the planter itself. Planter 1 showed bottom micro displacements because of slight loosening of the steel rod. Fracture of the one basalt rope of planter 3. Planter 5 and 2 showed bottom micro displacements. Intense rocking of all planters.
ST26	**Wnb0,2g (2)**	0.08	Rocking of all planters.
ST27	**EQ0,2g (2)**	0.2	Rocking of all planters.
ST28	**Wna0,2g**	0.08	Rocking of all planters.

Table 3.1.1w Summary of results (continued)

		Intensity (g)	Vertical living walls
ST1	Wnb0,07g (without)	0.05	
ST2	Wnb0,07g	0.05	
ST3	EQ0,07g	0.07	
ST4	EQ0,1g	0.1	
ST5	Wnb0,14g	0.08	
ST6	EQ0,14g	0.14	
ST7	EQ0,2g	0.2	
ST8	Wnb0,34g	0.08	
ST9	EQ0,34g	0.34	Initiation of loosening of basalt rope of LW1-4L and LW3-2L. Initiation of micro loosening of LW1-4R, LW3-2R, LW1-2L and LW1-2R.
ST10	Wnb0,5g	0.08	no change
ST11	EQ0,5g	0.5	no change
ST12	Wnb0,55g	0.08	no change
ST13	EQ0,55g	0.55	no change
ST14	Wnb0,74g	0.08	no change
ST15	EQ0,74g	0.74	no change
ST16	Wnb0,8g	0.08	no change
ST17	EQ0,8g	0.8	no change
ST18	Wnb1,1g	0.08	no change
ST19	EQ1,1g	1.1	Left living wall LW1-4L, showed basalt rope loosening without detachment of PU pads allowing micromovements for high direct horizontal loads (severe wind) but no living wall collapse was observed. Left vertical living wall LW3-2L showed basalt rope loosening without detachment of PU pads

			allowing micromovements for high direct horizontal loads (severe wind) but no living wall collapse was observed.
ST20	**Wnb1,3g**	0.08	no change
ST21	**EQ1,3g**	1.3	Left living wall LW1-4L, showed basalt rope loosening without detachment of PU pads allowing micromovements for low direct horizontal loads (frequent wind) but no living wall collapse was observed. Left vertical living wall LW3-2L showed basalt rope loosening without detachment of PU pads allowing micromovements for low direct horizontal loads (frequent wind) but no living wall collapse was observed.
ST22	**Wnb1,3g(2)**	0.08	no change
ST23	**EQ1,3g(2)**	1.3	Left living wall LW1-4L, showed basalt rope loosening leading to detachment of PU pads allowing micromovements for low direct horizontal loads (frequent wind) but no living wall collapse was observed. Left vertical living wall LW3-2L showed basalt rope loosening leading to detachment of PU pads allowing micromovements for low direct horizontal loads (frequent wind) but no living wall collapse was observed. Steel rod (hemlock) slight loosening at the top of living wall LW3-4R allowing micromovements for low direct horizontal loads (frequent wind) but no living wall collapse was observed.
ST24	**Wnb 1,4g**	0.08	no change
ST25	**EQ1,4g**	1.4	Steel rod or basalt rope loosening (in some cases) at very high accelerations of the structure, no living wall collapse was observed. Left living wall LW4-3L showed the best performance maintaining full capacity, in plane and out of plane (resistant to severe wind). Left living wall LW1-4L, showed basalt rope loosening leading to detachment of PU pads allowing micromovements for low direct horizontal loads (frequent wind) but no living wall collapse was observed. Living walls LW1-2L, LW2-3R, LW1-4R showed slight basalt rope loosening allowing micromovements for high direct horizontal loads (severe wind), but no living wall collapse was observed. Living wall LW1-2R showed basalt rope loosening allowing micromovements for medium direct horizontal loads (intense wind), but no living wall collapse was observed. Left vertical living wall LW2-3L showed basalt rope loosening leading to detachment of PU pads allowing micromovements for low direct horizontal loads (frequent wind) but no living wall collapse was observed. Steel rod (hemlock) slight loosening at the top of living wall LW4-3R allowing micromovements for low direct horizontal loads (frequent wind) but no living wall collapse was observed.

ST26	**Wnb0,2g (2)**	0.08	no change
ST27	**EQ0,2g (2)**	0.2	no change
ST28	**Wna0,2g**	0.08	no change

Table 3.1.1x Summary of results (continued)

		Intensity (g)	Renovated Structure
ST1	Wnb0,07g (without)	0.05	
ST2	Wnb0,07g	0.05	
ST3	EQ0,07g	0.07	
ST4	EQ0,1g	0.1	
ST5	Wnb0,14g	0.08	
ST6	EQ0,14g	0.14	
ST7	EQ0,2g	0.2	
ST8	Wnb0,34g	0.08	
ST9	EQ0,34g	0.34	
ST10	Wnb0,5g	0.08	
ST11	EQ0,5g	0.5	Already formed horizontal cracks opening and closing in brick wall 3-4 without brick wall stiffness reduction.
ST12	Wnb0,55g	0.08	no change
ST13	EQ0,55g	0.55	no change
ST14	Wnb0,74g	0.08	no change
ST15	EQ0,74g	0.74	no change
ST16	Wnb0,8g	0.08	no change
ST17	EQ0,8g	0.8	no change
ST18	Wnb1,1g	0.08	no change
ST19	EQ1,1g	1.1	no change
ST20	Wnb1,3g	0.08	no change
ST21	EQ1,3g	1.3	The columns entered yielding strain of their longitudinal steel reinforcements at the bottom. Damage with crushing of bottom brick at partial infill wall 2-3 and initiation of damage at the bottom brick at partial infill wall 3-4.

ST22	**Wnb1,3g(2)**	0.08	no change
ST23	**EQ1,3g(2)**	1.3	Damage with crushing of bottom brick at both partial infill walls occurred. The columns entered yielding strain of their longitudinal steel reinforcements at the bottom and at the top critical regions (columns 1, 2, 3, 4). PUFJ between concrete columns and brick infills maintained their integrity without fracture or debonding. FRPU jackets maintained their bonding on the PUFJs, on the concrete and on the bricks. No failure of brick infills 1 – 2 and 4 – 3 (out of plane) was observed.
ST24	**Wnb 1,4g**	0.08	no change
ST25	**EQ1,4g**	1.4	Damage with crushing of bottom brick at both partial infill walls occurred at very high displacement drift levels (2,62%). Local fracture of the FRPU jacket at the boundary between the crushed brick and the bottom foundation beam. Additional cracks at some mortar joints between bricks of the partial infill walls at their internal face (side with no FRPU jacket). Columns entered strain hardening of their longitudinal steel reinforcements.
ST26	**Wnb0,2g (2)**	0.08	no change
ST27	**EQ0,2g (2)**	0.2	no change
ST28	**Wna0,2g**	0.08	no change

3.2 Concluding assessment remarks

In table 3.1.1a – 3.1.1.d the maximum accelerations for each excitation are cited. Accelerometer Acc1 is located at the left corner of the slab along the direction x (direction of excitation). Accelerometer Acc4 is located at the right corner of the slab along direction x. Accelerometer Acc7 is located at the center of full infill along x direction. Acc10 is located at the center of foundation along x direction. The ratio between peak top slab and peak foundation acceleration fluctuates 1.75 at white noise before 0.07g (without bottom fixing of the vertical living walls), to 4 at white noise after 0.2g. The ratio between peak top slab and peak foundation seismic acceleration fluctuates 0.85 during ST25 that is EQ1.4g to 2 during ST4, that is EQ0.1g (table 3.1.1d). During ST15 excitation of EQ0.74g, infill wall 3-4 starts to significantly accelerate (1.19g). During ST25 excitation of EQ1.4g, infill wall 3-4 presents the highest out of plane acceleration (2.31g) at its center point. During this excitation EQ1.4g, all accelerometers acc1, acc4, acc7 and acc10 show the maximum values 2.05g, 1.86g, 2.31g and 2.56g respectively.

Table 3.1.1e – 3.1.1f provides the values from Draw wire displacement sensors (W1, W2, W3, W4). The max drift occurs during 1,4g excitation, with value 26.20%o. The minimum peak drift is 0.51%o at white noise before Wnb0.07g (without bottom fixing of the vertical living walls). The max residual drift is -2.37 mm (-1.93%o) at EQ1.4g excitation (Table 3.1.1l).

During excitation EQ0.5g, opening and closing of already formed (from the first phase) horizontal cracks in brick wall 3-4 was observed. However, no brick wall disintegration or stiffness reduction was noticed. During EQ1.3g, strain gauges SG5 (2693 ustrain), SG6 (-11803 ustrain) and SG15 (3230 ustrain) showed the highest values of variation. During EQ1.3g the columns entered yielding strain of their longitudinal steel reinforcements at the bottom. Also, damage with crushing of bottom brick at partial infill wall 2-3 and initiation of damage at the bottom brick at partial infill wall 3-4, was noticed.

During excitation EQ1.3g(2) , strain gauges SG5, SG6 and SG9 showed 10919 ustrain, -8657 ustrain and 2673 ustrain variation respectively. The columns entered yielding strain of their longitudinal steel reinforcements at the top critical regions as well (columns 1, 2, 3, 4). PUFJs between concrete columns and brick infills maintained their integrity without fracture or debonding while the maximum recorded horizontal top strain was 1173 ustrain, during excitation EQ1.4g. FRPU jackets at partial brick infills maintained their bonding on the PUFJs, on the concrete and on the bricks because of the protection of PUFJs. Therefore, strain gauges SG17-SG20 on the center of the partial brick infill face developed low values (maximum of 149 ustrain at excitation EQ0.55g). No failure of full brick infills 1 – 2 and 4 – 3 (out of plane) was observed. Basalt ropes wrapped around columns 3 and 4 developed extremely low strain values (max tensile strain of 58 ustrain SG23, SG24).

The Vertical Forest renovations resulted in a significant increase of the top slab mass. Yet, the innovative full green basalt rope wrapping of bottom and top critical regions of rc columns, the innovative construction of PUFJs between the wrapped concrete columns and the brick infills as well as of the one-sided FRPU jacketing of the brick infills resulted in increased stiffness and strength of the structure when compared to the as-built tested structure. The planters and vertical living walls are discussed in detail in the next section.

Table 3.1.1u shows the values of time (t14), at which (Acc1+Acc4)/2 receive maximum. Therefore, the time difference of the accelerometers between the peak top slab and the peak foundation Acc10, is given as Δt(t14-t10). The time difference for seismic excitations vary from -4.39 sec to 0.91 sec and for white noise from -0.08 sec to 15.85 sec. At white noise before WNb0.07g (without), the maximum difference Δt was observed.

3.3 Damage assessment

This section gathers the damage assessment of the planters, the vertical living walls and renovated reinforced concrete structure (table 3.1.1v – 3.1.1x).

Planters

The 5 planters with the trees (P) presented a remarkably resilient performance up to very severe seismic excitations. All different cases of Planters' anchoring with basalt ropes or steel rod on the top slab, sustained high displacement drifts and top slab accelerations. Despite, steel rod or basalt rope loosening or basalt rope fracture (in some cases) at very high accelerations of the structure, no planter collapse (or overturning) was observed. During certain excitations, the basalt rope anchors of the planters were cut or the prestressing devices were displaced. Then, the basalt rope anchors were easily replaced, and the prestressing devices corrected. In cases of rope loosening, it was easily tightened again. Most planters (except for planter 1) presented extreme rocking behavior with bottom micro or large displacement. During low seismic excitation, the rocking of planter 4 (without any anchoring but with PM pads) was negligible. However, for severe seismic excitations, extreme planter 4 rocking resulted in PM pads displacement and of the planter itself (no collapse or overturning). Planter 1 showed the best performance with bottom micro displacements because of slight loosening of the steel rod. Planter 5 (with double basalt rope and both ropes post-tensioned but without pads) showed excellent performance at low or severe seismic excitations with bottom micro displacements in most excitations.

During excitations Wnb0.07g (without), Wnb0.07g, EQ0.07g, EQ0.1g and Wnb0.14g, slight rocking of planter 5 was observed. During excitations EQ0.14, EQ0.2g, Wnb0.34g, Wnb0.5g, Wnb0.55g and Wnb0.74g, slight rocking of planter 2 and 5 was noticed. During EQ0.34g, rocking of planter 2, 3, 4 and 5 was observed. After excitation 0.34g, planter 2 basalt rope loosening was noted and the rope was tightened (post-tensioned again). After EQ0.5g, rocking of planter 2, 3, 4 and 5 as well as micro-displacement of planter 4 was noticed. After EQ0.55g, planter 3 displacement of prestressing device was noticed and it was tightened again. Rocking of planter 2, 3, 4 and 5 was observed. Planter 4 showed micro displacements. At excitation 0.74g, fracture of the basalt rope of planter 3 occured. Basalt rope loosening of planters 2,5 was evidenced and the rope was tightened again. Micro-displacement of planter 4 was noticed. After excitation EQ0.8g, rocking of planter 4 was evidenced, leading to micro displacement of the PM pads and of the planter itself. In planter 3 basalt rope was loose. After excitation EQ1.1g, rocking of planter 4 resulted in micro displacement of the PM pads and of the planter itself. The one basalt rope of planter 3 fractured. Displacement of prestressing devices of planter 2 and 5 and loosening of basalt ropes was noticed. After EQ1.3g, rocking of planter 4 leading to displacement (+-3 cm) of the PM pads and of the planter itself was observed. Planter 1 showed bottom micro displacements because of slight loosening of the steel rod. The one basalt rope of planter 2 was fractured. Planters 2, 3 and 5 showed bottom displacements. After excitation EQ1.3g(2), rocking of planter 4 leading to displacement (+-3 cm) of the PM pads and of the planter itself, was noticed. The basalt rope of planter 3 was fractured. Both basalt ropes of planter 5 were fractured. The prestressing device of planter 2 was displaced. All damages were restored easily. At excitation EQ1.4g, rocking of planter 4 leading to displacement (+-4 cm) of the PM pads and of the planter itself was noticed. Planter 1 showed bottom micro displacements because of slight loosening of the steel rod. The one basalt rope of planter 3 was fractured. Planter 5 and 2 showed bottom micro displacements. Finally, after all excitations, planter 1 showed the best performance with bottom micro displacements because of slight loosening of the steel rod. Planter 5 showed excellent performance with bottom micro displacements.

Wnb0.07g(without), Wnb0.07g, EQ0.07g, EQ0.1g, Wnb0.14g

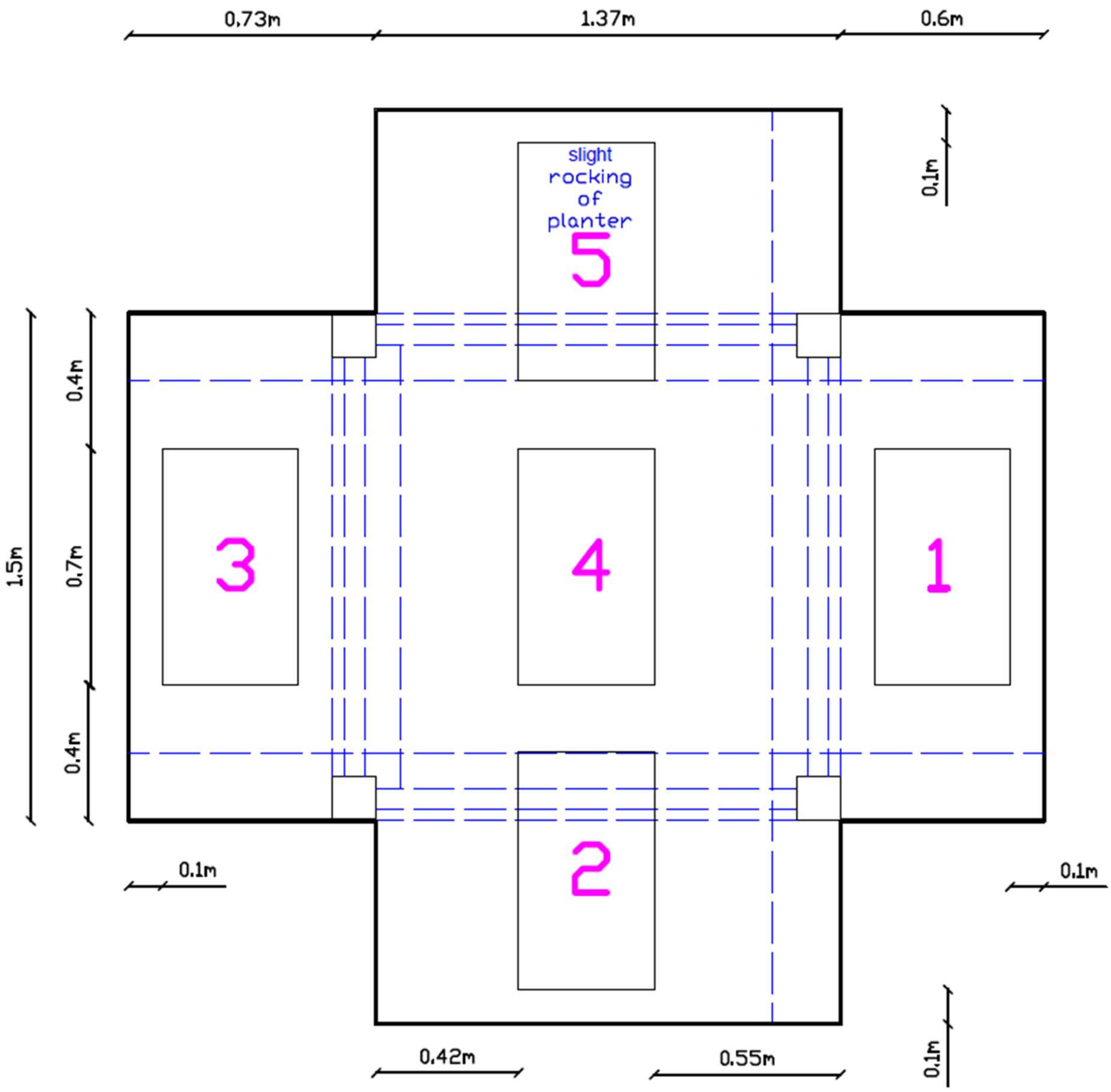

Figure 3.3.1 Observed damage after Wnb0.07g(without), Wnb0.07g, EQ0.07g, EQ0.1g, Wnb0.14g tests:. Slight rocking of planter 5.

EQ0.14g, EQ0.2g, Wnb0.34g, Wnb0.5g, Wnb0.55g

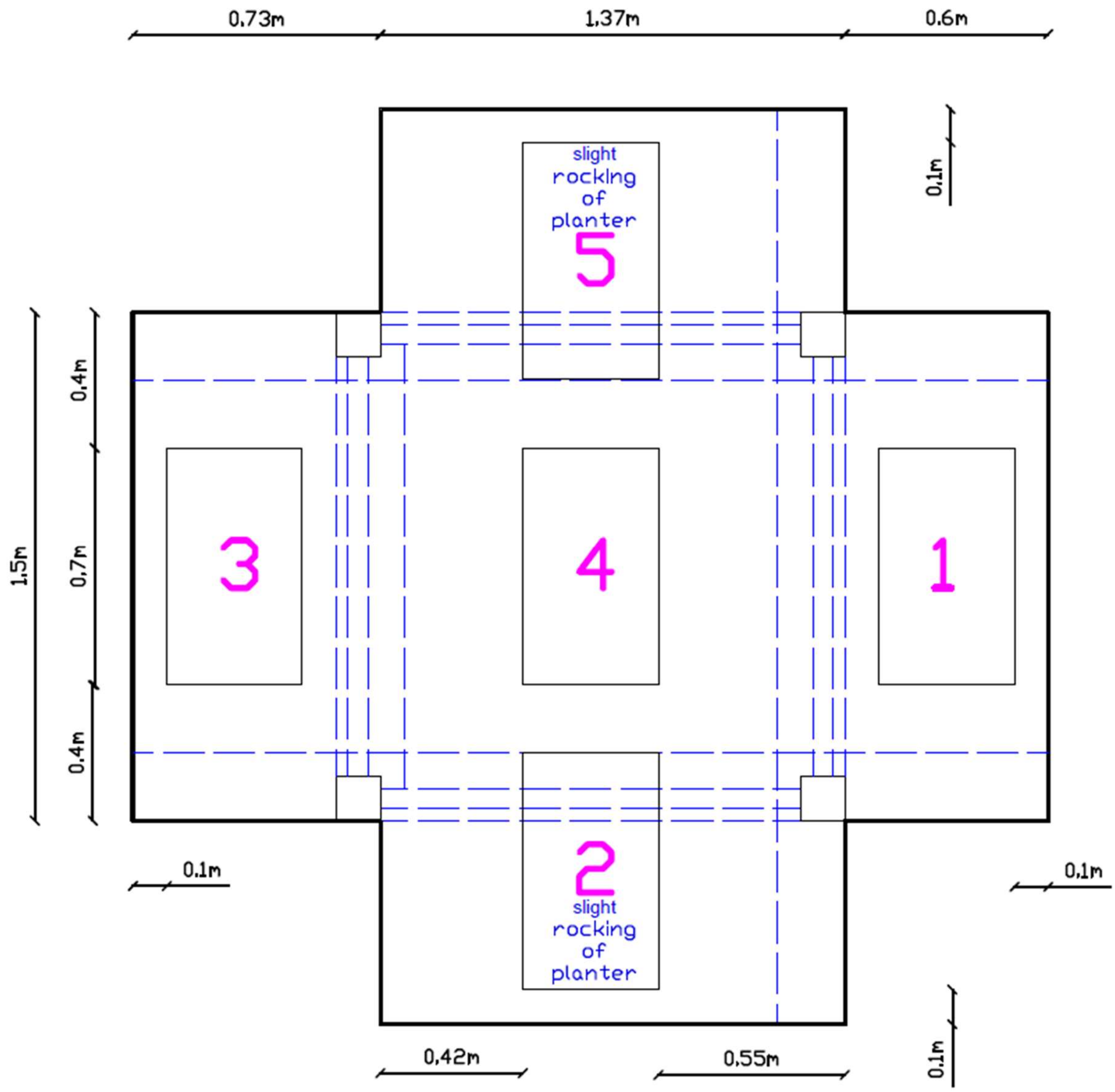

Figure 3.3.2 Observed damage after EQ0.14g, EQ0.2g, Wnb0.34g, Wnb0.5g, Wnb0.55g tests:. Slight rocking of planter 2 and 5.

EQ0.34g

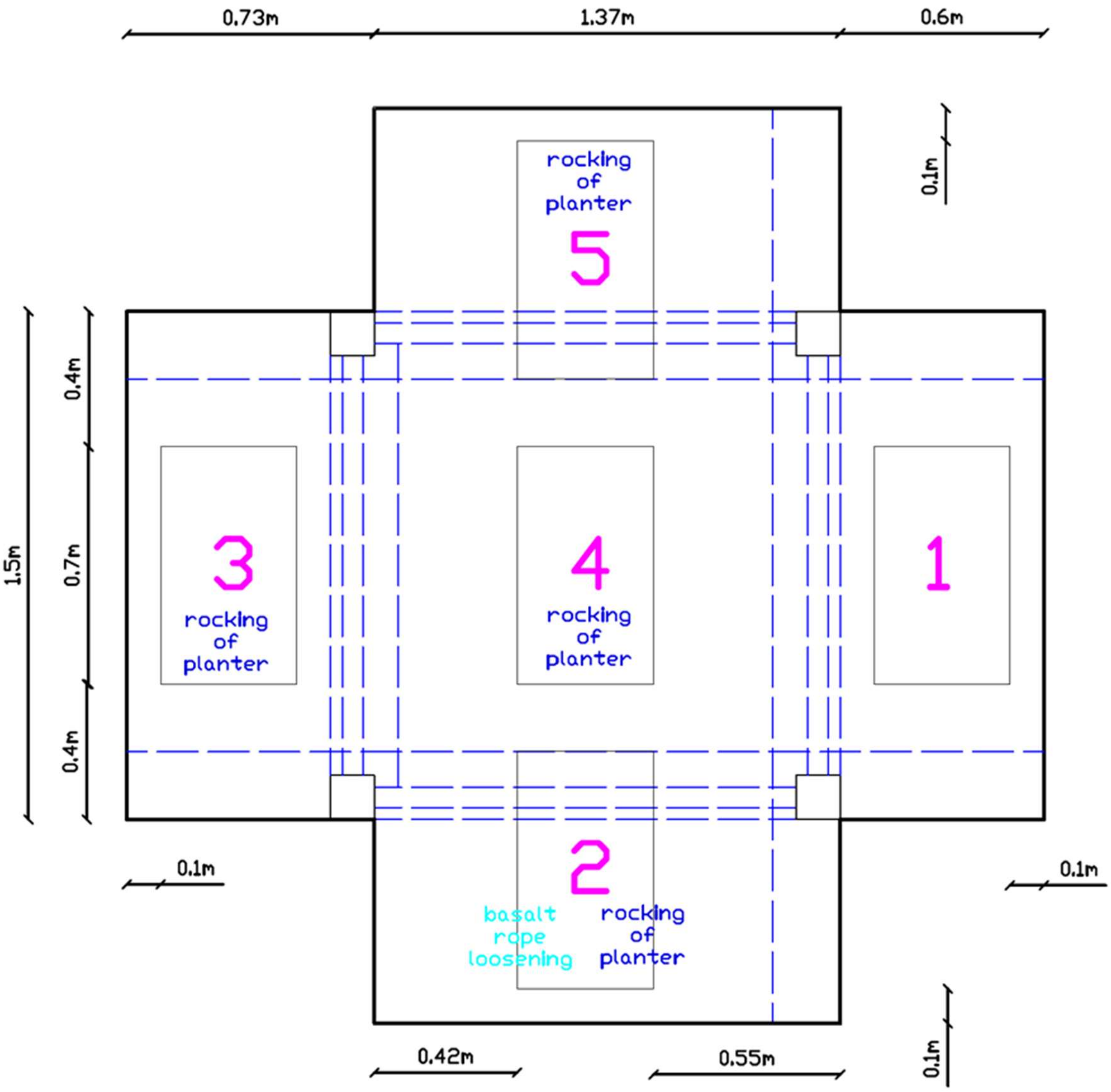

Figure 3.3.3 Observed damage after EQ0.34 test: Planter 2 basalt rope loosening was observed, then it was tightened. Rocking of planter 2, 3, 4 and 5.

EQ0.5g

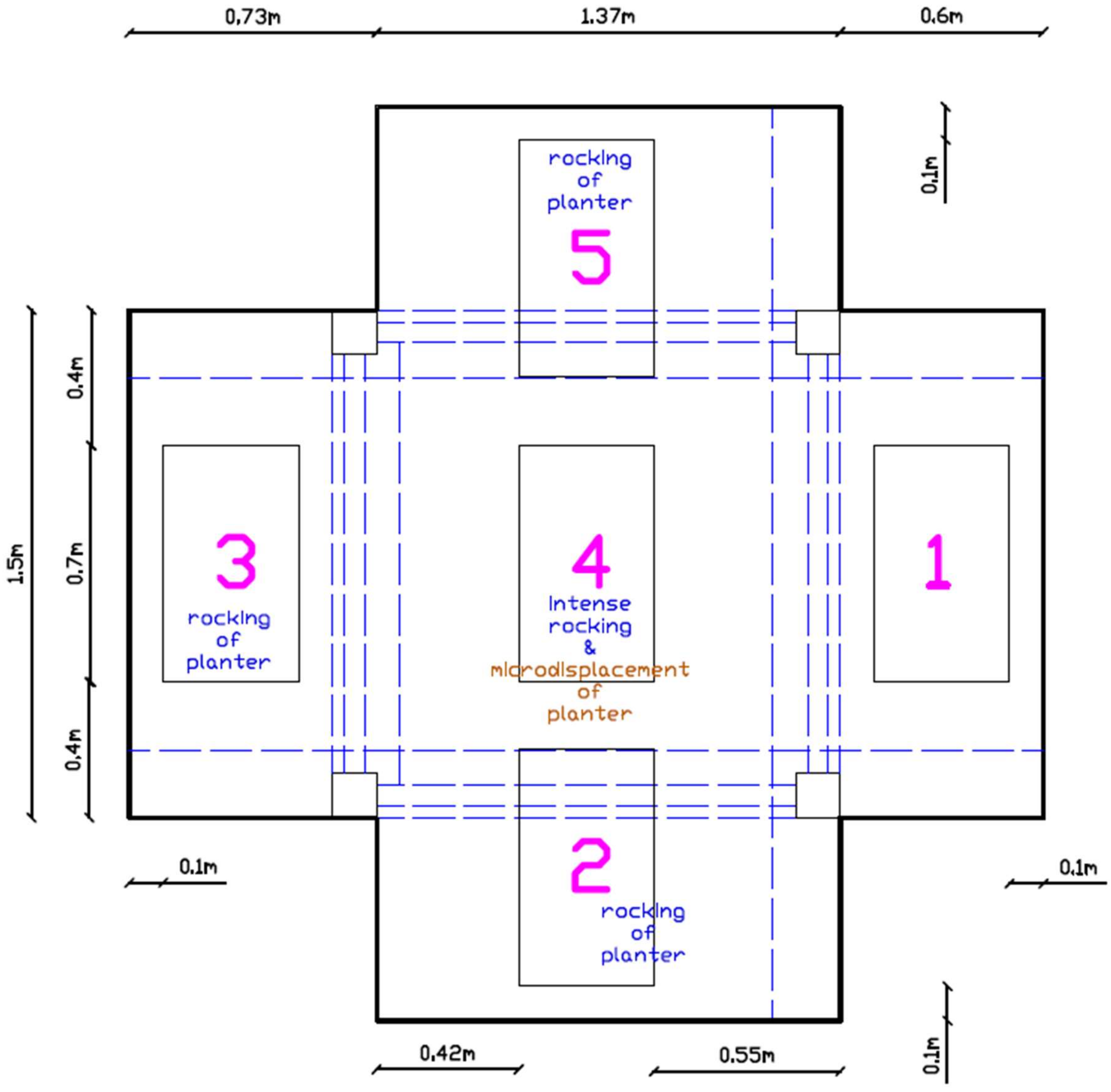

Figure 3.3.4 Observed damage after EQ0.5g test: Rocking of planter 2, 3, 4 and 5. Micro-displacement of planter 4.

Wnb0.55g, WNb0.74g, Wnb0.8g

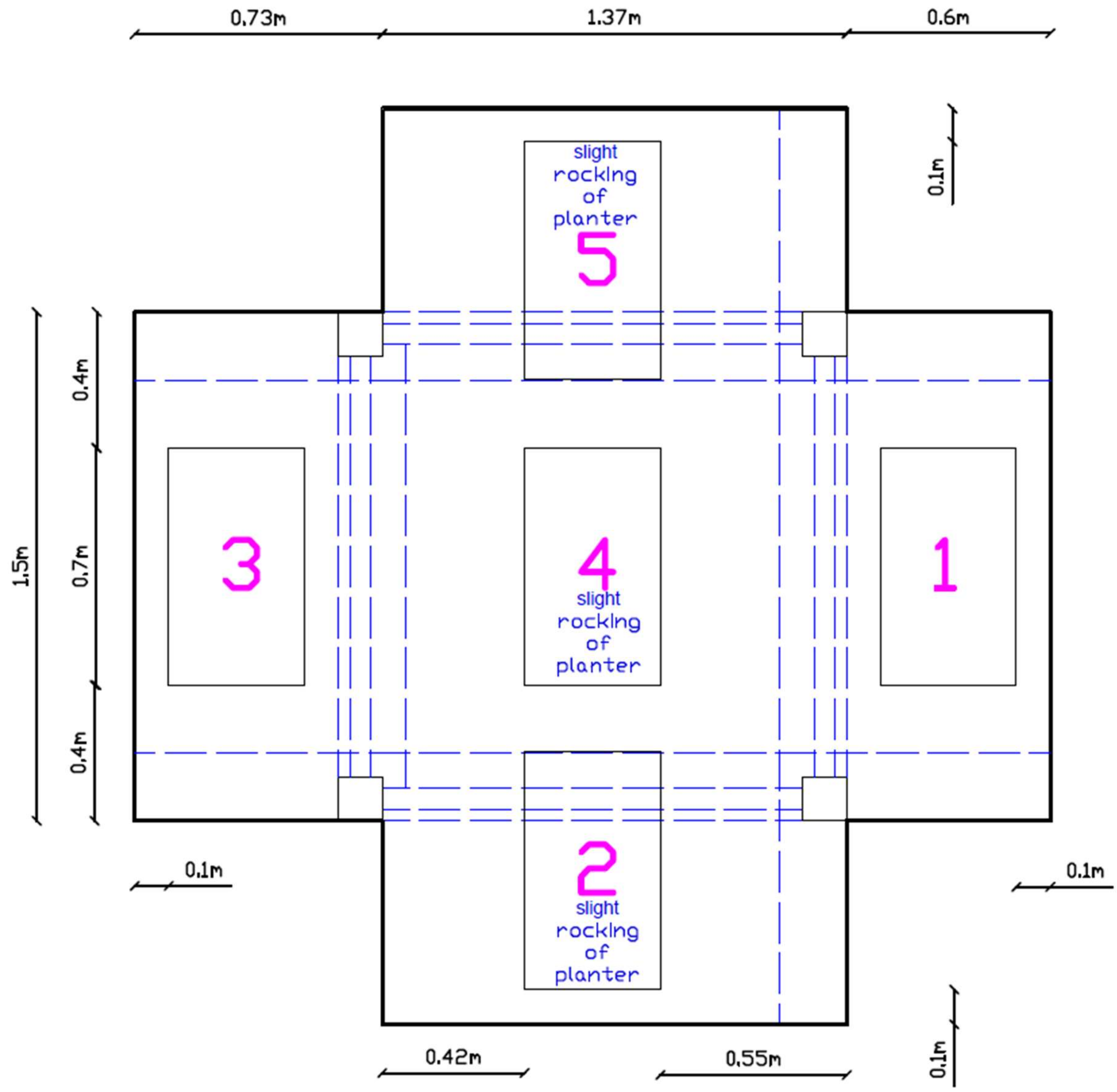

Figure 3.3.5 Observed damage after Wnb0.55g, WNb0.74g, Wnb0.8g tests: Rocking of planter 2, 3, 4 and 5. Micro-displacement of planter 4.

EQ0.55g

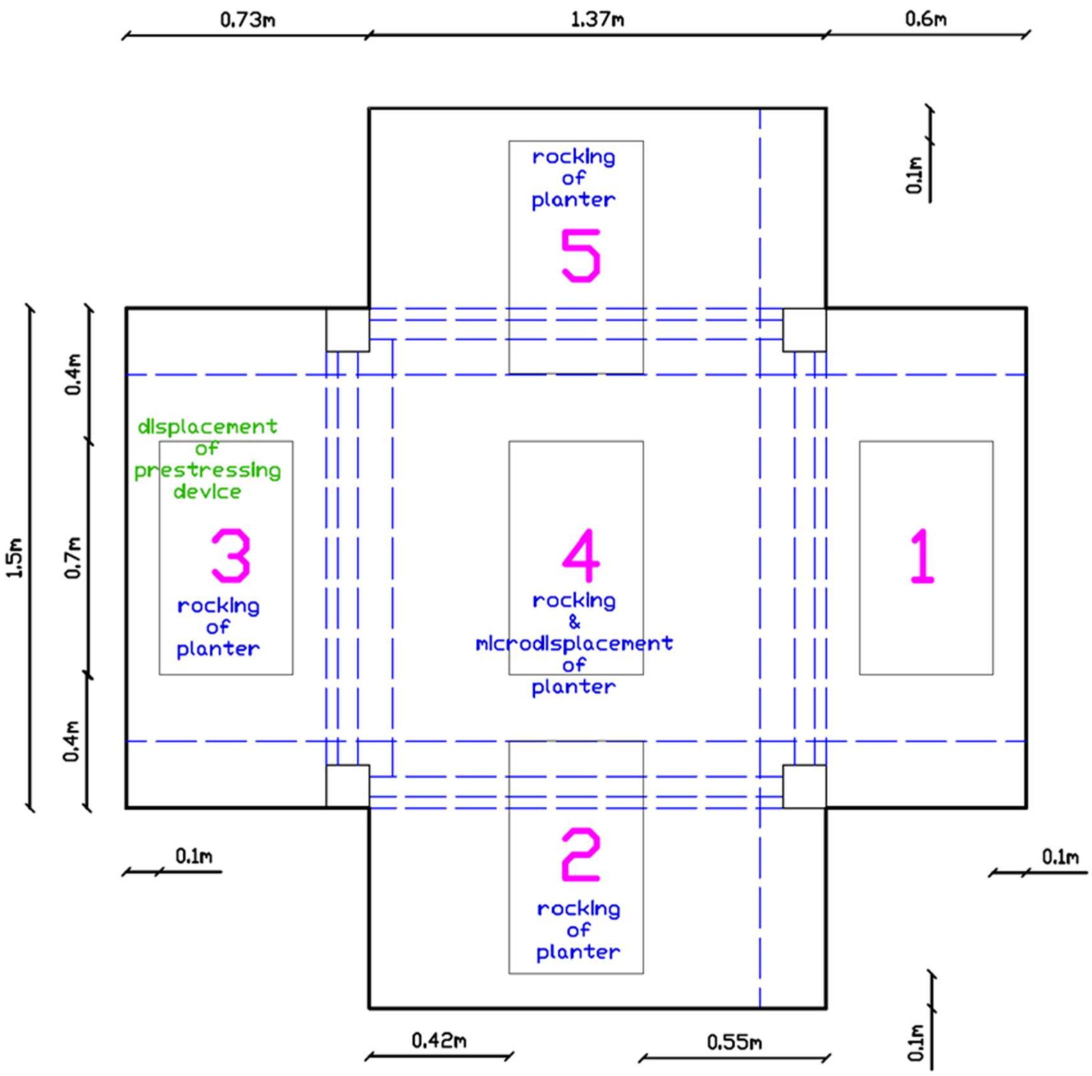

Figure 3.3.6 Observed damage after EQ0.55 test: Planter 3 displacement of prestressing device was noticed and it was tightened again. Rocking of planter 2, 3, 4 and 5. Micro-displacement of planter 4.

EQ0.74g

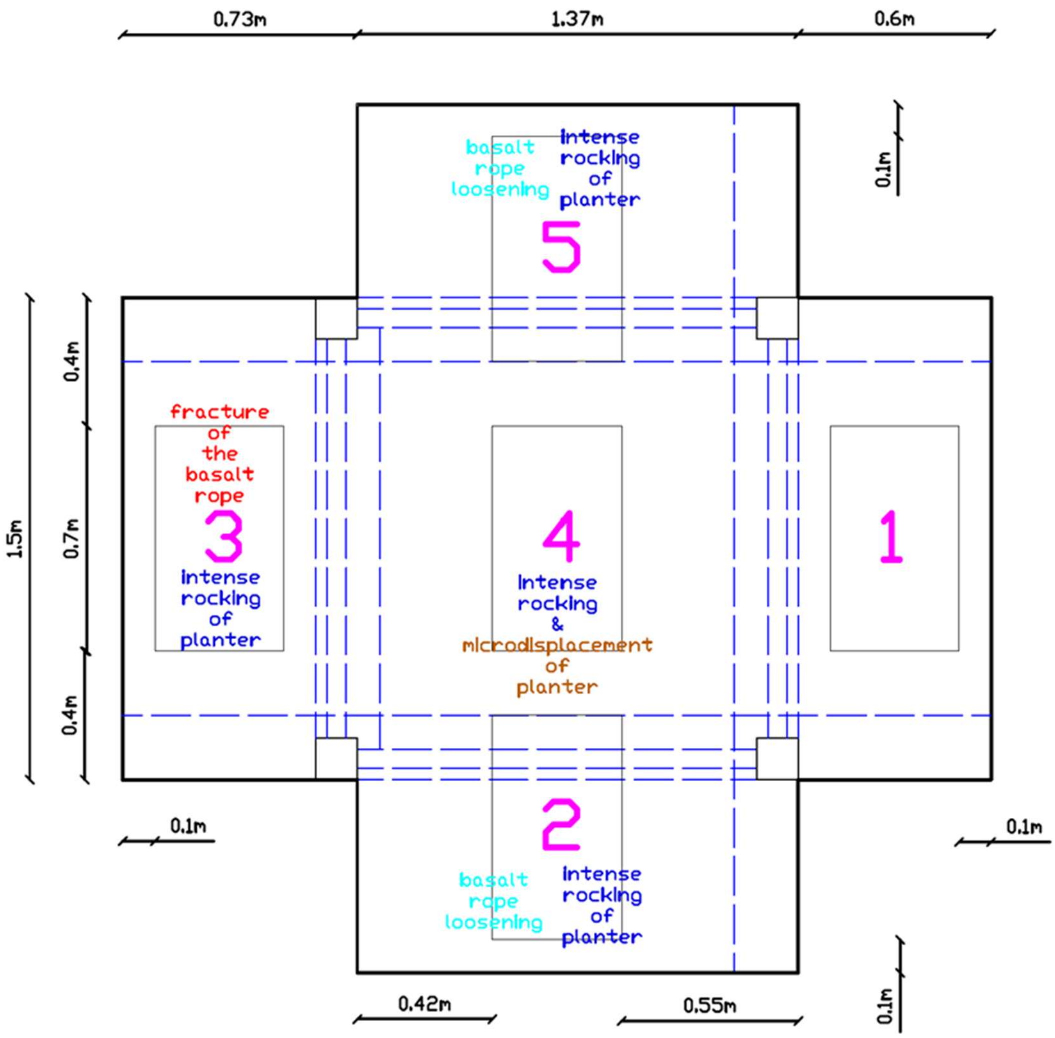

Figure 3.3.7 Observed damage after EQ0.74g test: Fracture of the basalt rope of planter 3. Basalt rope loosening of planters 2,5 and tightened again. Intense rocking of planter 2, 3, 4 and 5. Micro-displacement of planter 4.

EQ0.8g

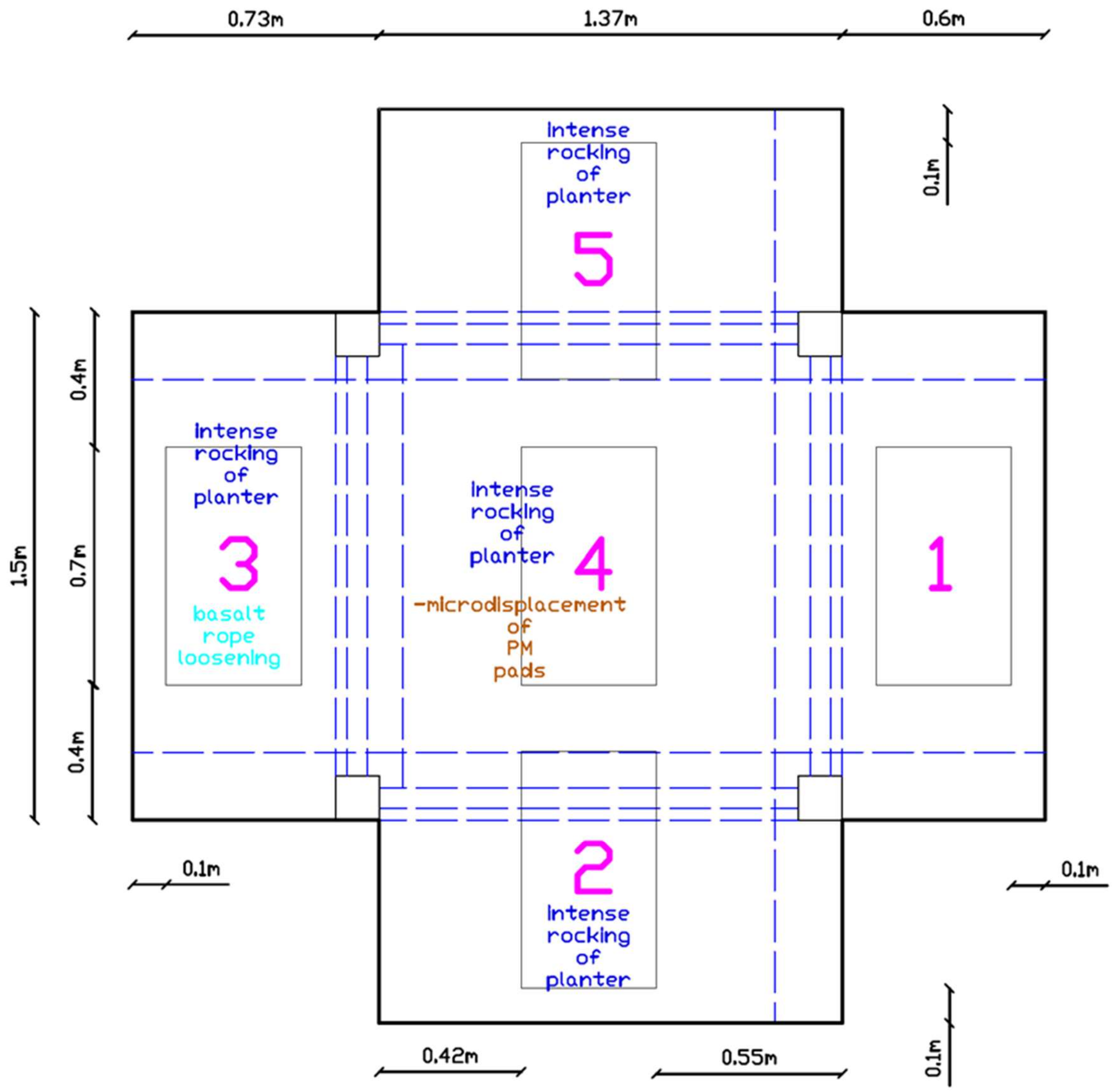

Figure 3.3.8 Observed damage after EQ0.80g test: Intense rocking of planter 4 leading to micro displacement of the PM pads and of the planter itself. Planter 3 basalt rope was loosening. Intense rocking of planter 2, 3 and 5.

Wnb1.1g, Wnb1.3g, Wnb1.4

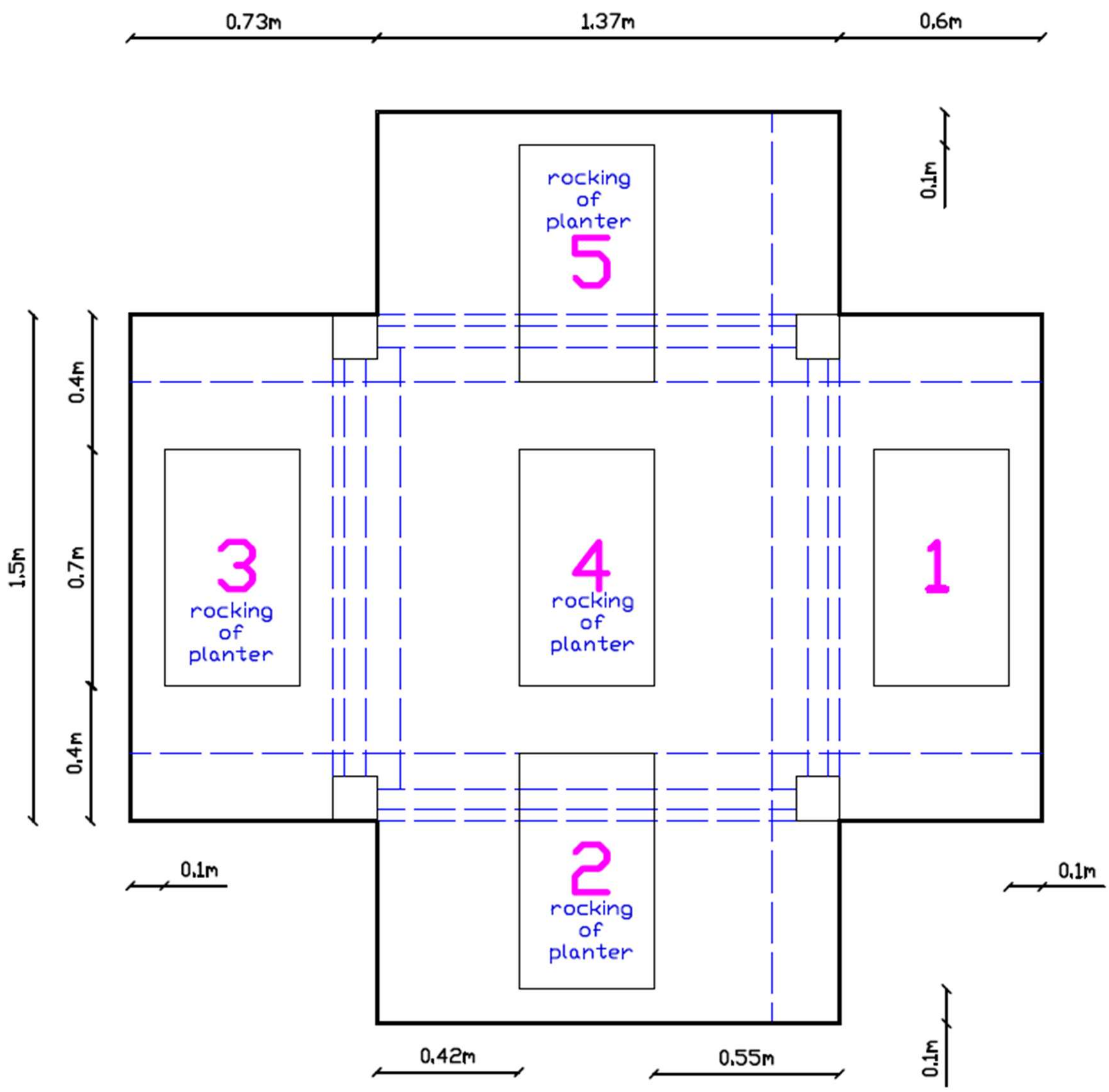

Figure 3.3.9 Observed damage after Wnb1.1g, Wnb1.3g, Wnb1.4 test: Rocking of planter 5, 4, 3 ,2.

EQ1.1g

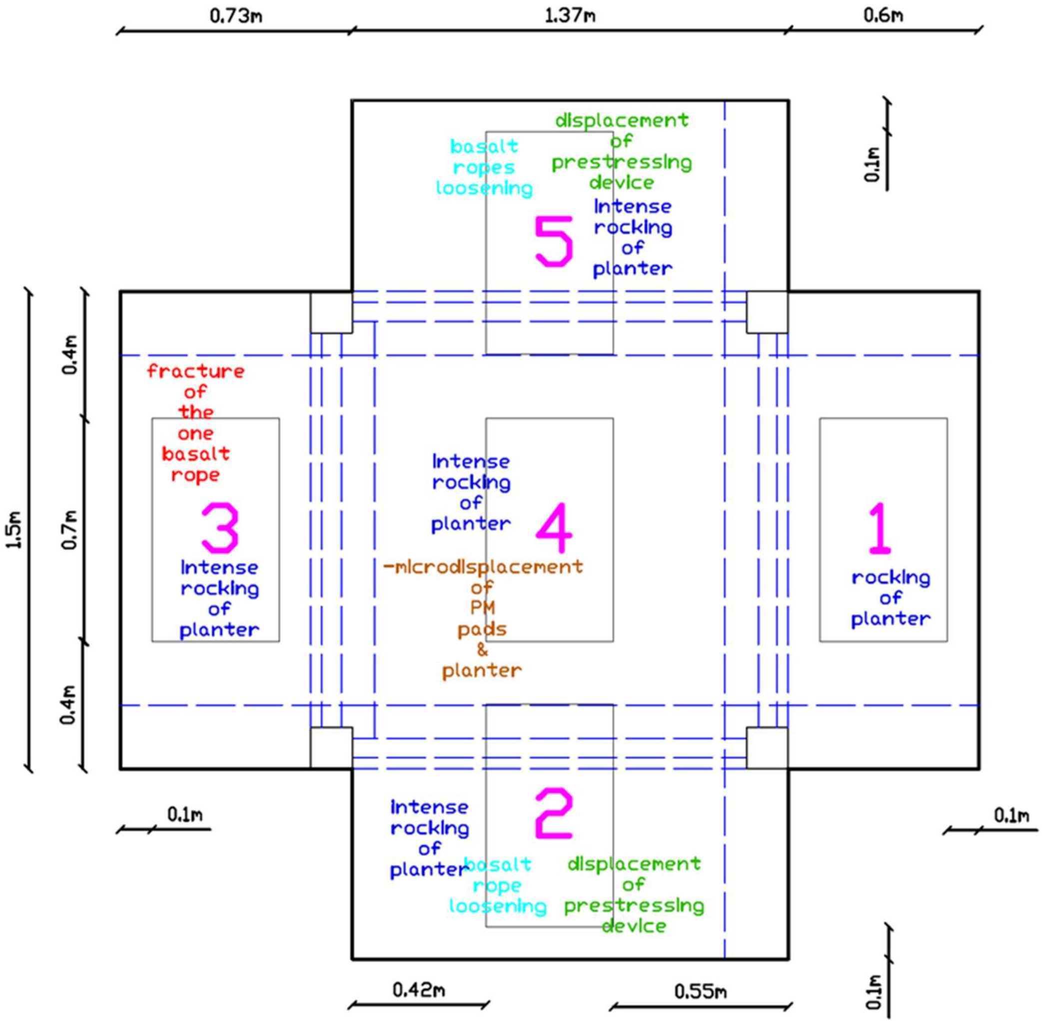

Figure 3.3.10 Observed damage after EQ1.1g test: intense rocking of planter 4 leading to micro displacement of the PM pads and of the planter itself. Fracture of the one basalt rope of planter 3. Displacement of prestressing devices of planter 2 and 5 and loosening of basalt ropes. Intense rocking of planter 2, 3, 5 and rocking of planter 1.

EQ1.3g

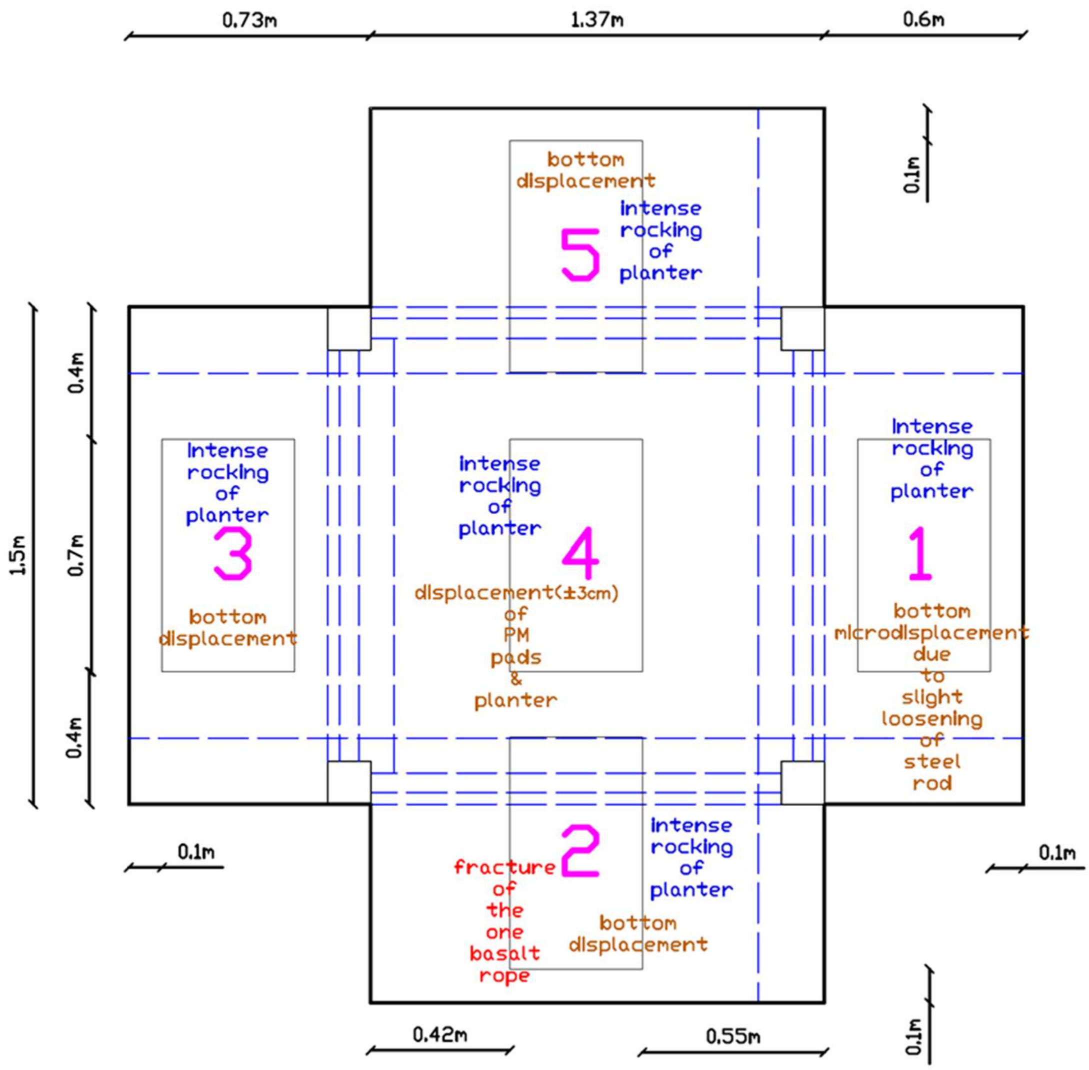

Figure 3.3.11 Observed damage after EQ1.3g test: Intense rocking of planter 4 leading to displacement (+-3 cm) of the PM pads and of the planter itself. Planter 1 showed bottom microdisplacements because of slight loosening of the steel rod. Fracture of the one basalt rope of planter 2. Planters 2,3 and 5 showed bottom displacements. Intense rocking of all planters.

Wnb1.3g(2)

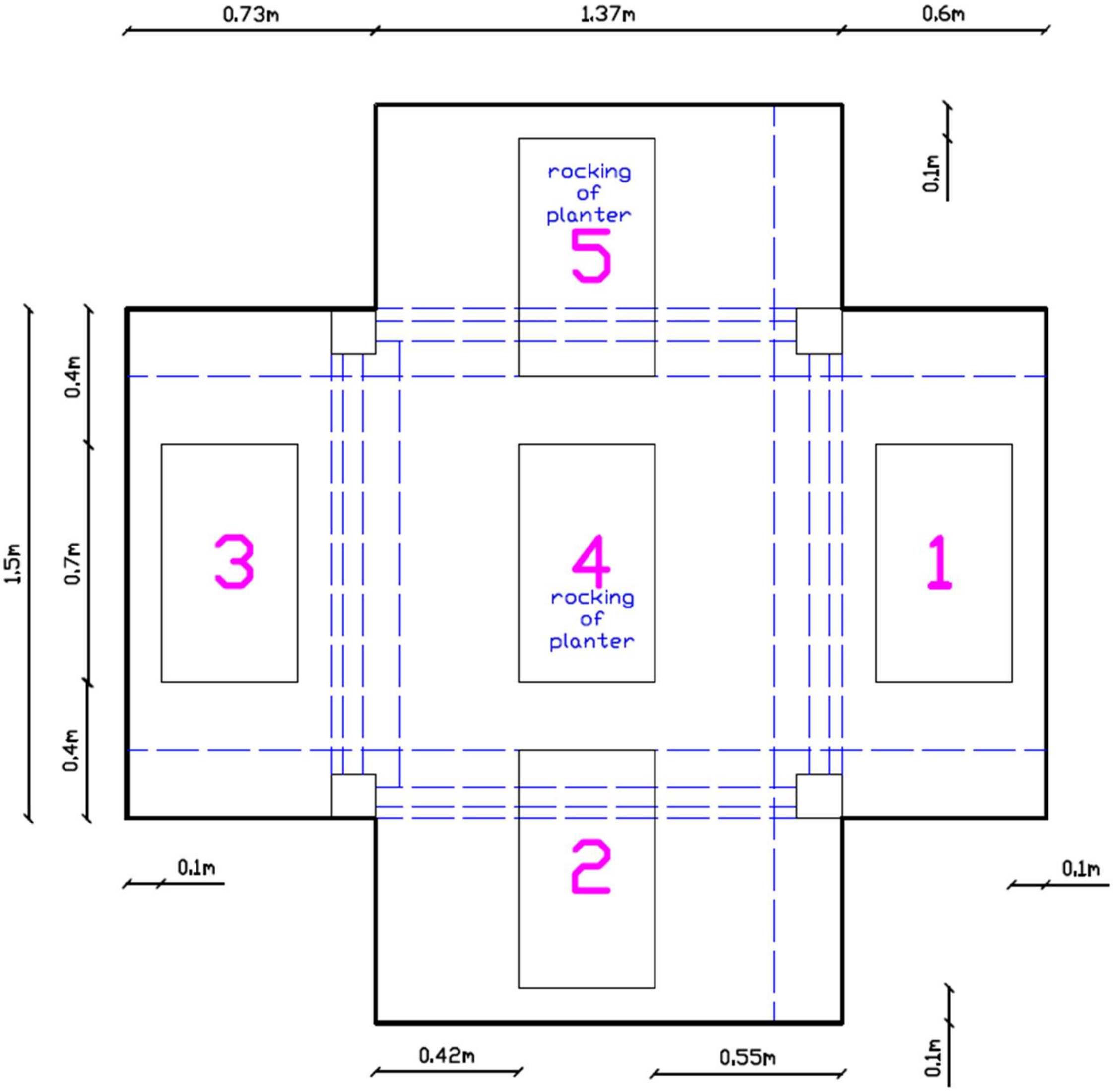

Figure 3.3.12 Observed damage after Wnb1.3g (2) test: Rocking of planter 4 and 5.

EQ1.3g(2)

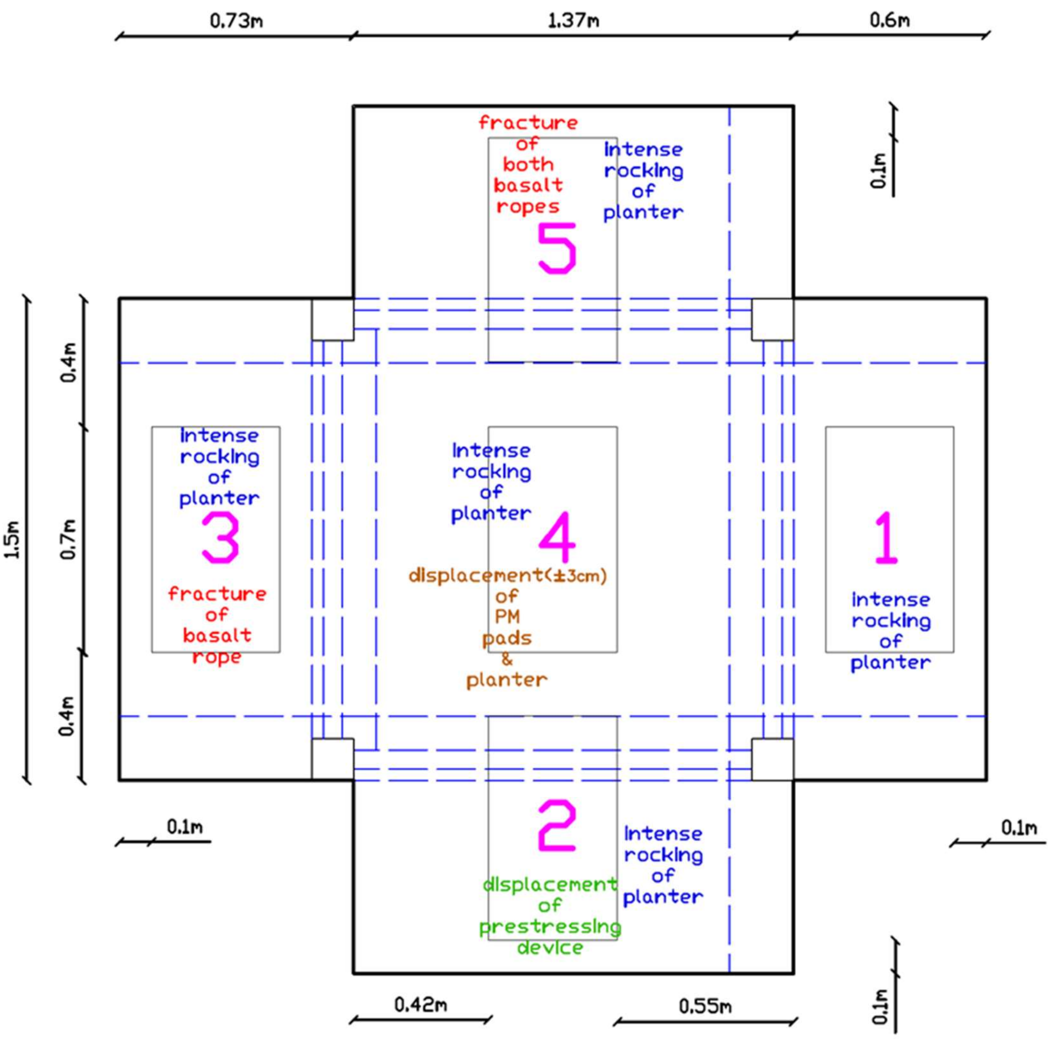

Figure 3.3.13 Observed damage after EQ1.3g(2) test: Intense rocking of planter 4 leading to displacement (+-3 cm) of the PM pads and of the planter itself. Fracture of basalt rope of planter 3. Fracture of both basalt ropes of planter 5. Displacement of prestressing device of planter 2. Intense rocking of all planters.

EQ1.4g

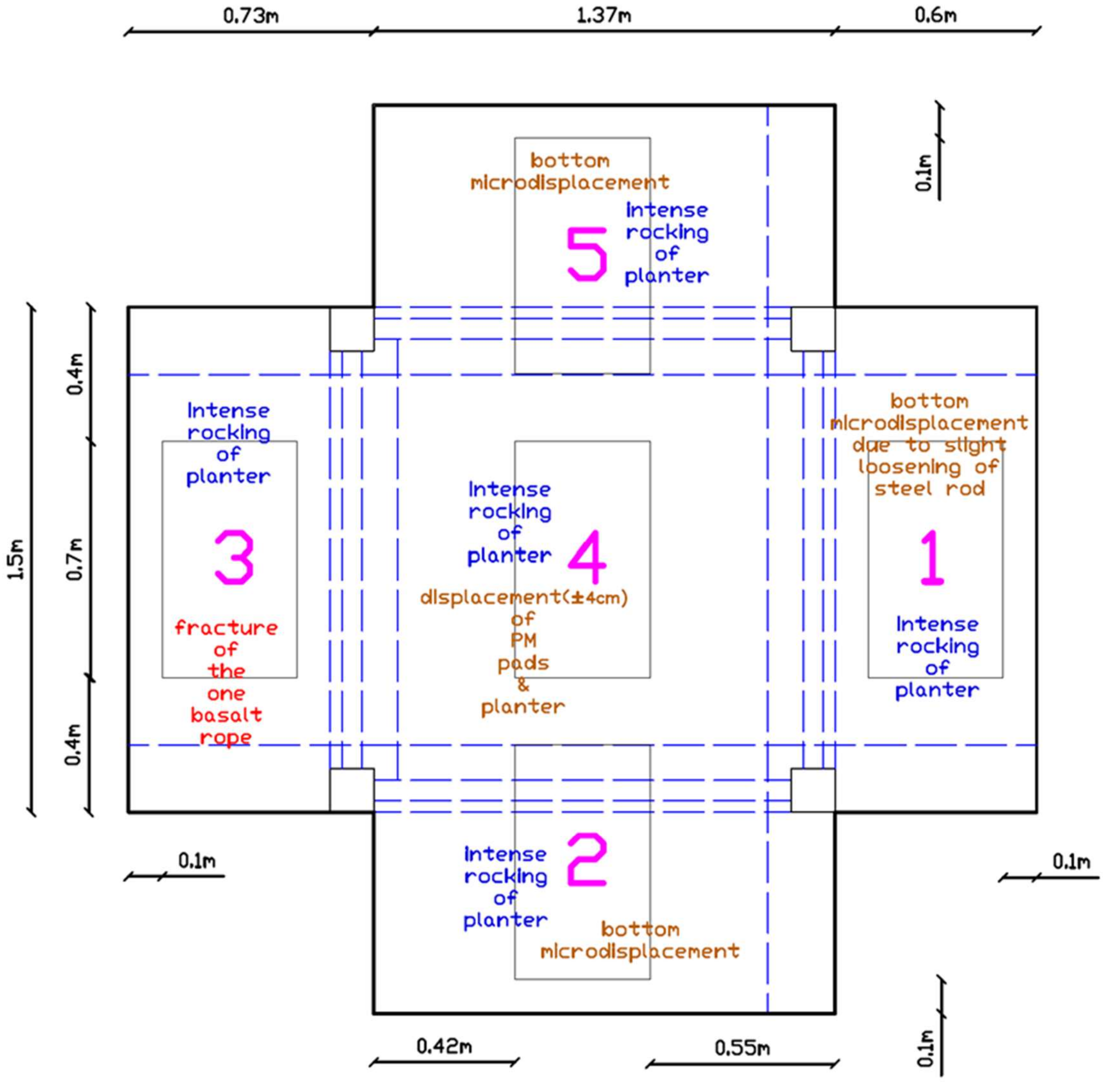

Figure 3.3.14 Observed damage after EQ1.3g(2) test : Intense rocking of planter 4 leading to displacement (+-4 cm) of the PM pads and of the planter itself. Planter 1 showed bottom micro displacements because of slight loosening of the steel rod. Fracture of the one basalt rope of planter 3. Planter 5 and 2 showed bottom micro displacements. Intense rocking of all planters.

Wnb0.2g, EQ0.2g, Wna0.2g

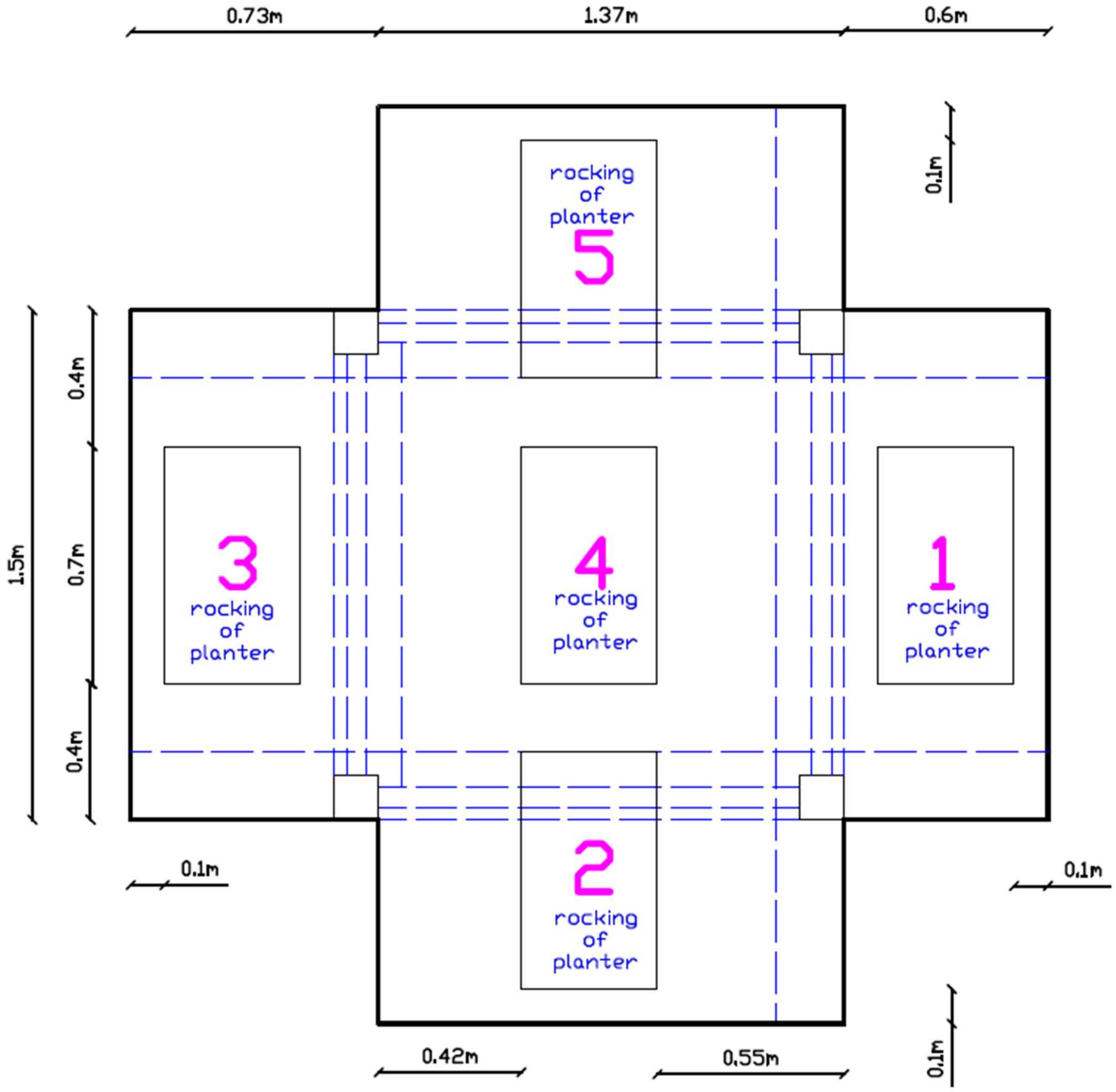

Figure 3.3.15 Observed damage after Wnb0.2g, EQ0.2g, Wna0.2g tests: Rocking of all planters.

Vertical living walls

The 8 vertical living walls (LW) presented a remarkably resilient performance up to very severe seismic excitations. All different cases of vertical Living Wall attachment on the concrete elements with basalt ropes and PU pads, sustained high displacement drifts and top slab accelerations respectively. Despite, steel rod or basalt rope loosening (in some cases) at very high accelerations of the structure, no living wall collapse was observed. It is important to mention that LW4-3L, LW1-2L and LW1-2R showed better performance than LW4-3R at very high displacement drifts. Similar high performance showed LW1-4L and LW2-3R.

Initiation of loosening of basalt rope of LW1-4L and LW3-2L was observed. Also, initiation of micro loosening of LW1-4R, LW3-2R, LW1-2L and LW1-2R, was observed. No severe loosening of vertical living walls, before EQ0.74g was observed. More specifically, after EQ0.8g left living wall LW1-4L, showed basalt rope loosening without detachment of PU pads allowing micromovements for high direct horizontal loads (severe wind) but no living wall collapse was observed. Left vertical living wall LW3-2L showed basalt rope loosening without detachment of PU pads allowing micromovements for high direct horizontal loads (severe wind) but no living wall collapse was observed. After excitation EQ1.1g, left living wall LW1-4L, showed basalt rope loosening without detachment of PU pads allowing micromovements for high direct horizontal loads (severe wind) but no living wall collapse was observed. Also, left vertical living wall LW3-2L showed basalt rope loosening without detachment of PU pads allowing micromovements for high direct horizontal loads (severe wind) but no living wall collapse was observed. After excitation EQ1.3g, left living wall LW1-4L, showed basalt rope loosening without detachment of PU pads allowing micromovements for low direct horizontal loads (frequent wind) but no living wall collapse was observed. Left vertical living wall LW3-2L showed basalt rope loosening without detachment of PU pads allowing micromovements for low direct horizontal loads (frequent wind) but no living wall collapse was observed. After excitation EQ1.3g(2), left living wall LW1-4L, showed basalt rope loosening leading to detachment of PU pads allowing micromovements for low direct horizontal loads (frequent wind) but no living wall collapse was observed. Left vertical living wall LW3-2L showed basalt rope loosening leading to detachment of PU pads allowing micromovements for low direct horizontal loads (frequent wind) but no living wall collapse was observed. Steel rod (hemlock) slight loosening at the top of living wall LW3-4R allowing micromovements for low direct horizontal loads (frequent wind) but no living wall collapse was observed. Finally, after the maximum intensity excitation EQ1.4g, steel rod or basalt rope loosening (in some cases) at very high accelerations of the structure, no living wall collapse was observed. Left living wall LW3-4L showed the best performance maintaining full capacity, in plane and out of plane (resistant to severe wind). Left living wall LW1-4L, showed basalt rope loosening leading to detachment of PU pads allowing micromovements for low direct horizontal loads (frequent wind) but no living wall collapse was observed. Living walls LW1-2L, LW2-3R, LW1-4R showed slight basalt rope loosening allowing micromovements for high direct horizontal loads (severe wind), but no living wall collapse was observed. Living wall LW1-2R showed basalt rope loosening allowing micromovements for medium direct horizontal loads (intense wind), but no living wall collapse was observed. Left vertical living wall LW3-2L showed basalt rope loosening leading to detachment of PU pads allowing micromovements for low direct horizontal loads (frequent wind) but no living wall collapse was observed. Steel rod (hemlock) slight loosening at the top of living wall LW3-4R allowing micromovements for low direct horizontal loads (frequent wind) but no living wall collapse was observed.

EQ1.1g

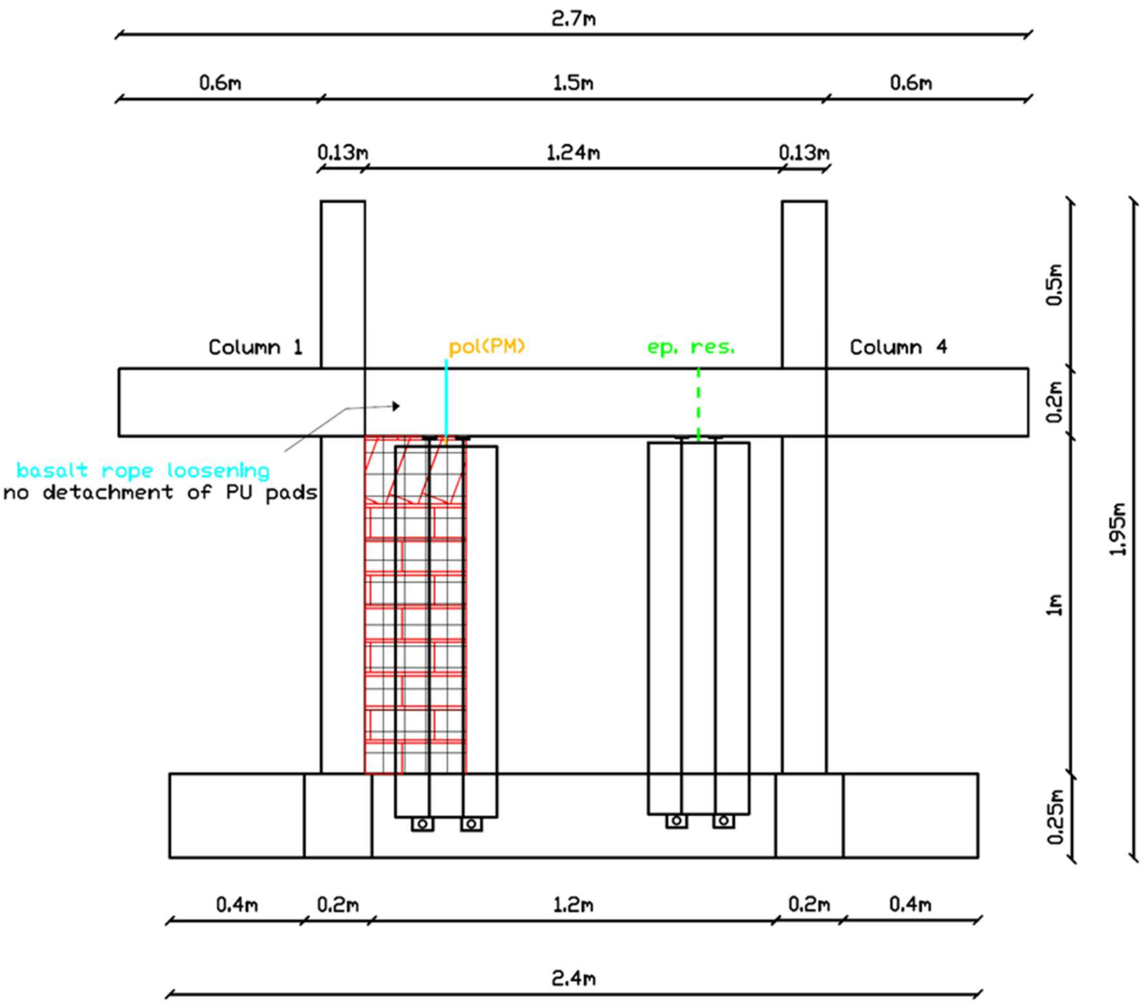

Figure 3.3.16 Observed damage after 1.1g test: Left living wall LW1-4L, showed basalt rope loosening without detachment of PU pads allowing micromovements for high direct horizontal loads (severe wind) but no living wall collapse was observed.

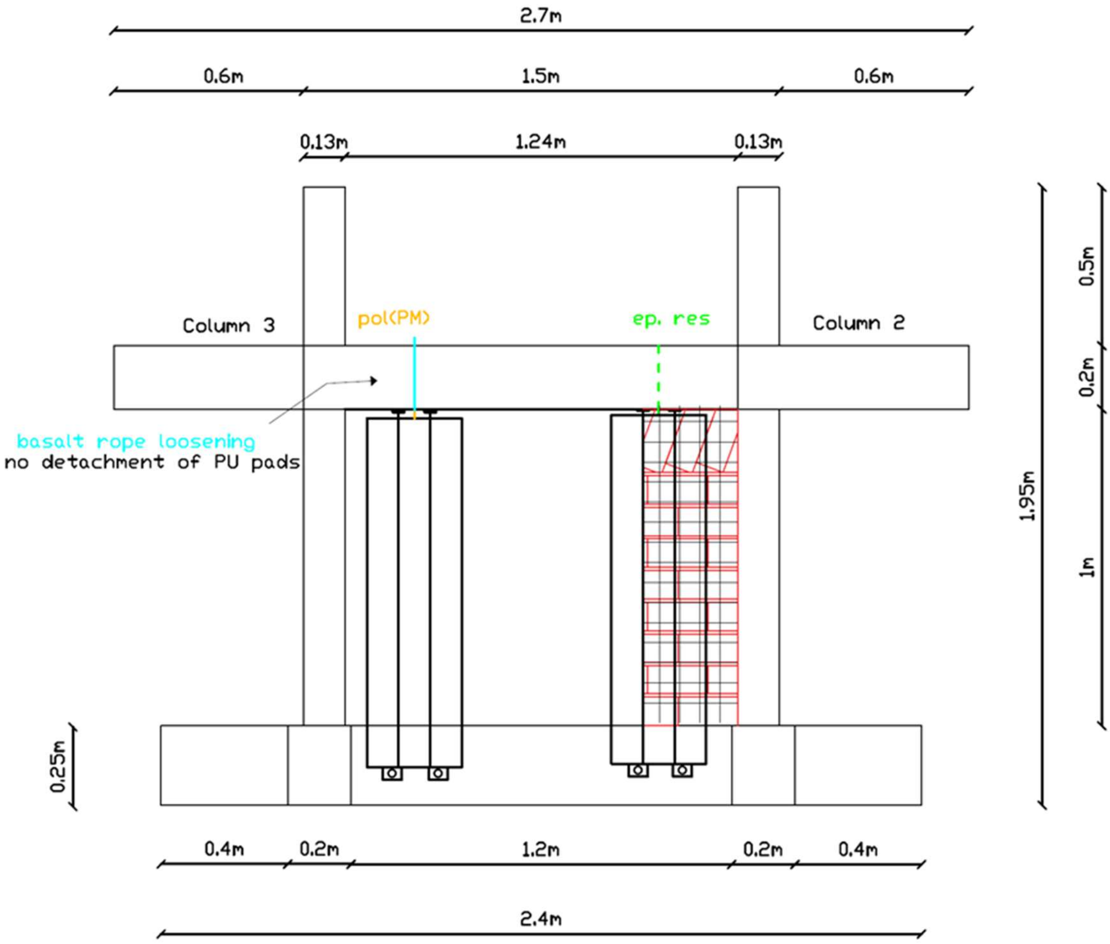

Figure 3.3.17 Observed damage after 1.1g test: Left vertical living wall LW3-2L showed basalt rope loosening without detachment of PU pads allowing micromovements for high direct horizontal loads (severe wind) but no living wall collapse was observed.

EQ1.3g

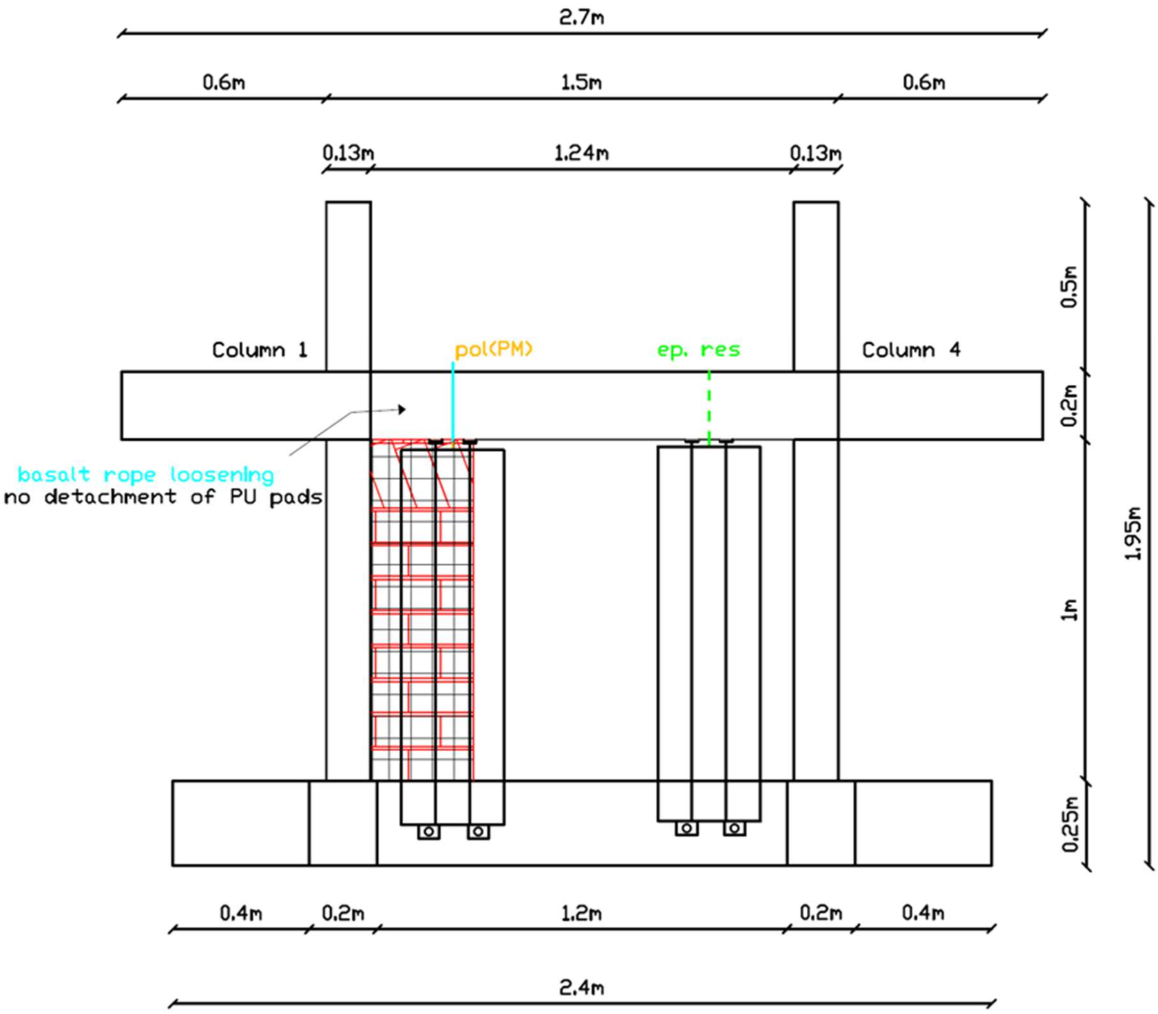

Figure 3.3.18 Observed damage after 1.3g test: Left living wall LW1-4L, showed basalt rope loosening without detachment of PU pads allowing micromovements for low direct horizontal loads (frequent wind) but no living wall collapse was observed.

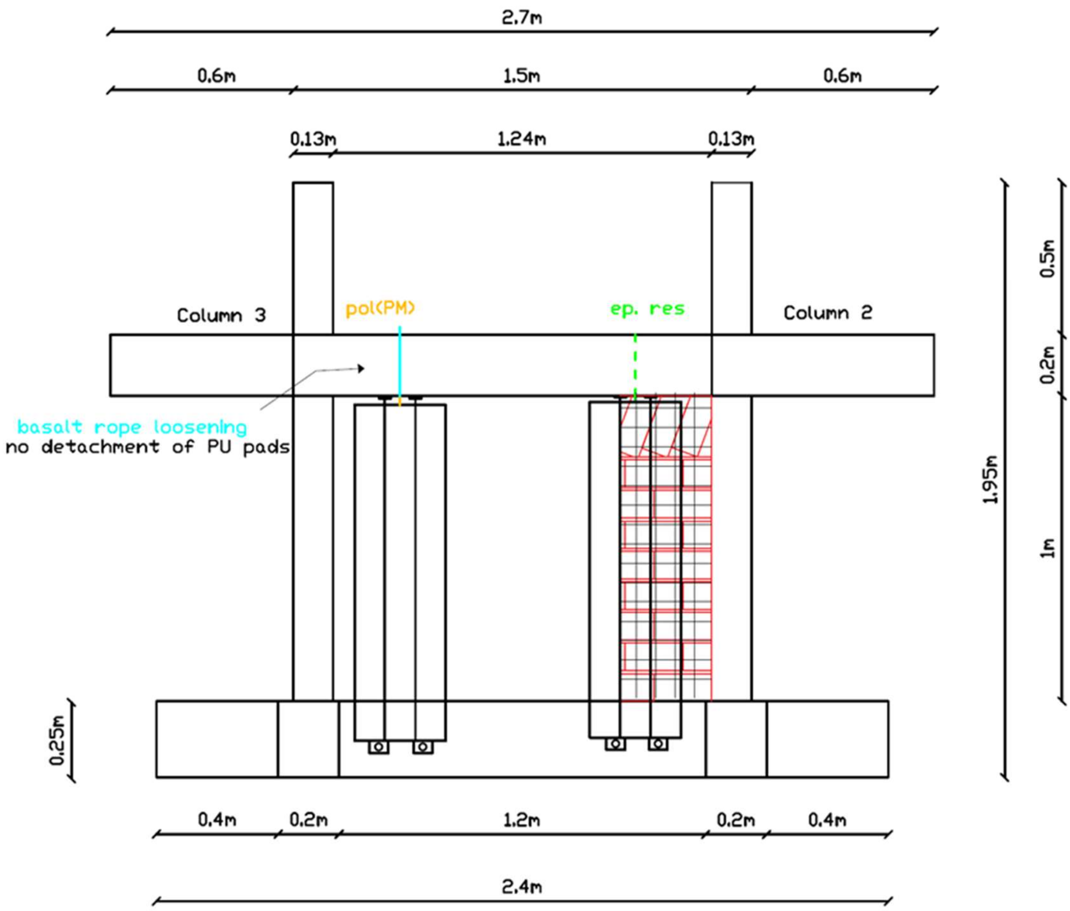

Figure 3.3.19 Observed damage after 1.3g test: Left vertical living wall LW3-2L showed basalt rope loosening without detachment of PU pads allowing micromovements for low direct horizontal loads (frequent wind) but no living wall collapse was observed.

EQ1.3g(2)

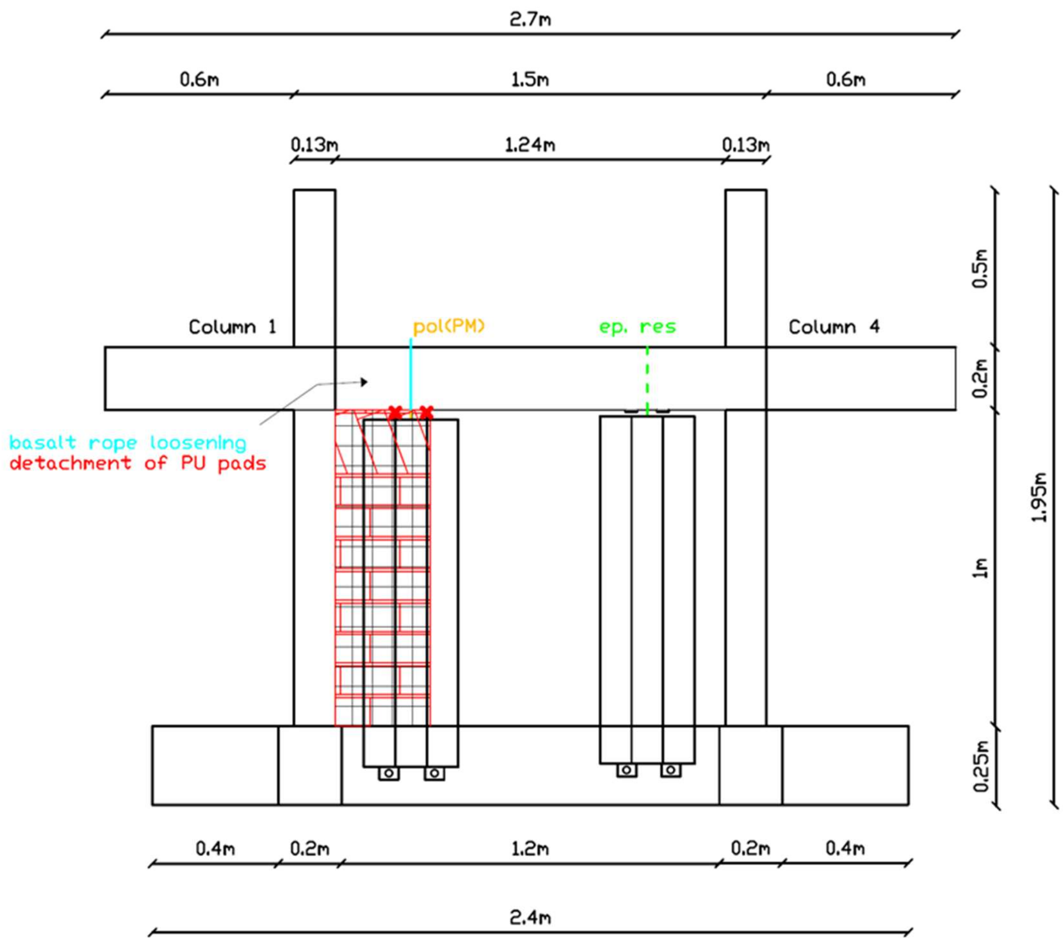

Figure 3.3.20 Observed damage after 1.3g(2) test: Left living wall LW1-4L, showed basalt rope loosening leading to detachment of PU pads allowing micromovements for low direct horizontal loads (frequent wind) but no living wall collapse was observed.

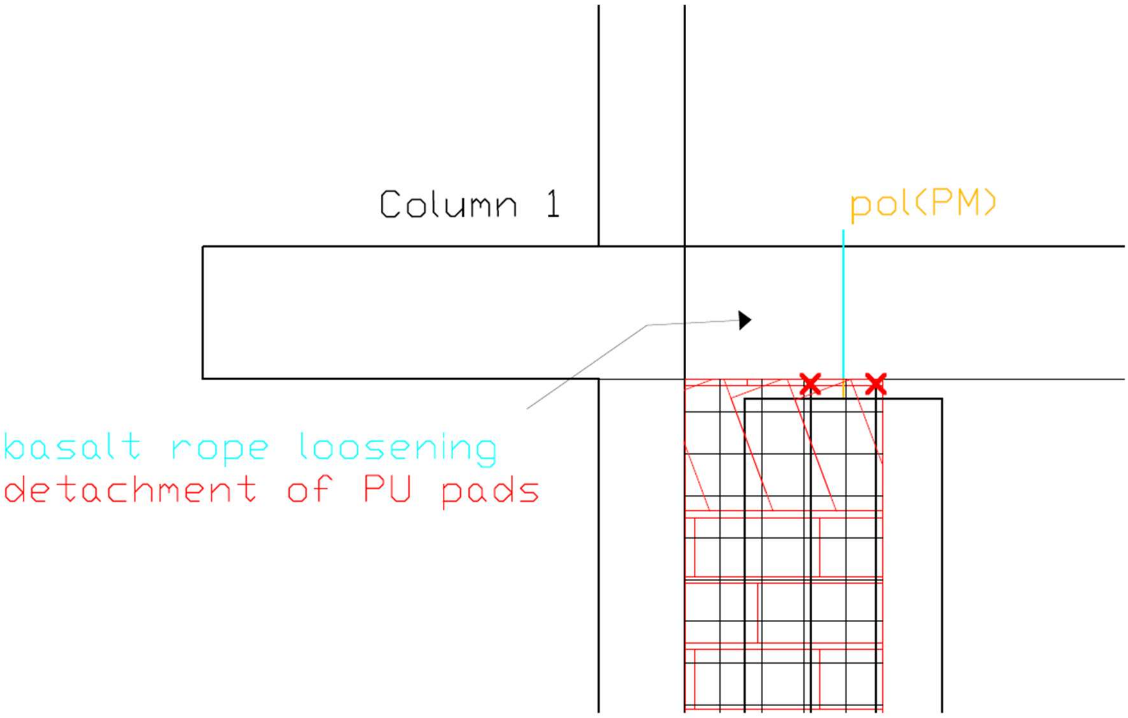

Figure 3.3.21 Anchoring details and PU pads dimensions (under the top slab), left living wall LW1-4L: detachment of PU pads after EQ1.3g (2)

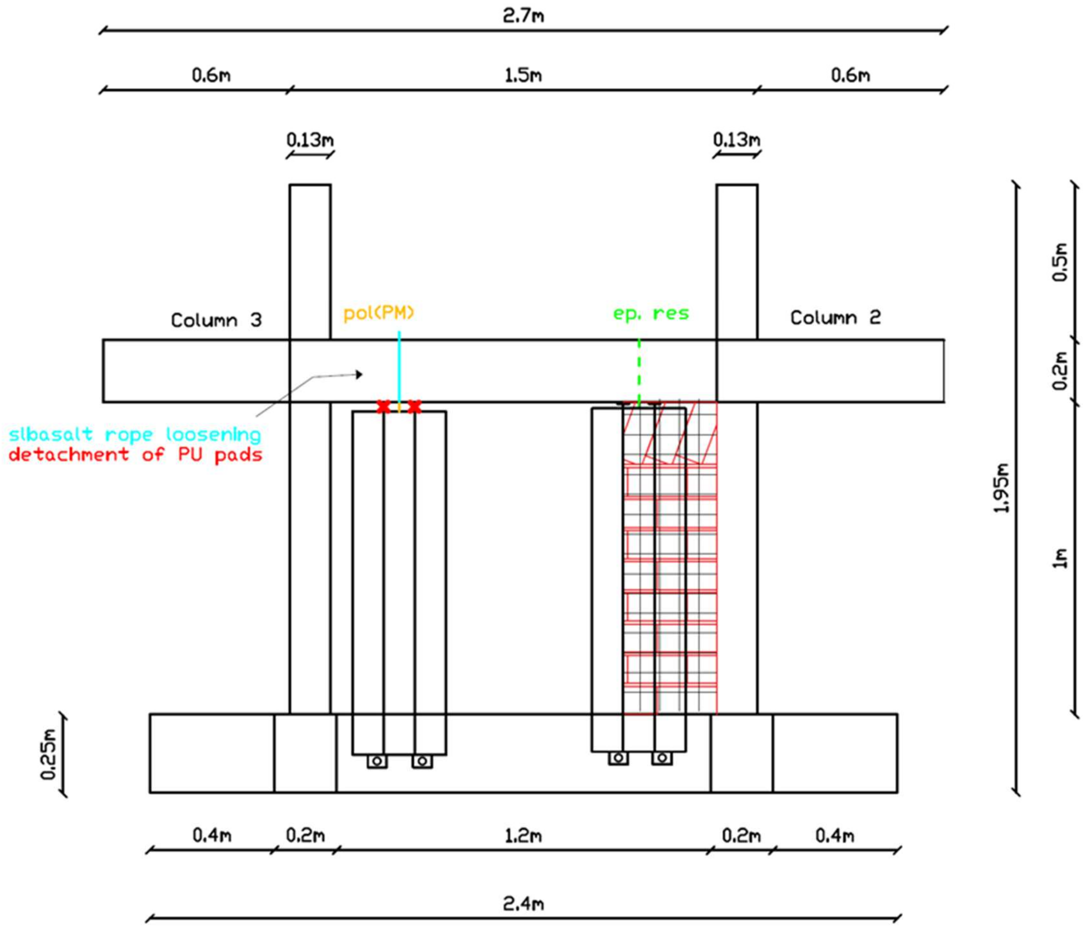

Figure 3.3.22 Observed damage after 1.3g(2) test: Left vertical living wall LW3-2L showed basalt rope loosening leading to detachment of PU *pads* allowing micromovements for low direct horizontal

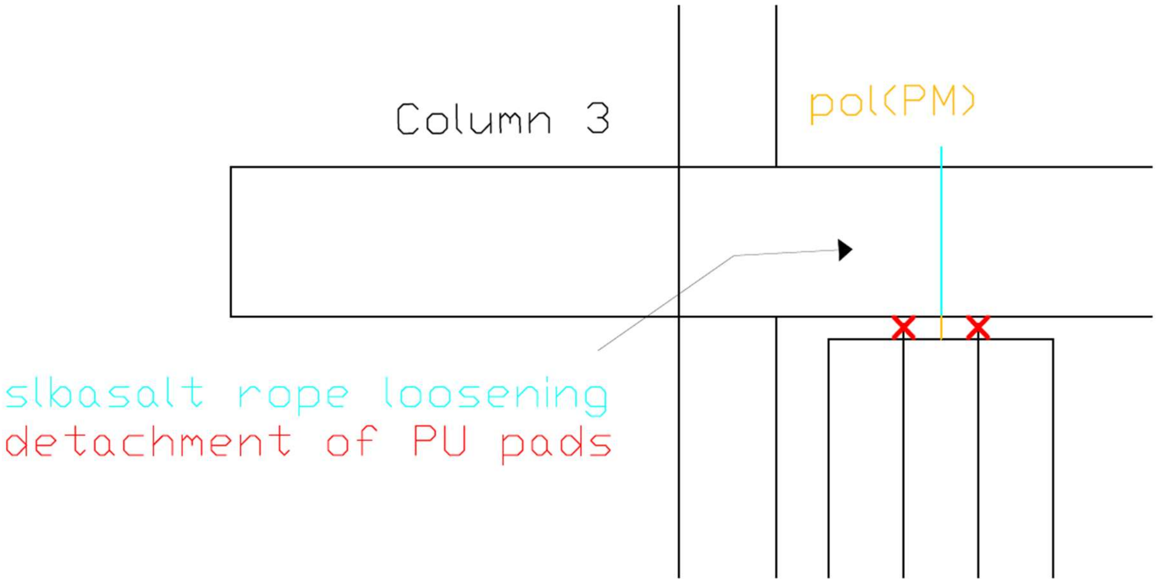

Figure 3.3.23 Anchoring details and PU pads dimensions (under the top slab), left living wall LW3-2L: detachment of PU pads after EQ1.3g (2)

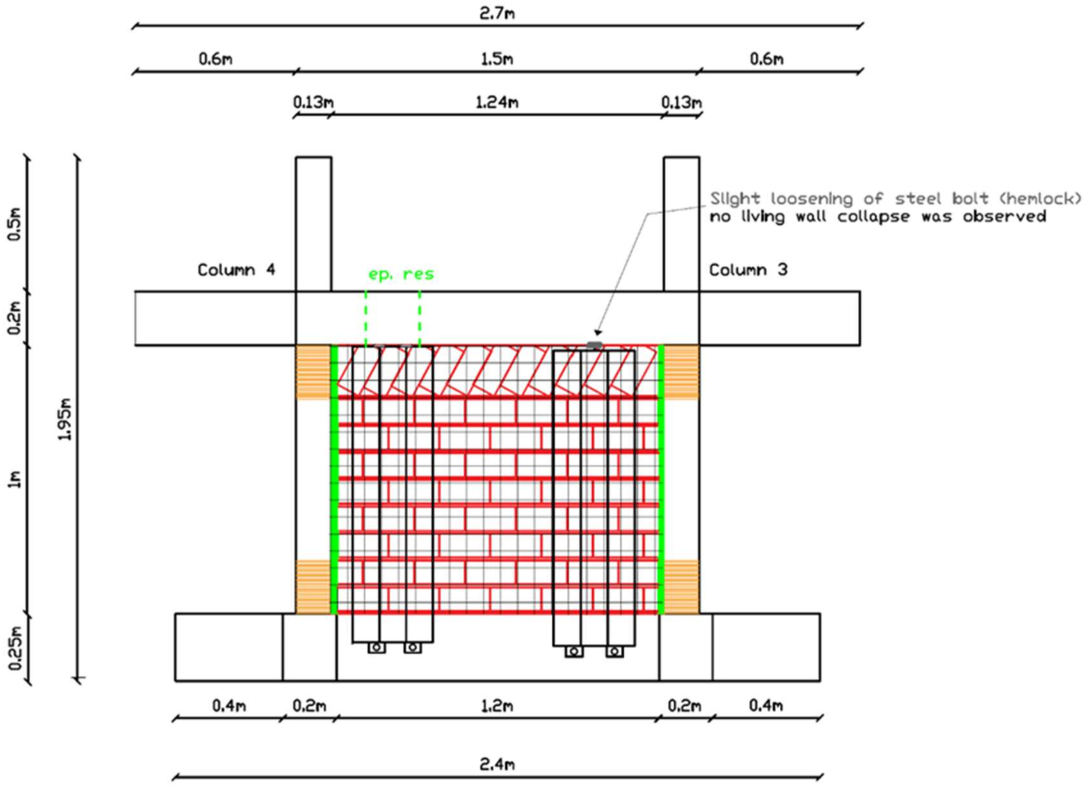

Figure 3.3.24 Observed damage after 1.3g(2) test: Steel rod (hemlock) slight loosening at the top of living wall LW3-4R allowing micromovements for low direct horizontal loads (frequent wind) but no living wall collapse was observed.

EQ1.4g

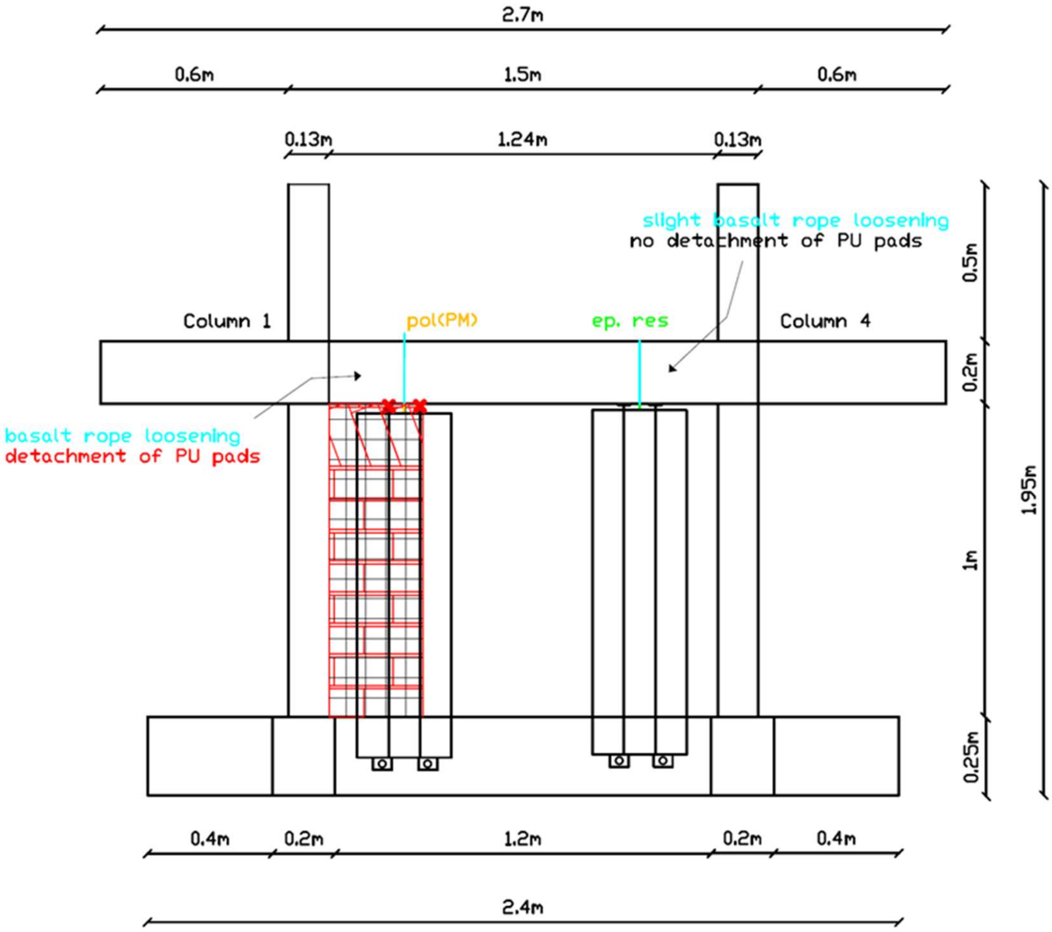

Figure 3.3.25 Observed damage after 1.4g test: Left living wall LW1-4L, showed basalt rope loosening leading to detachment of PU pads allowing micromovements for low direct horizontal loads (frequent wind) but no living wall collapse was observed. LW1-4R showed slight basalt rope loosening allowing

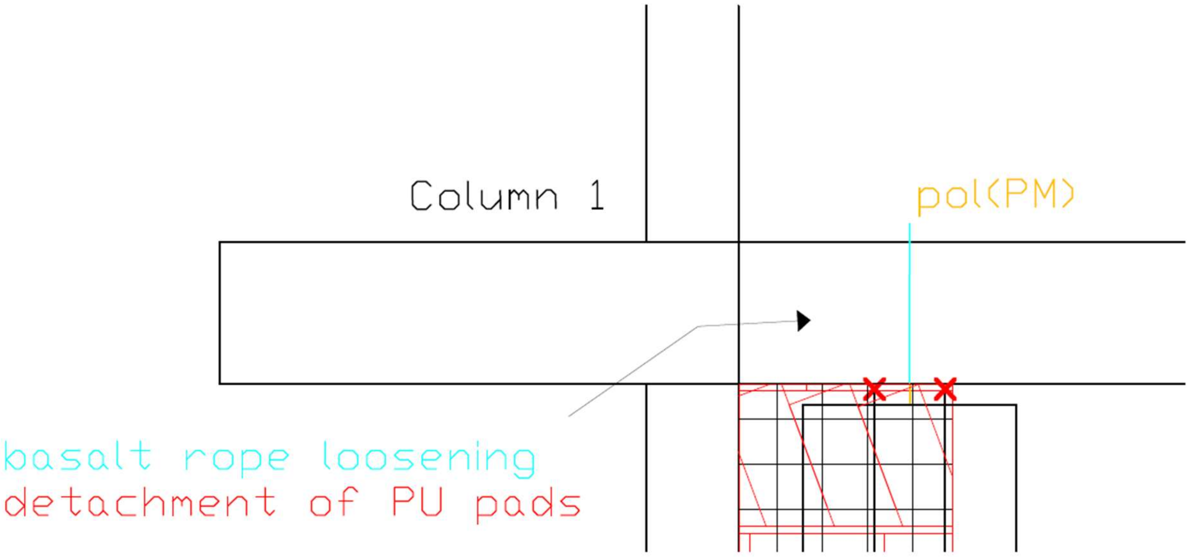

Figure 3.3.26 Anchoring details and PU pads dimensions (under the top slab), left living wall LW1-4L: detachment of PU pads after EQ1.4g

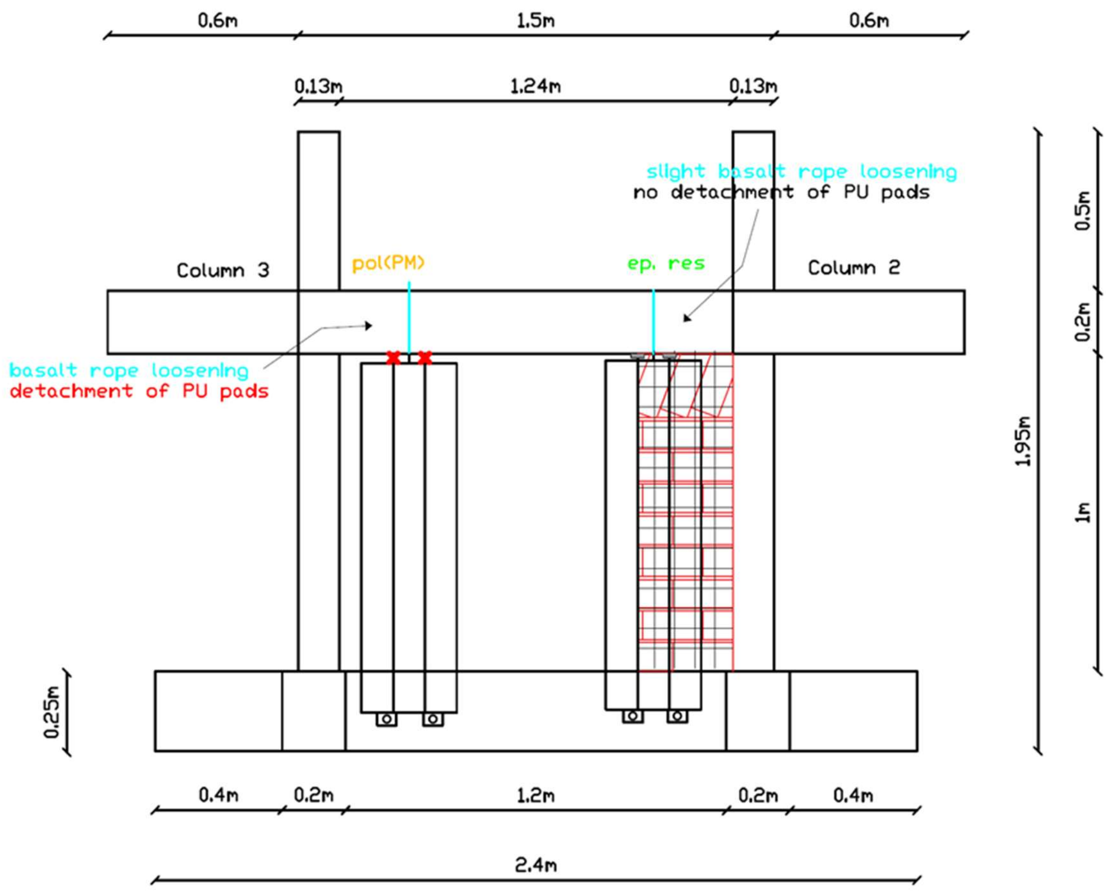

Figure 3.3.27 Observed damage after 1.4g test: Living walls LW2-3R showed slight basalt rope loosening allowing micromovements for high direct horizontal loads (severe wind), but no living wall collapse was observed. Left vertical living wall LW2-3L showed basalt rope loosening leading to detachment of PU pads allowing micromovements for low direct horizontal loads (frequent wind) but no living wall collapse was observed.

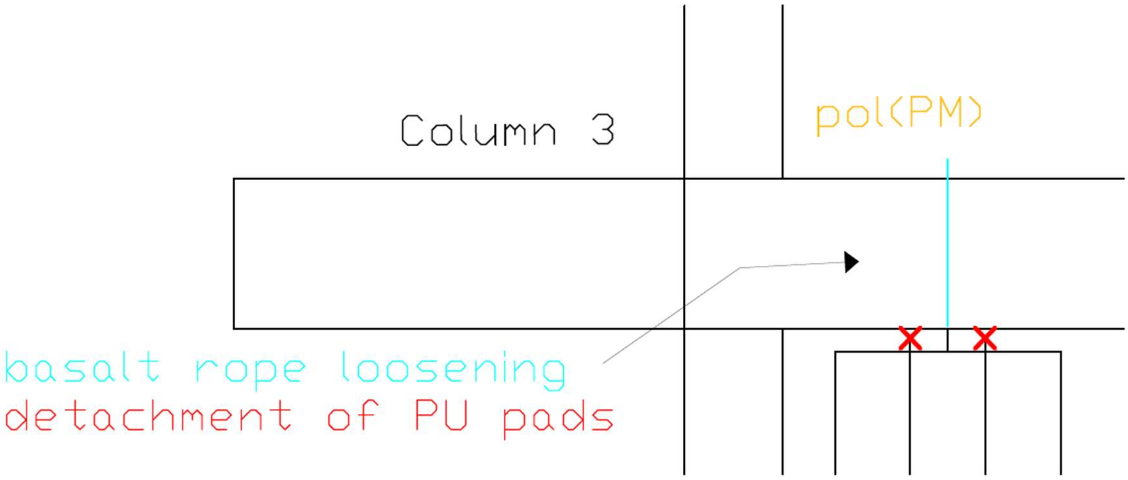

Figure 3.3.28 Anchoring details and PU pads dimensions (under the top slab), left living wall LW3-2L: detachment of PU pads after EQ1.4g

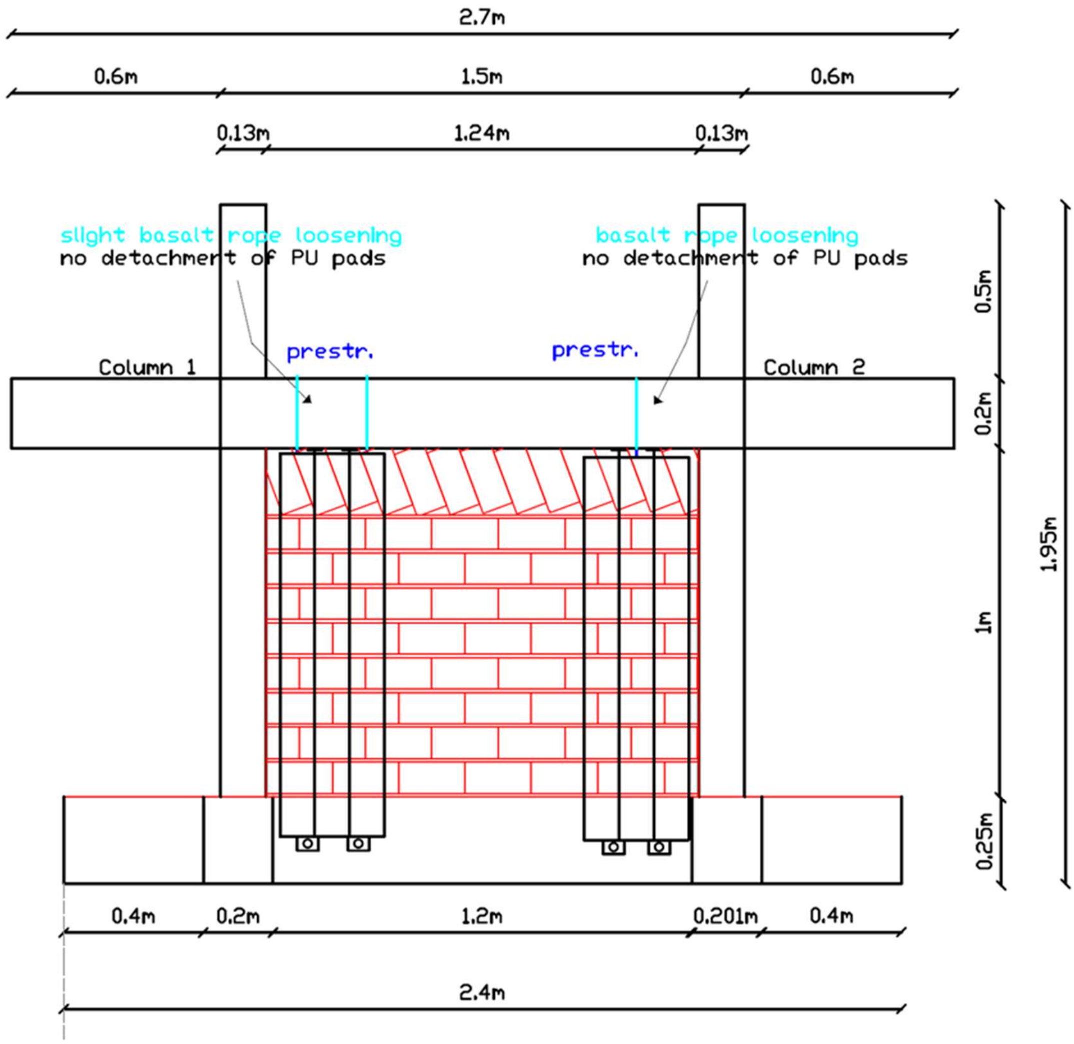

Figure 3.3.29 Observed damage after 1.4g test: Living walls LW1-2Lshowed slight basalt rope loosening allowing micromovements for high direct horizontal loads (severe wind), but no living wall collapse was observed. Living wall LW1-2R showed basalt rope loosening allowing micromovements for medium direct horizontal loads (intense wind), but no living wall collapse was observed.

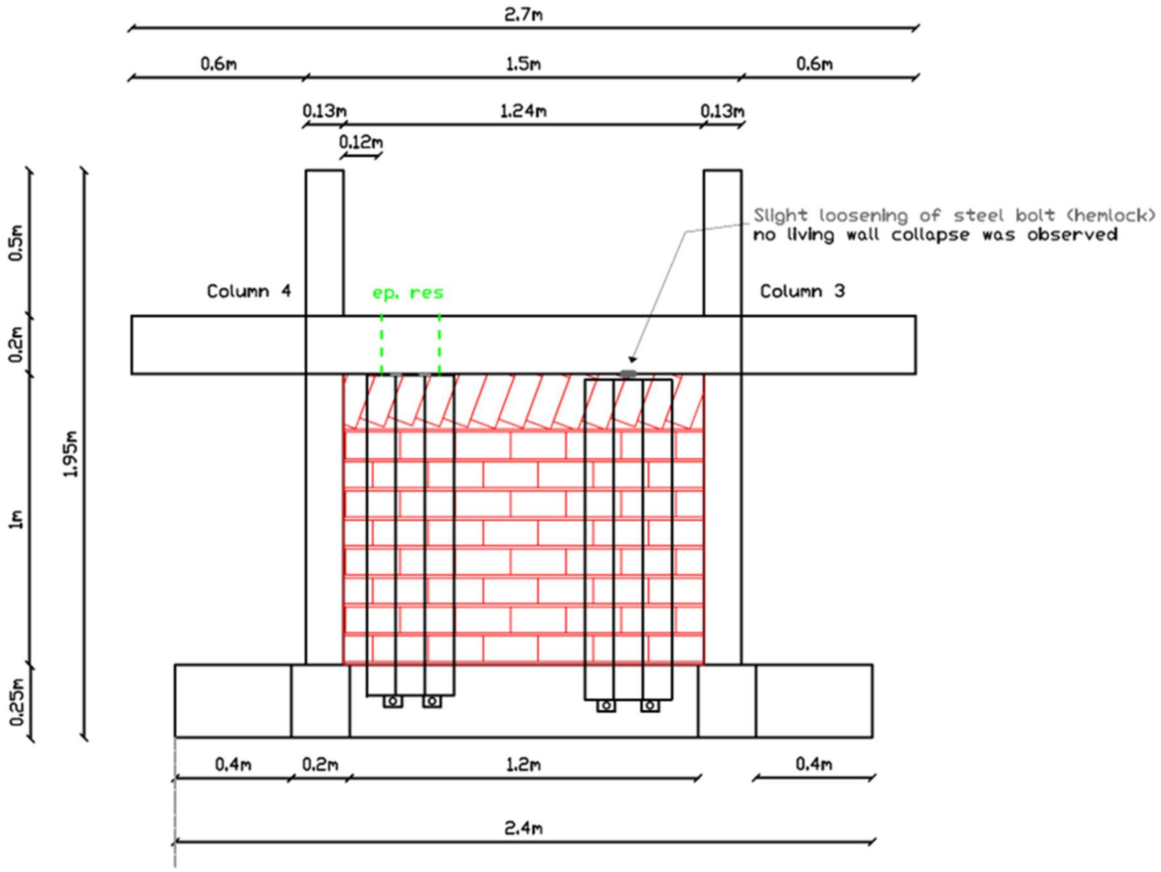

Figure 3.3.30 Observed damage after 1.4g test: Steel rod (hemlock) slight loosening at the top of living wall LW4-3R allowing micromovements for low direct horizontal loads (frequent wind) but no living wall collapse was observed.

Renovated Structure

After all seismic tests the partial brick infill 1- 4 suffered crushing of the bottom brick and local fracture of the FRPU jacket at the boundary between the crushed brick and the bottom foundation beam. The same is valid for partial brick infill 2 – 3. PUFJ between concrete columns and brick infills maintained their integrity without fracture or debonding. FRPU jackets maintained their bonding on the PUFJs, on the concrete and on the bricks. No failure of brick infills 1 – 2 and 4 – 3 (out of plane) was observed. The columns entered yielding strain of their longitudinal steel reinforcements at the bottom and at the top critical regions (columns 1, 2, 4). Damage with crushing of bottom brick at both partial infill walls occurred at very high displacement drift levels (2,62%), characteristic for rc structures at ULS, and for EQ1,4g. Therefore, the second phase of the seismic testing of the VF renovated structure is completed successfully, after the execution of 28 dynamic tests. The innovative renovations avoided partial or global collapse of the structure while at the end of all tests the structure showed extremely low stiffness around zero displacement drift. However, it reveals a recovery potential with negligible residual drift. The PZTs reveal remarkable sensitivity to the damage accumulation inside concrete core or at the brick – mortar joints, feeling also the rocking behavior of planters. PZT recordings coincide with photographic validation and observations and demonstrate the ability of the PZT-enabled SHM system to detect changes in the health condition at different locations after each loading sequence. The PZTs reveal remarkable sensitivity to the damage accumulation inside concrete core or at the brick – mortar joints, feeling also the rocking behavior of planters. PZT recordings coincide with photographic validation and observations and demonstrate the ability of the PZT-enabled SHM system to detect changes in the health condition at different locations after each loading sequence.

No severe damages before EQ1.1g was observed. After EQ1.1g cracks with debonding between bricks was noticed. After EQ1.3g, values of strain gauges showed that the columns entered yielding strain of their longitudinal steel reinforcements at the bottom. Crushing of bottom brick at partial infill wall 2-3 was observed. After EQ1.3g(2), damage with crushing of bottom brick at both partial infill walls occurred. The columns entered yielding strain of their longitudinal steel reinforcements at the bottom and at the top critical regions (columns 1, 2, 3, 4), according to strain gauges. PUFJ between concrete columns and brick infills maintained their integrity without fracture or debonding. FRPU jackets maintained their bonding on the PUFJs, on the concrete and on the bricks. No failure of brick infills 1 – 2 and 4 – 3 (out of plane) was observed. Finally, after EQ1.4g, damage with crushing of bottom brick at both partial infill walls occurred at very high displacement drift levels (2,62%). Local fracture of the FRPU jacket at the boundary between the crushed brick and the bottom foundation beam was noticed. Additional cracks at some mortar joints between bricks of the partial infill walls at their internal face (side with no FRPU jacket).

Figure 3.3.31 Observed damage after EQ1.3g test: The columns entered yielding strain of their longitudinal steel reinforcements at the bottom. Damage with crushing of bottom brick at partial infill wall 2-3

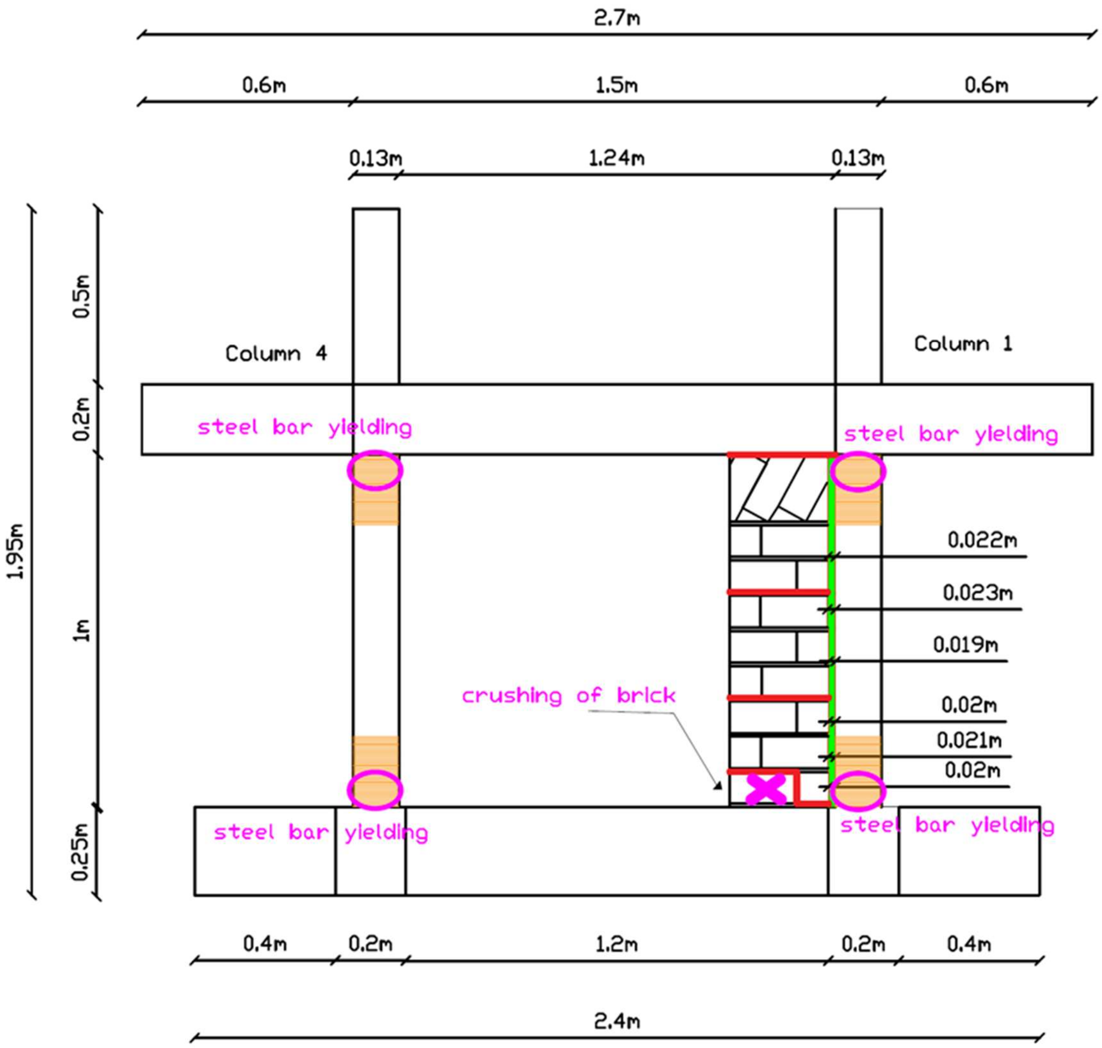

Figure 3.3.32 Observed damage after EQ1.3g(2) test: Damage with crushing of bottom brick at partial infill wall occurred. The columns entered yielding strain of their longitudinal steel reinforcements at the bottom and at the top critical regions (columns 1, 4).

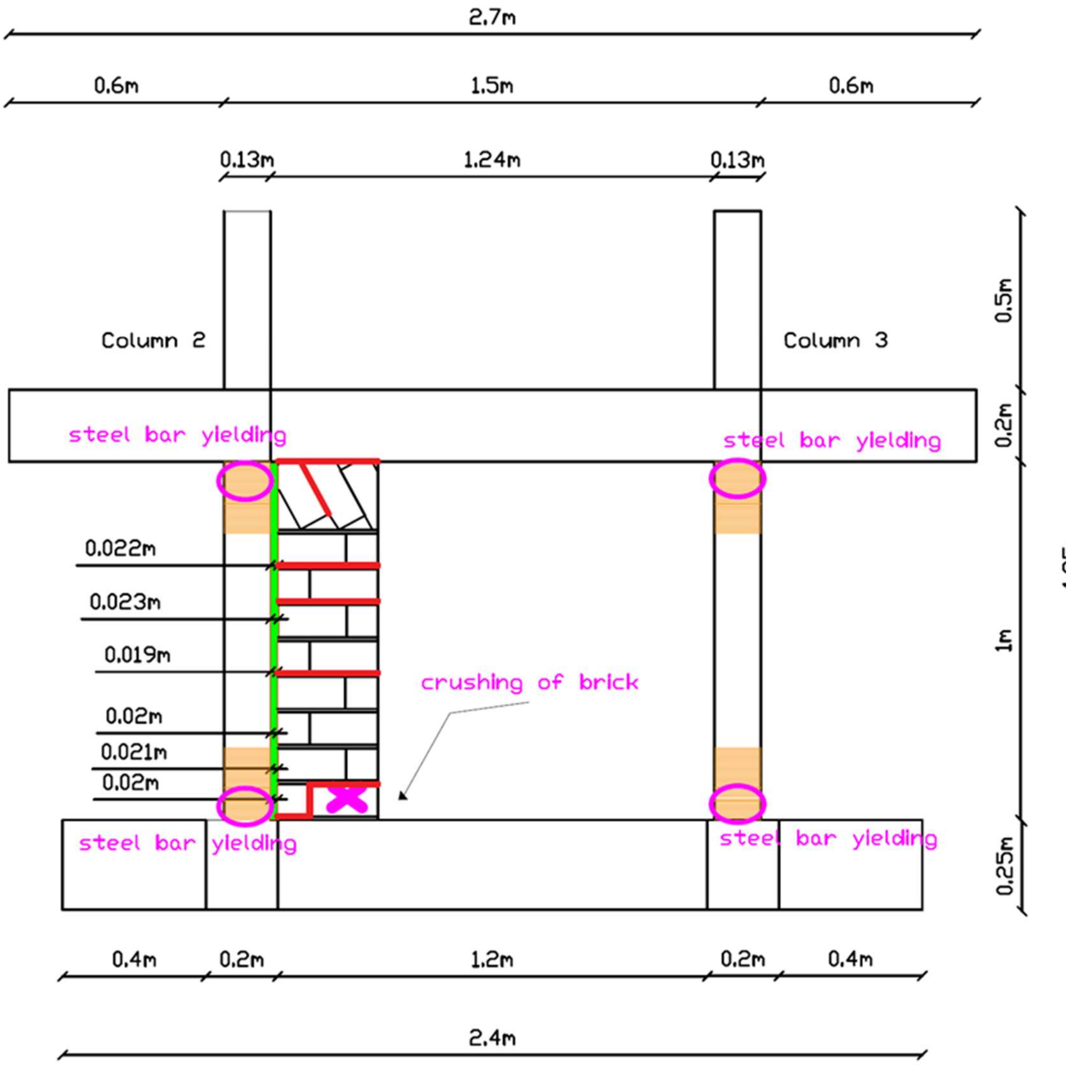

Figure 3.3.33 Observed damage after EQ1.3g(2) test: Damage with crushing of bottom brick at partial infill wall occurred. The columns entered yielding strain of their longitudinal steel reinforcements at the bottom and at the top critical regions (columns 2, 3).

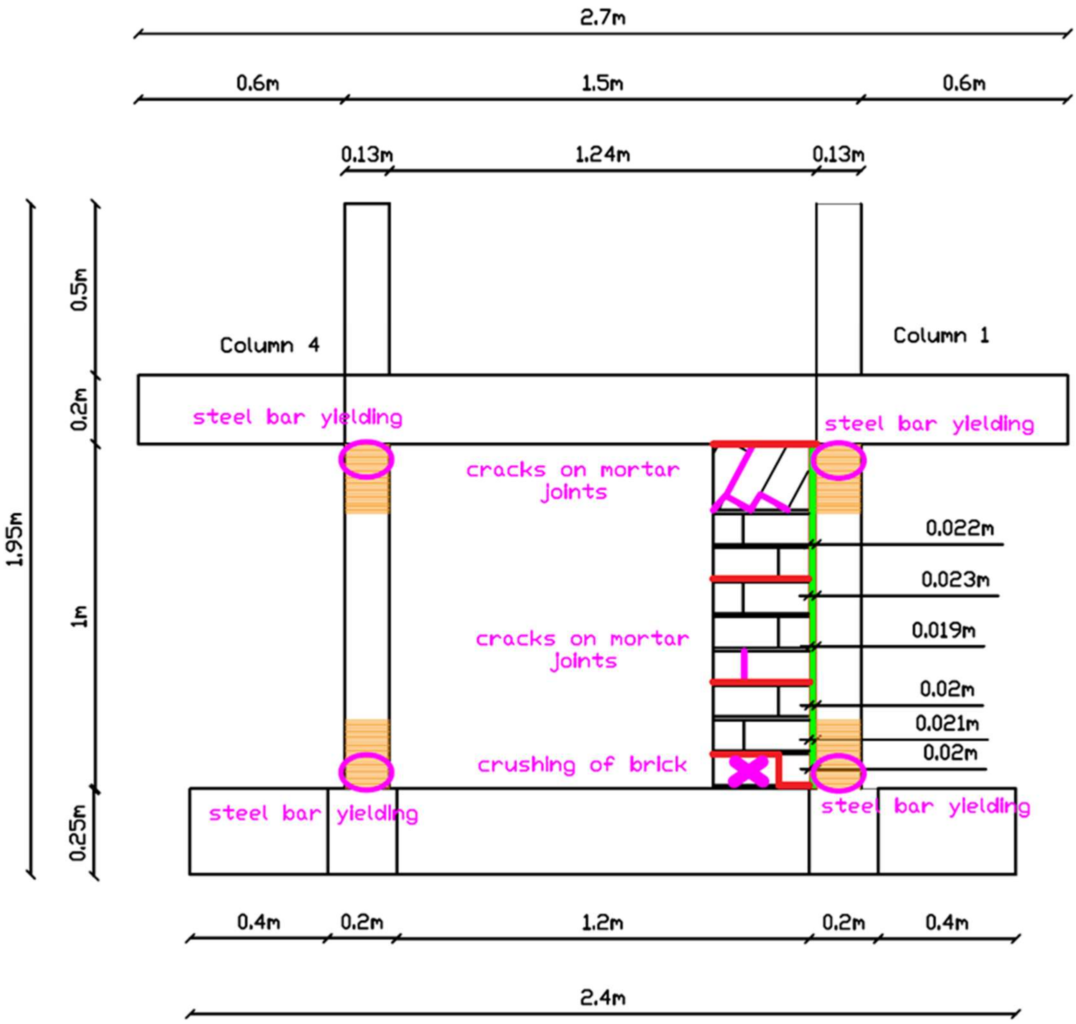

Figure 3.3.34 Observed damage after EQ1.4g test: Damage with crushing of bottom brick at both partial infill walls occurred at very high displacement drift levels (2,62%). Local fracture of the FRPU jacket at the boundary between the crushed brick and the bottom foundation beam. Additional cracks at some mortar joints between bricks of the partial infill walls at their internal face (side with no FRPU jacket). The columns entered yielding strain of their longitudinal steel reinforcements at the bottom and at the top critical regions (columns 1, 2, 3, 4).

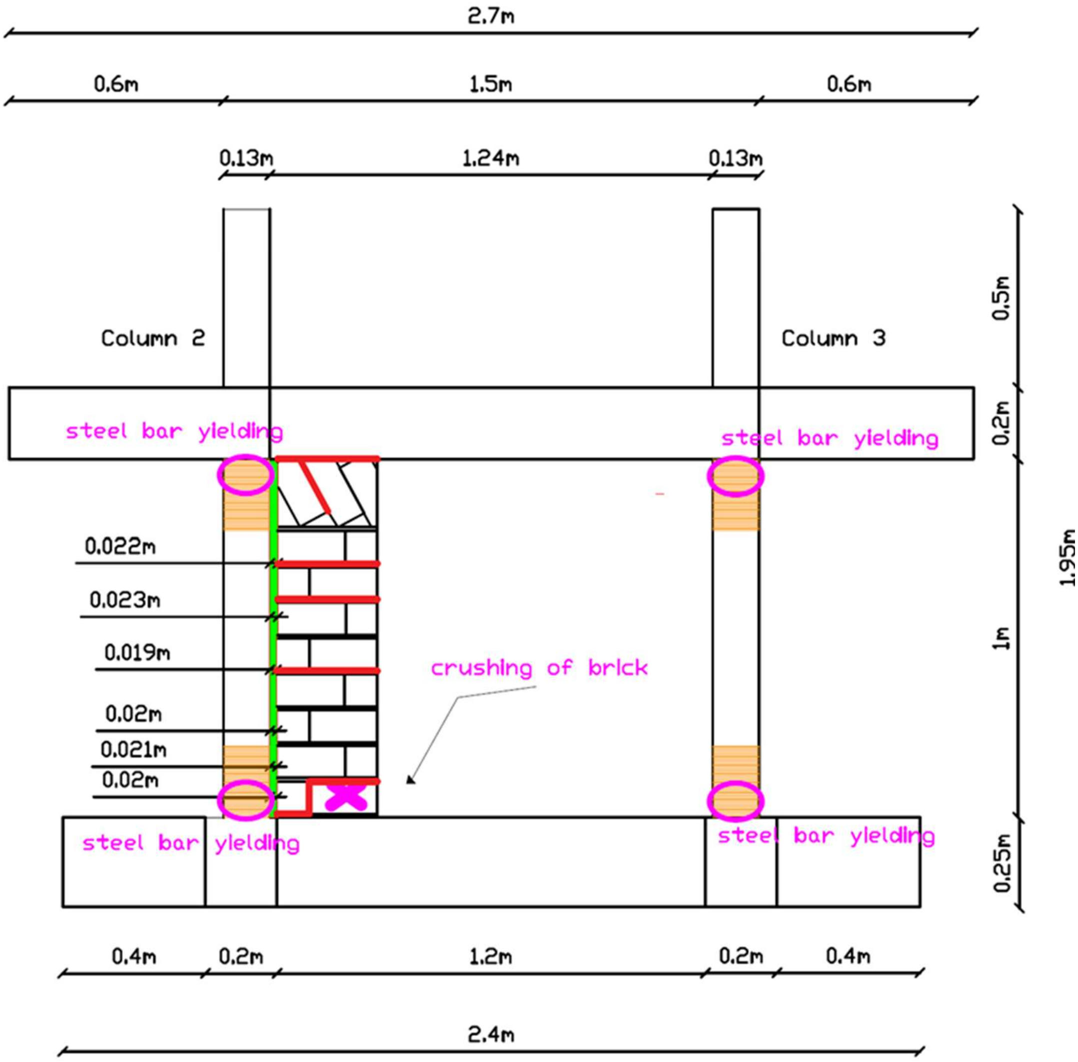

Figure 3.3.35 Observed damage after EQ1.4g test: Observed damage after 1.4g test: Damage with crushing of bottom brick at both partial infill walls occurred at very high displacement drift levels (2,62%). Local fracture of the FRPU jacket at the boundary between the crushed brick and the bottom foundation beam. Additional cracks at some mortar joints between bricks of the partial infill walls at their internal face (side with no FRPU jacket). The columns entered yielding strain of their longitudinal steel reinforcements at the bottom and at the top critical regions (columns 1, 2, 3, 4).

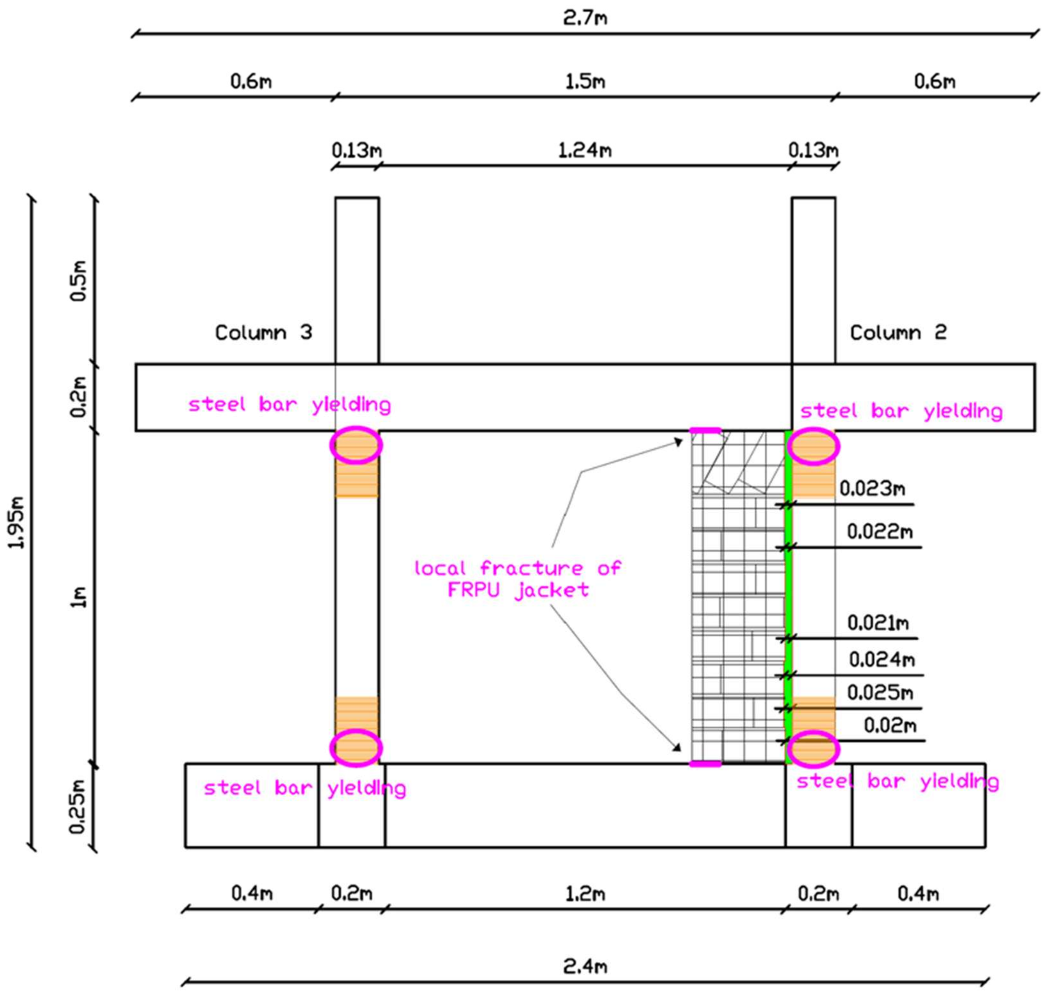

Figure 3.3.36 Observed damage after EQ1.4g test: Observed damage after 1.4g test: Damage with crushing of bottom brick at both partial infill walls occurred at very high displacement drift levels (2,62%). Local fracture of the FRPU jacket at the boundary between the crushed brick and the bottom foundation beam. Additional cracks at some mortar joints between bricks of the partial infill walls at their internal face (side with no FRPU jacket). The columns entered yielding strain of their longitudinal steel reinforcements at the bottom and at the top critical regions (columns 1, 2, 3, 4).

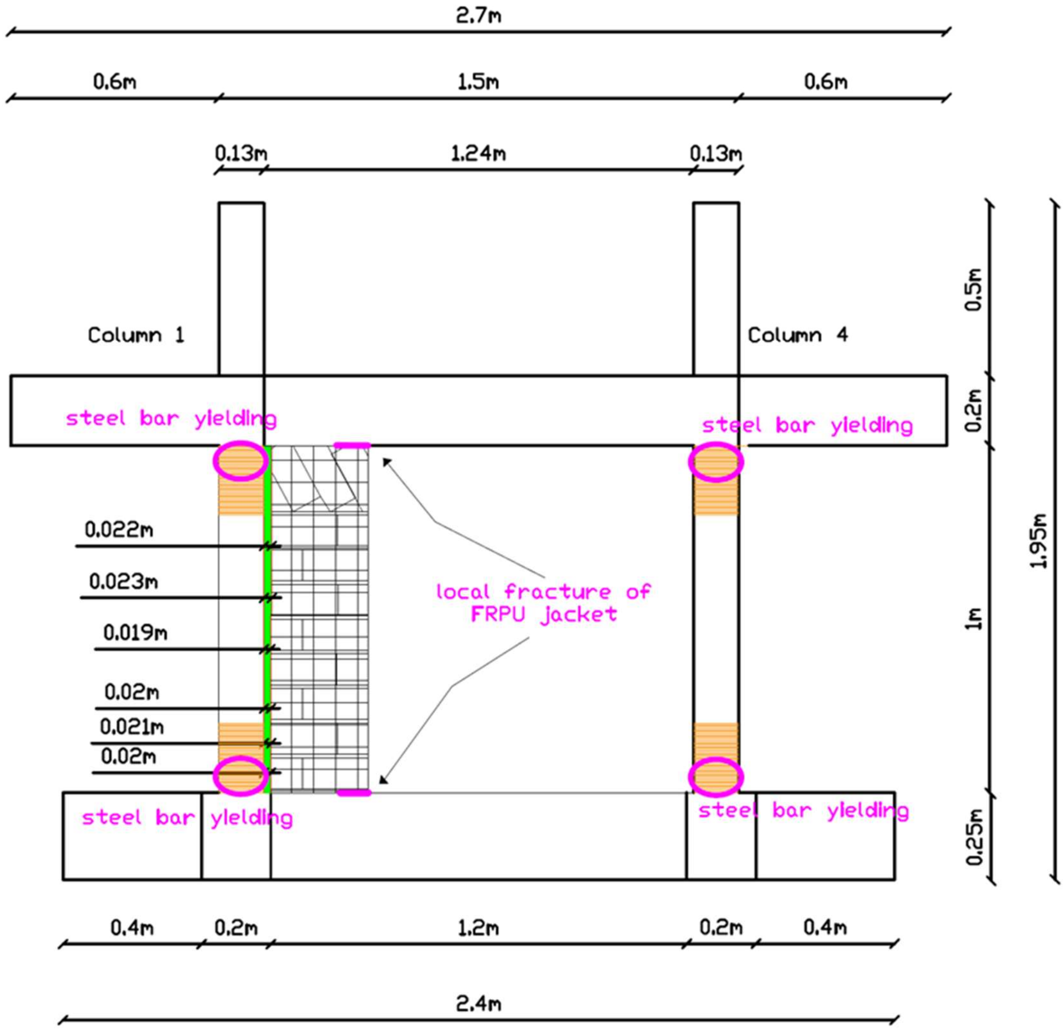

Figure 3.3.37 Observed damage after EQ1.4g test: Observed damage after 1.4g test: Damage with crushing of bottom brick at both partial infill walls occurred at very high displacement drift levels (2,62%). Local fracture of the FRPU jacket at the boundary between the crushed brick and the bottom foundation beam. Additional cracks at some mortar joints between bricks of the partial infill walls at their internal face (side with no FRPU jacket). The columns entered yielding strain of their longitudinal steel reinforcements at the bottom and at the top critical regions (columns 1, 2, 3, 4).


(a) (b) (c) (d)

Figure 3.3.38 Characteristic observed damage after all seismic tests: (a) interior side of wall infill 1-4 parallel to the direction of movement of seismic table (b) wall infill 2-3 parallel to the direction of movement of seismic table (c) Interior top side of wall infill 1-4, parallel to the direction of movement of the seismic table (d) detachment of PU pads

3.4 Assessment of the performance of the tested as-built VF renovated structure using PZT sensors

The proposed methodology for real-time damage assessment in reinforced concrete (RC) structures using piezoelectric (PZT) sensors offers significant potential for early detection of damage and the provision of critical failure warnings before visible signs appear. The system utilizes a total of 48 PZT sensors, installed both internally and externally on the structure prior to renovation. Extra PZTs are installed as patches at specific locations to monitor the health of the retrofits and the connection (anchoring) of the structures created by the presence of the vertical forest. More specifically, 13 extra PZTs were placed on the strengthened structure, for a total of 61 PZT sensors used to evaluate the structural performance of the renovated frame structure.

Measurements obtained via the EMI method reflect the electromechanical response of PZT patches. Analyzing these signals using statistical methods helps convert changes between healthy and potentially damaged states into damage index metrics, aiding in structural health assessment. Integrating advanced monitoring technologies into retrofitting applications provides valuable insights into the performance and durability of the retrofit system (Naoum et al. 2024, Papadopoulos at al. 2023, 2024, Zapris et al. 2023).

By applying statistical methods, variations in EMI signatures can be translated into numerical indices. One of the most widely used indices in the literature is the Root Mean Square Deviation (RMSD). This damage index is considered one of the most effective and reliable metrics across various fields of Structural Health Monitoring (SHM) (Voutetaki et al. 2016, Chalioris et al. 2020, Chalioris et al. 2021, Na and Baek, 2018). The damage index of RMSD was applied for the statistical analysis of the EMI responses:

$$\mathrm{RMSD} = \sqrt{\frac{\sum_1^M \left(\left|V_p(f_r)\right|_D - \left|V_p(f_r)\right|_0\right)^2}{\sum_1^M \left(\left|V_p(f_r)\right|_0\right)^2}}$$

Where $\left|V_p(f_r)\right|_0$ is the absolute value of the voltage output signal as extracted from the PZT at the healthy pristine state of the specimen, $\left|V_p(f_r)\right|_D$ is the absolute value of the corresponding voltage output signal as measured from the same PZT at any damage level, and M is the number of measurements in the frequency band. Each SHM device records the EMI response of a PZT sensor within a specified frequency range of 10 to 240 kHz, using a resolution of 1 kHz.

In assessing the structural condition of the Vertical Forest (VF) structure, the well-established statistical index, Root Mean Square Deviation (RMSD), is used. The healthy state recorded is the baseline measurement for each PZT sensor, used in the RMSD statistical analysis. Here in the healthy pristine state of the specimen is considered the PZT recording after the completion of all renovations with basalt rope wrapping, PUFJ, FRPU jacketing, vertical living wall or planter attachment and before any seismic table excitations of the second phase. Changes in the frequency response signals caused by damage are assessed through the RMSD index, with different values indicating structural damage.

Higher RMSD values suggest the presence of damage. It was observed that elevated RMSD values were not present in the PZTs situated in regions where no cracking was detected.

RMSD values are calculated from the absolute voltage output responses and utilized to assess the effectiveness of the SHM method in damage detection and evaluation. For this purpose, Figures 3.4.1 το 3.4.16 illustrate the range of RMSD values calculated based on the PZT voltage output signals from most of the PZT sensors inside and on the renovated structure.

No significant values were observed in the RMSD indices for the PZT cases installed on the beams, where no structural damage was detected. However, there is a trend of increasing RMSD values that could trigger further actions to assess internal micro damages in the beams. The same is valid for the slab sensors. The PZT installed in the middle of the slab, shows increased RMSD values, indicating that damage has developed in this vicinity. The PZTs reveal remarkable sensitivity to the damage accumulation inside the concrete core feeling the rocking behavior of planters. Lower values were observed in the RMSD for the PZT cases installed on the edge of the slab.

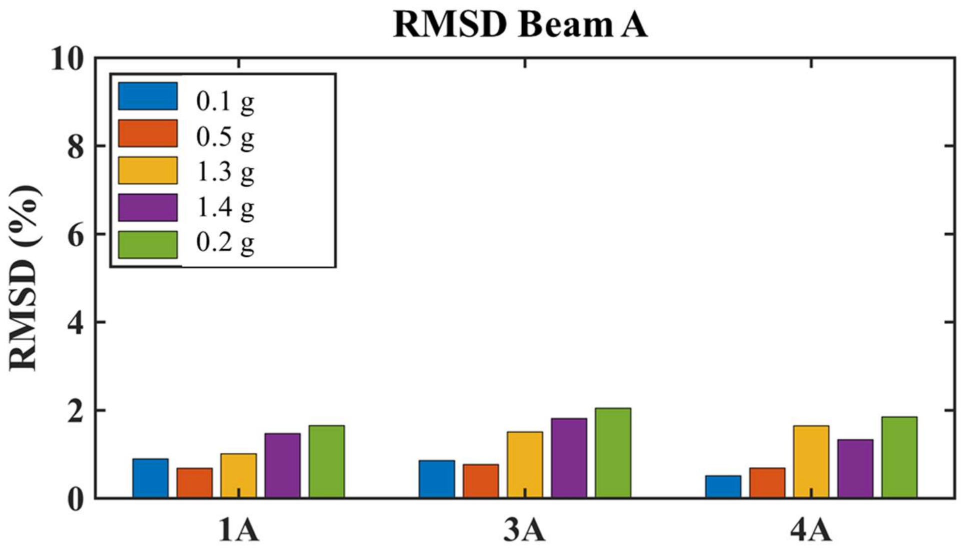

Figure 3.4.1: Voltage frequency responses of the PZT sensors inside beam B14

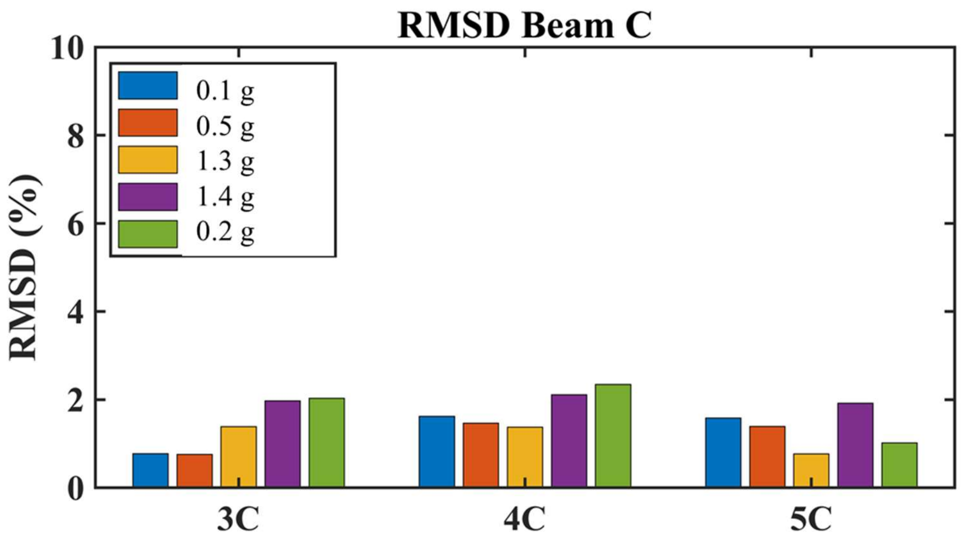

Figure 3.4.2: Voltage frequency responses of the PZT sensors inside beam B12

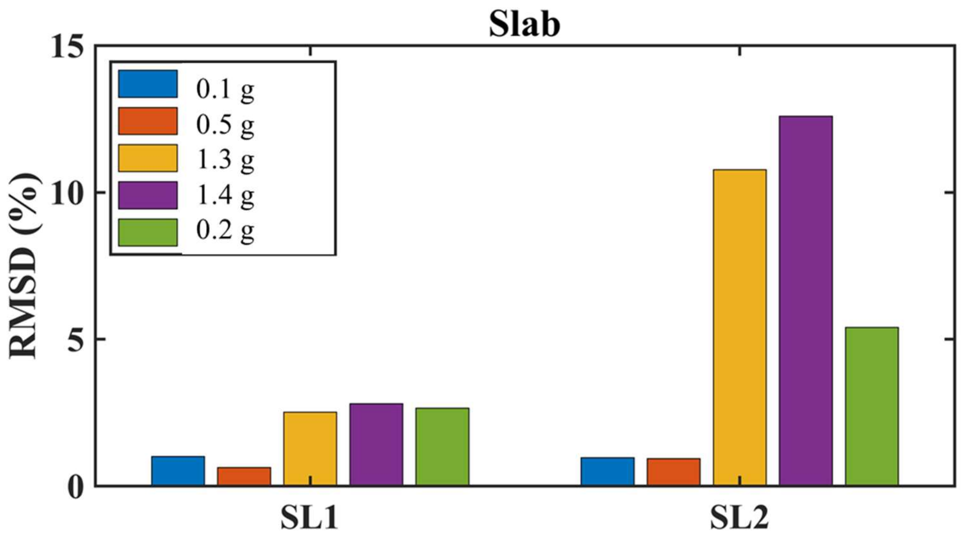

Figure 3.4.3: Voltage frequency responses of the PZT sensors inside the slab

All columns show increased RMSD values at all areas (down, mid, up), indicating that increasing additional damage has developed within concrete core (added to the damage of phase A). After 1.3g, all columns exhibited higher RMSD values compared to excitations 0.1g and 0.5g. Following the 1.3g excitation, the PZT sensors recorded higher RMSD values compared to the 0.1g and 0.5g excitations. Notably, the RMSD values show an increasing trend in the response from the 1.3g excitation onward, continuing through the subsequent 1.3g and 0.2g excitations (especially in column 3). Relatively lower RMSD values in columns 1 and 2 compared with the ones in columns 3 and 4 may denote that basalt rope wrapping together with PUFJ and FRPU jacketed infills in two directions (full and partial infill in columns 1 and 2) could restrict better additional concrete core disintegration within the critical regions of columns (than in columns 3 and 4 with only full infill).

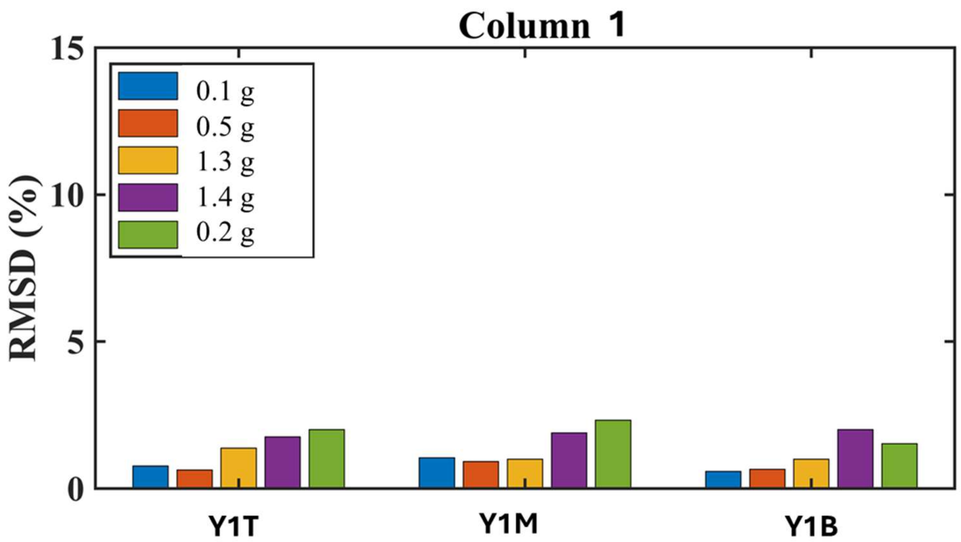

Figure 3.4.4: Voltage frequency responses of the PZT sensors inside column 1 (Top, Middle, Bottom)

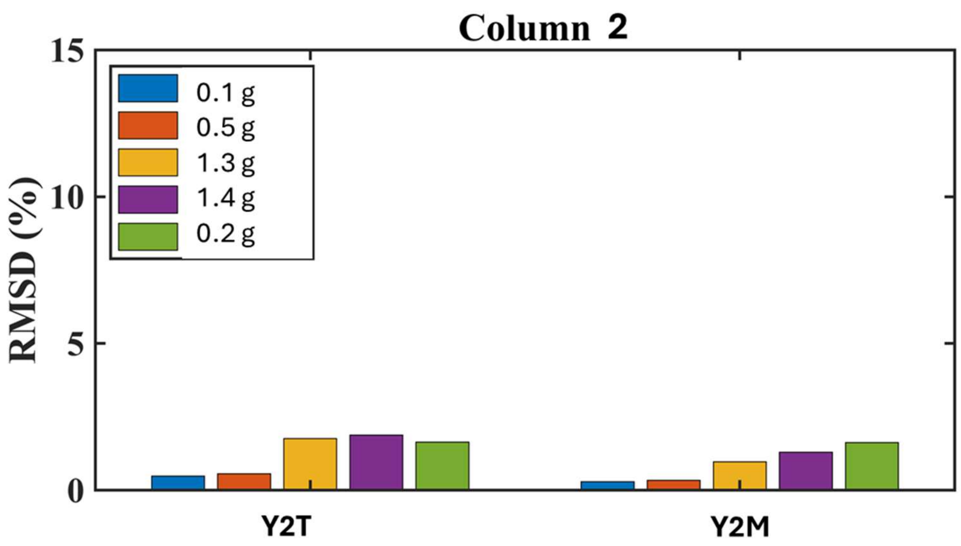

Figure 3.4.5: Voltage frequency responses of the PZT sensors inside column 2 (Top, Middle)

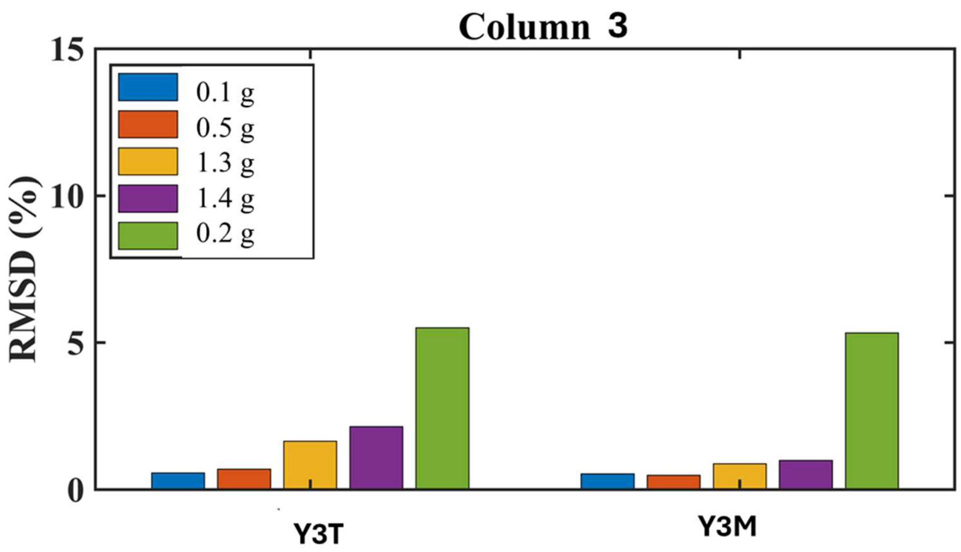

Figure 3.4.6: Voltage frequency responses of the PZT sensors inside column 3 (Top, Middle,)

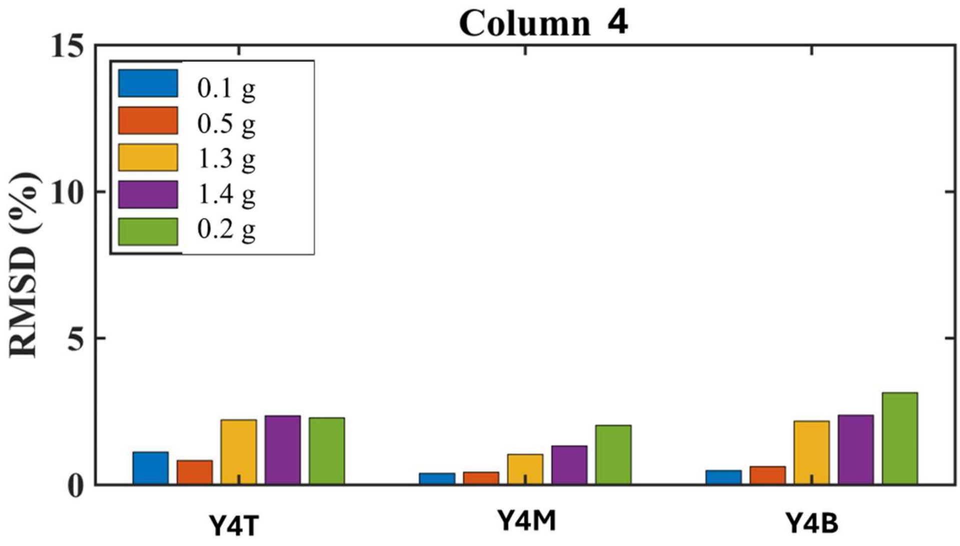

Figure 3.4.7: Voltage frequency responses of the PZT sensors inside column 4 (Top, Middle, Bottom)

Slight differences were observed in the RMSD of PZTs installed on the surface of the partial infill walls and full infill wall within the polyurethane. After EQ1.3g, the RMSD values are higher regarding the excitations EQ0.1g and EQ0.5g.

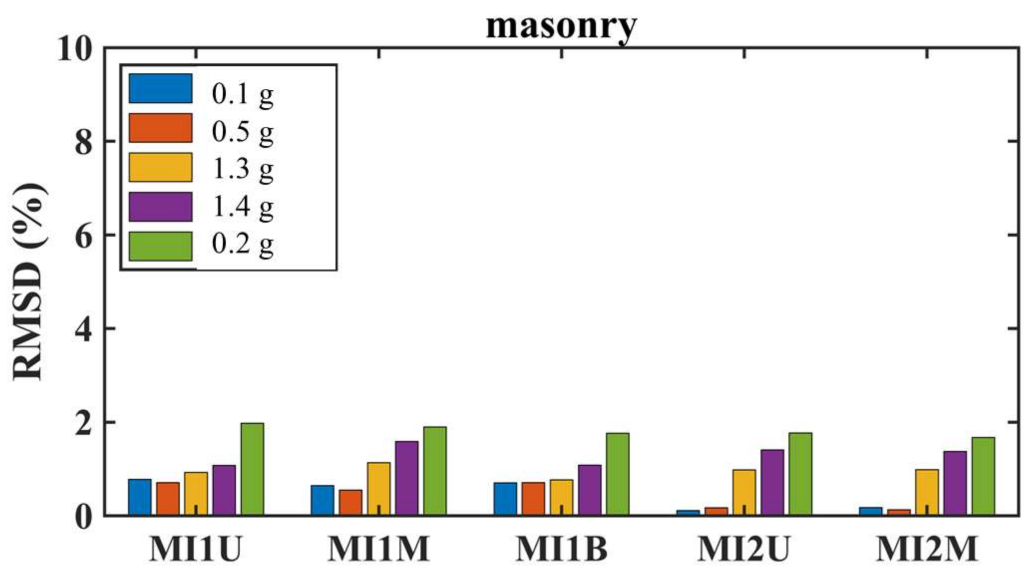

Figure 3.4.8: Voltage frequency responses of the PZT sensors on partially infilled walls (Upper, Middle, Bottom)

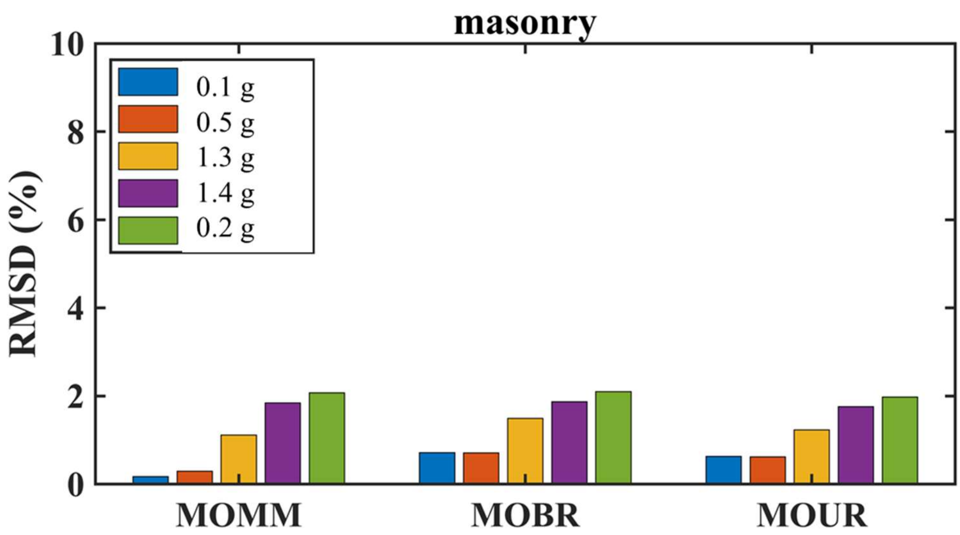

Figure 3.4.9: Voltage frequency responses of the PZT sensors on full Infill wall between columns 1-2

PZT patches are installed at the surface of RC column 1, MORJPuT at the infill wall and MI1JPuT at the partial infill wall. Elevated RMSD values were recorded at the PZTs after more intense excitations, which were externally attached to the **surface of Column** Y1 at the top, particularly for the partial infill wall (in-plane).

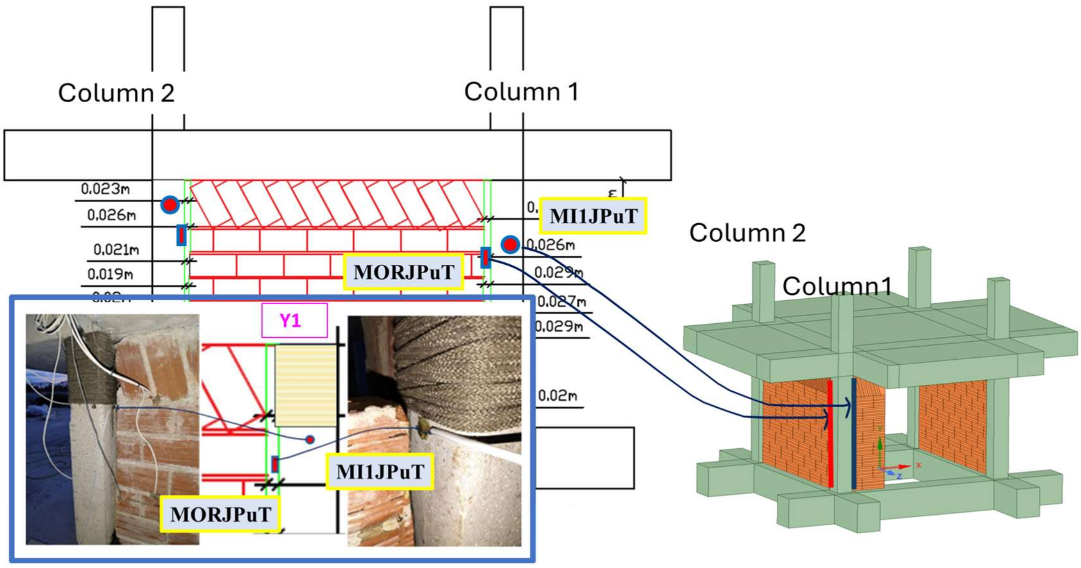

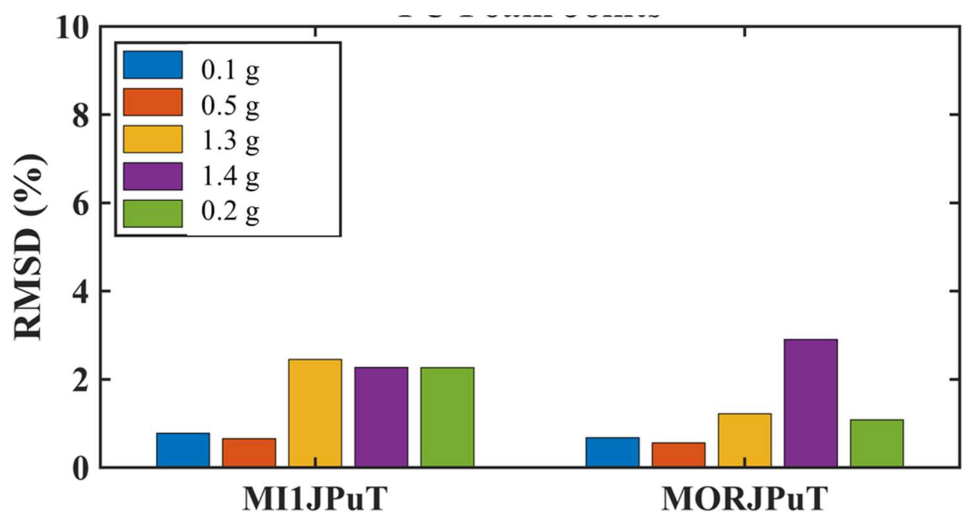

Figure 3.4.10: Voltage frequency responses of the PZT sensors placed on top of column 1 : MORJPuT at the infill wall and MI1JPuT at the partial infill wall

PZT patches were externally attached to the basalt ropes at the top of the living wall, anchored to the roof using resin on basalt ropes. They showed no significant changes in voltage frequency response and exhibited relatively low RMSD values while capturing the increasing trend with increasing seismic intensity. The recordings align with the observation that no collapse of the living walls LW2-3R (VFAnBF, close to column 2) and LW1-4R (VFAnBS, close to column 4) occurred (fig. 3.4.11) while the basalt ropes suffered higher tension for higher seismic intensity. PZT patches installed on the anchoring metal structure of planter 1 (VFZnS) exhibited elevated RMSD values after 1.3g excitation which agrees with the slight loosening of the steel rod (anchoring of the planter, figure 3.4.11 and figure 3.3.11).

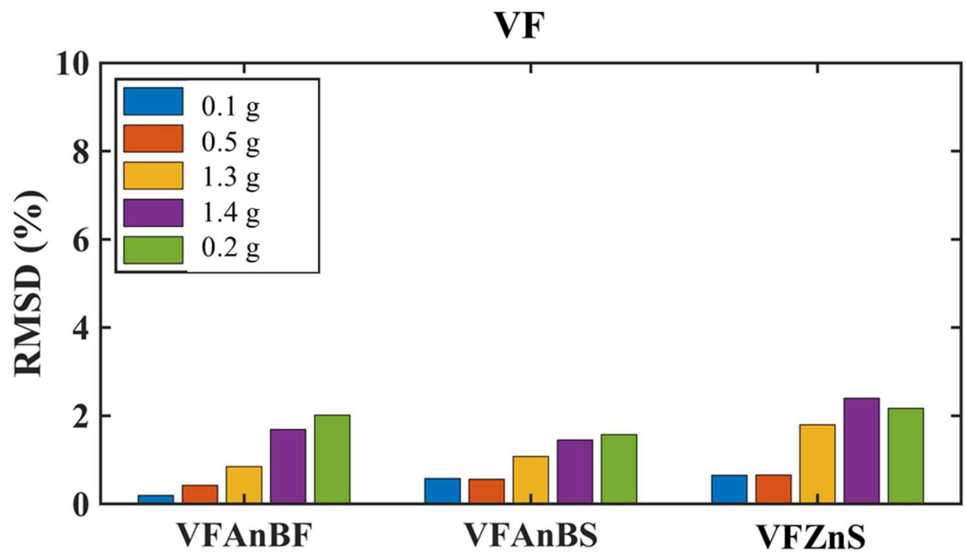

Figure 3.4.11: Voltage frequency responses of the PZT sensors (column 2: VFAnBF, LW2-3R, column 4: VFAnBS, LW1-4R anchoring metal structure for living wall as well as anchoring metal structures for planter 1, VFZnS)

H.F.R.I. Hellenic Foundation for Research & Innovation
Greece 2.0 NATIONAL RECOVERY AND RESILIENCE PLAN
Funded by the European Union NextGenerationEU
GREENERGY

PZT patches installed on basalt rope wrap of columns 3 and 4 exhibit different voltage frequency responses compared to usual. While the efficacy of the EMI method for SHM in reinforced concrete (RC) structural elements has been thoroughly examined in the literature, a notable research gap exists concerning its investigation for materials such as basalt. The PZT recordings capture the increasing trend of basalt tightening despite the extremely low strain values measured in table 3.1.1t.

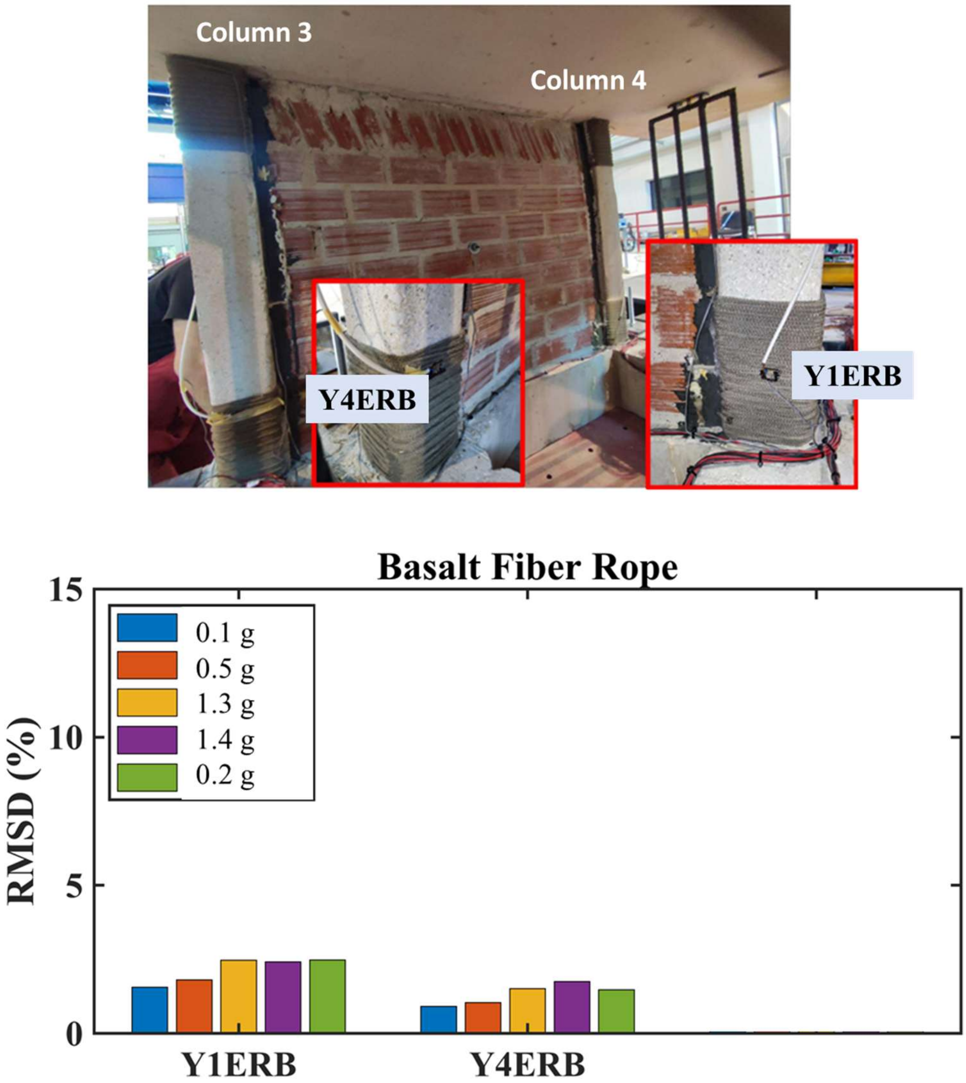

Figure 3.4.12: Voltage frequency responses of the PZT sensors externally attached (Y4ERB and Y1ERB – columns 3 and 4 bottom) on the basalt rope

Figures 3.4.13 to 3.4.16 illustrate the range of RMSD values calculated based on the PZT voltage output signals from the PZT sensors inside the columns at all loading states compared to the healthy state. The RMSD values exhibit an increasing trend from excitation 0.1g to the subsequent seven excitations.

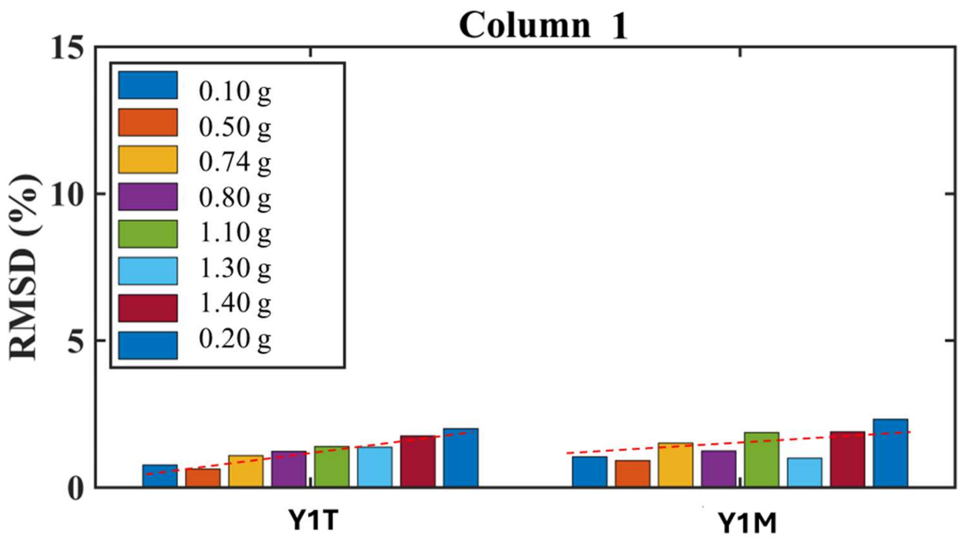

Figure 3.4.13: Voltage frequency responses of the PZT sensors inside column 1 (Top, Middle) at all excitations

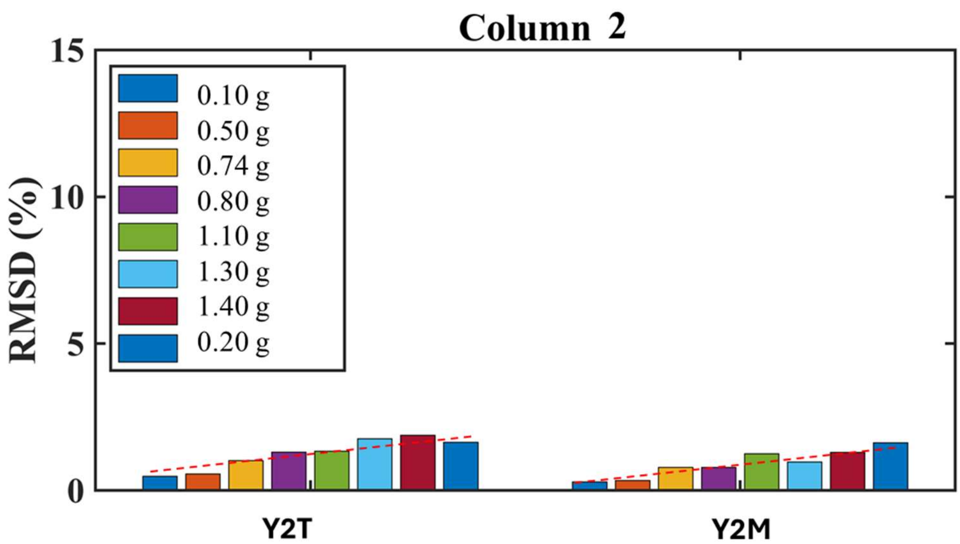

Figure 3.4.14: Voltage frequency responses of the PZT sensors inside column 2 (Top, Middle) at all excitations

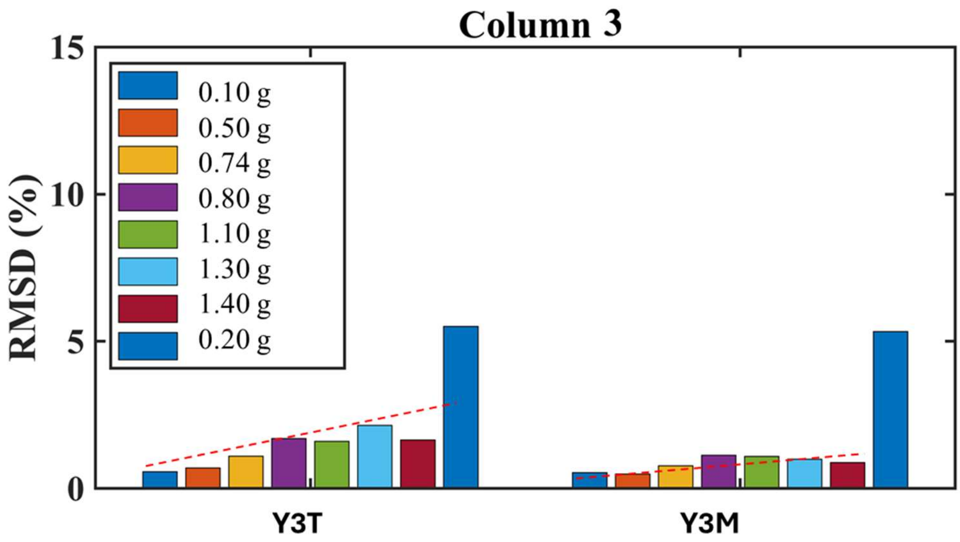

Figure 3.4.15: Voltage frequency responses of the PZT sensors inside column 3 (Top, Middle) at all excitations

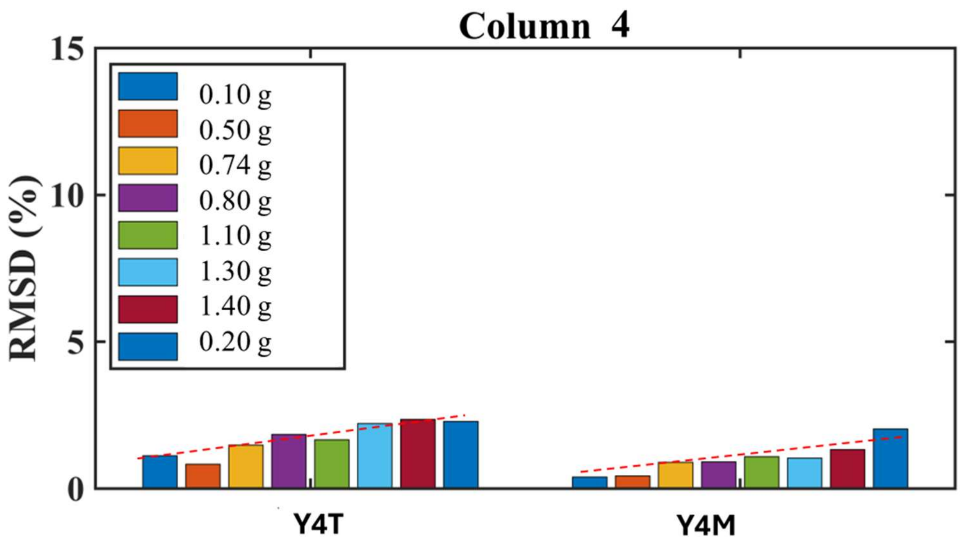

Figure 3.4.16: Voltage frequency responses of the PZT sensors inside column 4 (Top, Middle) at all excitations

These results support the effectiveness and reliability of the implemented instrumentation and the adopted EMI-based monitoring method for structural health assessment.

4 Conclusions

The report cites all critical results from the different accelerometers, relative top and bottom accelerations and displacement drifts of the structure during each testing. Further, numerous strain gauges glued at different positions of longitudinal steel bars within critical regions of columns, allow for straight foreword assessment of their axial strain level.

The detailed assessment of the renovated structure after the second phase of testing concludes that the partial infill walls suffer bed joint cracking. Damage with crushing of bottom brick at both partial infill walls occurred. No further disintegration of brick infills 1 – 2 and 4 – 3 (out of plane) was observed. No collapse of brick infills was observed for severe seismic excitations, higher than 2g. The columns entered yielding strain of their longitudinal steel reinforcements at the bottom and at the top critical regions (columns 1, 2, 3, 4), leading to a ductile behavior, without disintegration of the concrete core under compression. Basalt rope wrapping of the columns, together with PUFJs and FRPU jacketing of the brick infills resulted in a resilient renovation allowing for interesting damage redistribution and damage barrier mechanisms (through elastic materials). No damage of the retrofit was observed, other than the local fracture of the glass grid of the FRPU near the crushed brick of the partial infill. The structure sustained extremely severe earthquake excitations and developed 2.62% relative displacement drift without accumulation of severe local structural damages or collapse. The tests were terminated as after the successive severe seismic excitations and the crushing of two bottom bricks, the structure exhibited very low stiffness (development of horizontal displacement for very low horizontal loads) but with recovery capacity (because of the elastic PUFJ and FRPU jacketing and VF renovations) and relatively low residual drift. The crushing of two bottom bricks did not pose any threat to human life at advanced ULS performance levels for brick infills or RC structure.

The 5 different simulated planters with the trees (P) presented a remarkably resilient performance up to very severe seismic excitations, avoiding planter overturning or damage. The different anchoring detailing provided a holistic insight on the design of common steel or green, natural recyclable, replaceable, non-corrosive, lightweight and fire-resistant anchoring through basalt ropes. PM pads offered a very resilient alternative foundation of planter 4 up to significant seismic excitations. The 8 different simulated vertical living walls (LW) presented a remarkably resilient performance up to very severe seismic excitations offering several alternatives for top elastic support through basalt ropes and flexible PM pads against the concrete slab to avoid local damage and non-desirable interaction or slip. No serious damage accumulation for different LWs was observed up to severe seismic excitations.

PZTs provide a reliable framework for assessing the health condition of renovated RC structures at various locations. They also show potential for evaluating additional materials incorporated into the VF structure. This assessment is based on RMSD values obtained from PZT measurements, which enable a detailed correlation between sensor data and the location and extent of damage observed in situ. For all PZTs, including those attached to VF materials, the RMSD values demonstrate a consistent increasing trend from the initial 0.1g excitation through subsequent excitations.

The VF renovated showed lower displacement drifts for equivalent acceleration top mass levels (accounting for the additional top mass because of the planters and living wall structures) because of the innovative lightweight, non-corrosive, flexible retrofits. That is an interesting increase of stiffness. For EQ1.1g the drift of the renovated structure was similar to the one during the first phase despite the significantly increased top mass of the VF renovated structure. The second phase of the seismic testing is completed successfully, based on the advanced ULS level damages of the VF renovated structure after the execution of 28 dynamic tests, including 13 levels of earthquake excitations. The large number of severe excitations reveal a high potential for energy absorption by the VF renovated structure.

References

Anagnostou, E., Rousakis, T.C., Karabinis, A.I., Seismic retrofitting of damaged RC columns with lap-spliced bars using FRP sheets, Composites Part B: Engineering, 2019, 166, pp. 598–612.

Chalioris, C.E.; Karayannis, C.G.; Angeli, G.M.; Papadopoulos, N.A.; Favvata, M.J.; Providakis, C.P. Applications of Smart Piezoelectric Materials in a Wireless Admittance Monitoring System (WiAMS) to Structures-Tests in RC Elements. Case Stud. Constr. Mater. 2016, 5, 1-18, doi:10.1016/j.cscm.2016.03.003.

Chalioris, C.E.; Papadopoulos, N.A.; Angeli, G.M.; Karayannis, C.G.; Liolios, A.A.; Providakis, C.P. Damage Evaluation in Shear-Critical Reinforced Concrete Beam Using Piezoelectric Transducers as Smart Aggregates. Open Eng. 2015, 5, 373-384, doi:10.1515/eng-2015-0046.

Chalioris, C.E.; Voutetaki, M.E.; Liolios, A.A. Structural health monitoring of seismically vulnerable RC frames under lateral cyclic loading. Earthq. Struct. 2020, 19, 29-44.

Chalioris CE, Kytinou VK, Voutetaki ME, Karayannis CG. Flexural Damage Diagnosis in Reinforced Concrete Beams Using a Wireless Admittance Monitoring System—Tests and Finite Element Analysis. Sensors 2021; 21(3). DOI: https://doi.org/10.3390/s21030679.

Gams M, Tomaževič M, Berset T. Seismic strengthening of brick masonry by composite coatings: an experimental study. Bulletin of Earthquake Engineering 2017; 15(10): 4269–4298.

Golias E, Zapris AG, Kytinou VK, Osman M, Koumtzis M, Siapera D, Chalioris CE, Karayannis CG. Application of X-Shaped CFRP Ropes for Structural Upgrading of Reinforced Concrete Beam–Column Joints under Cyclic Loading–Experimental Study. Fibers 2021; 9(7).

Guo R, Zhang H, Chen K, et al. Seismic Performance Analysis of Concrete Columns Reinforced with Prestressed Wire Ropes Embedded in Polyurethane Cement Composites. *Buildings*. 2024 ; 14 (4) : 993. doi:10.3390/buildings14040993.

Haq M., Bhalla S., Naqvi T., Piezo-impedance based fatigue damage monitoring of restrengthened concrete frames, Composite Structures 280 (2022), 114868, https://doi.org/10.1016/J.COMPSTRUCT.2021.114868.

Helman D, Yungstein Y, Mulero G, Michael Y. High-Throughput Remote Sensing of Vertical Green Living Walls (VGWs) in Workplaces. Remote Sensing 2022; 14(14): 3485.

Hojdys Ł, Krajewski P, Kwiecien A, Rousakis T, Vanian V, Marcin T, Viskovic A, Ilki A, Gams M, Rakicevic Z, Zajac B, Bogdanovic A. Quick Repair of Damaged Infill Walls with Externally Bonded FRPU Composites: Shake Table Tests. Journal of Composites for Construction ASCE. Volume 27, Issue 1. February: 2023. https://doi.org/10.1061/(ASCE)CC.1943-5614.0001268

Hou S, Zhang H, Han X, Ou J. Damage monitoring of the RC frame shaking table test and comparison with FEM results. Procedia Engineering 2017; 210: 393–400.

Irga PJ, Torpy FR, Griffin D, Wilkinson SJ. Vertical Greening Systems: A Perspective on Existing Technologies and New Design Recommendation. *Sustainability*. 2023;15(7):6014. doi:10.3390/su15076014.

Karabini, M., Rousakis, T., Golias, E., Karayannis, C., Seismic Tests of Full Scale Reinforced Concrete T Joints with Light External Continuous Composite Rope Strengthening—Joint Deterioration and Failure Assessment. Materials, 2023, 16(7), 2718.

Karayannis CG, Voutetaki ME, Chalioris CE, Providakis CP, Angeli GM. Detection of flexural damage stages for RC beams using Piezoelectric sensors (PZT). Smart Structures and Systems, An International Journal 2015; 15(4): 997–1018.

Kwiecień A, Gams M, Rousakis T, Viskovic A, Korelc J. Validation of a New Hyperviscoelastic Model for Deformable Polymers Used for Joints between RC Frames and Masonry Infills. Engineering Transactions 2017; 65(1): 113–121.

Kwiecień A. Shear bond of composites-to-brick applied with highly deformable, in relation to resin epoxy, interface materials. Materials and Structures 2014; 47(12): 2005–2020.

Kwiecień A, Zając B. Dynamic response of the cracked masonry building repaired with the flexible joint method – an innovative earthquake protection. In: Brennan MJ, editor. Proceedings of the 7th European Conference on Structural Dynamics, 7-9 July 2008, Southampton: University of Southampton. Institute of Sound & Vibration Research; 2008.

Kwiecień A, de Felice G, Oliveira DV, Zając B, Bellini A, De Santis S, et al. Repair of composite-to masonry bond using flexible matrix. Materials and Structures 2016; 49(7): 2563–2580.

Na, W.S; Baek, J., A Review of the Piezoelectric Electromechanical Impedance Based Structural Health Monitoring Technique for Engineering Structures, Sensors 2018, 18(5), 1307; doi:10.3390/s18051307.

Naoum, M.C.; Papadopoulos, N.A.; Sapidis, G.M.; Voutetaki, M.E. Efficacy of PZT Sensors Network Different Configurations in Damage Detection of Fiber-Reinforced Concrete Prisms under Repeated Loading. Sensors 2024, 24, 5660. https://doi.org/10.3390/s24175660 .

Naoum, M.C.; Papadopoulos, N.A.; Sapidis, G.M.; Chalioris, C.E. Advanced Structural Monitoring Technologies in Assessing the Performance of Retrofitted Reinforced Concrete Elements. Appl. Sci. 2024, 14, 9282. https://doi.org/ 10.3390/app14209282.

Naoum, M.C.; Papadopoulos, N.A.; Voutetaki, M.E.; Chalioris, C.E. Structural Health Monitoring of Fiber-Reinforced Concrete Prisms with Polyolefin Macro-Fibers Using a Piezoelectric Materials Network under Various Load-Induced Stress. Buildings 2023, 13, 2465. https://doi.org/10.3390/buildings13102465.

Nakashima M, Nagae T, Enokida R, Kajiwara K. Experiences, accomplishments, lessons, and challenges of E-defense—Tests using world's largest shaking table. *Japan Architectural Review*. 2018;1(1):4-17. doi:10.1002/2475-8876.10020.

Ozden S, Akguzel U, Ozturan T. Seismic strengthening of infilled reinforced concrete frames with composite materials. ACI Structural Journal 2011; 108(4): 414–422.

Papadopoulos, N.A.; Naoum, M.C.; Sapidis, G.M.; Chalioris, C.E. Cracking and Fiber Debonding Identification of Concrete Deep Beams Reinforced with C-FRP Ropes against Shear Using a Real-Time Monitoring System. Polymers 2023, 15, 473, doi:10.3390/polym15030473.

Papadopoulos, N.A.; Naoum, M.C.; Sapidis, G.M.; Chalioris, C.E. Resilient and Sustainable Structures through EMI-Based SHM Evaluation of an Innovative C-FRP Rope Strengthening Technique. Appl. Mech. 2024, 5, 405–419. https://doi.org/ 10.3390/applmech5030024.

Providakis C, Tsistrakis S, Voutetaki M, Tsompanakis Y, Stavroulaki M, Agadakos J, Kampianakis E, Pentes G. A new damage identification approach based on impedance-type measurements and 2D error statistics. Structural Monitoring and Maintenance 2015; 2(4): 319–338.

Providakis C, Tsistrakis S, Voutetaki M, Tsompanakis J, Stavroulaki M, Agadakos J, Kampianakis E, Pentes G, Liarakos E. An Innovative Active Sensing Platform for Wireless Damage Monitoring of Concrete Structures. Current Smart Materials 2016; 1(1): 49–62.

Padanattil A, Karingamanna J, K.M M. Novel hybrid composites based on glass and sisal fiber for retrofitting of reinforced concrete structures. Construction and Building Materials 2017; 133: 146–153.

Rouka D, Kaloudaki A, Rousakis T, Fanaradelli T, Anagnostou E, Kwiecień A, et al. Response of RC buildings with Low-strength Infill Walls Retrofitted with FRP sheets with Highly Deformable Polymer-Effects of Infill Wall Strength. 25th International Conference on Composites/Nano Engineering, Rome 2017.

Rousakis TC, Tourtouras IS. RC columns of square section – Passive and active confinement with composite ropes. Composites Part B: Engineering 2014; 58: 573–581.

Rousakis TC. Reusable and recyclable nonbonded composite tapes and ropes for concrete columns confinement. Composites Part B: Engineering 2016; 103: 15–22.

Rousakis T, Anagnostou E, Fanaradelli T. Advanced Composite Retrofit of RC Columns and Frames with Prior Damages—Pseudodynamic Finite Element Analyses and Design Approaches. Fibers 2021a; 9(9).

Rousakis T, Vanian V, Fanaradelli T, Anagnostou E. 3D FEA of Infilled RC Framed Structures Protected by Seismic Joints and FRP Jackets. Applied Sciences 2021b; 11(14).

Rousakis TC, Panagiotakis GD, Archontaki EE, Kostopoulos AK. Prismatic RC columns externally confined with FRP sheets and pre-tensioned basalt fiber ropes under cyclic axial load. Composites Part B: Engineering 2019; 163: 96–106. DOI: https://doi.org/10.1016/j.compositesb.2018.11.024.

Rousakis T, Tourtouras I. RC columns of square section – Passive and active confinement with composite ropes. *Composites Part B: Engineering*. 2014;58:573-581. doi:10.1016/j.compositesb.2013.11.011.

Rousakis T, Macha M. External Confinement with Basalt Fiber Ropes in Existing Reinforced Concrete Structures. *ce papers*. 2023;6(5):277-285. doi:10.1002/cepa.2109.

Rousakis T, Ilki A, Kwiecien A, Viskovic A, Gams M, Triller P, Ghiassi B, Benedetti A, Rakicevic Z,Colla C, Halici OF, Zając B, Hojdys Ł, Krajewski P, Rizzo F, Vanian V, Sapalidis A, Papadouli E, Bogdanovic A. Deformable Polyurethane Joints and Fibre Grids for Resilient Seismic Performance of Reinforced Concrete Frames with Orthoblock Brick Infills. Polymers 2020; 12(12). DOI: https://doi.org/10.3390/polym12122869.Thomoglou, A.K.; Falara, M.G.; Gkountakou, F.I.; Elenas, A.; Chalioris, C.E. Smart Cementitious Sensors with Nano-, Micro-, and Hybrid-Modified Reinforcement: Mechanical and Electrical Properties. Sensors 2023, 23, 2405. https://doi.org/10.3390/s23052405.

Sam-Daliri, O.; Faller, L.M.; Farahani M.; Roshanghias, A.; Araee, A.; Baniassadi, M.; Oberlercher, H.; Zangl, H., Impedance analysis for condition monitoring of single lap CNT-epoxy adhesive joint. International Journal of Adhesion and Adhesives, 88, 59-65, doi:10.1016/j.ijadhadh.2018.11.003.

Sam-Daliri, O.; Faller, L.M.; Farahani M.; Zangl, H., Structural health monitoring of adhesive joints under pure mode I loading using the electrical impedance measurement. Engineering Fracture Mechanics, 245, 107585, doi:10.1016/j.engfracmech.2021.107585.Thomoglou, A.K.; Voutetaki, M.E.; Fantidis, J.G.; Chalioris, C.E. Novel Natural Bee Brick with a Low Energy Footprint for "Green" Masonry Walls: Mechanical Properties. Eng. Proc. 2024, 60, 9. https://doi.org/10.3390/engproc2024060009.

Sharma R, Hsiao FP, Liu KY, Pon CE. Shaking table test of a half-scale three-story non-ductile RC building subjected to near-fault ground motions: Experimental and numerical modeling. *Structures*. 2022;45:721-747. doi:10.1016/j.istruc.2022.09.041.

Thomoglou, A.K., Voutetaki M.E., Fantidis J.G. and Chalioris C.E. Novel Natural Bee Brick with a Low Energy Footprint for "Green" Masonry Walls: Mechanical Properties†, Engineering Proceedings 2024; 60(1). DOI: https://doi.org/10.3390/engproc2024060009.

Talakokula V, Bhalla S, Gupta A. Corrosion assessment of reinforced concrete structures based on equivalent structural parameters using electro-mechanical impedance technique. Journal of Intelligent Material Systems and Structures 2014; 25(4): 484–500. DOI: https://doi.org/10.1177/1045389X13498317.

Talakokula V, Bhalla S. Reinforcement corrosion assessment capability of surface bonded and embedded piezo sensors for reinforced concrete structures. Journal of Intelligent Material Systems and Structures 2015; 26(17): 2304–2313. DOI: https://doi.org/10.1177/1045389X14554133.

Tedeschi C, Kwiecień A, Valluzzi MR, Zając B, Garbin E, Binda L. Effect of thermal ageing and salt decay on bond between FRP and masonry. Materials and Structures 2014; 47(12): 2051–2065.

Triantafillou TC, Papanicolaou CG, Zissimopoulos P, Laourdekis T. Concrete confinement with textile- reinforced mortar jackets. ACI Structural Journal 2006; 103(1): 28.

Triantafyllou, G.G., Rousakis, T.C., Karabinis, A.I., Effect of patch repair and strengthening with EBR and NSM CFRP laminates for RC beams with low, medium and heavy corrosion, Composites Part B: Engineering, 2018, 133, pp. 101–111.

Triller Petra, Konrad Kwiecień, Arkadiusz Kwiecień, Uroš Bohinc, Bogusław Zając, Marcin Tekieli, Magdalena Szumera, Rousakis Theodoros, Vanian Vachan, Ahmet Tugrul Akyildiz, Alberto Viskovic, Efficiency of FRPU strengthening of a damaged masonry infill wall under in-plane cyclic shear loading and elevated temperatures. Engineering Structures, Volume 317, 15 October 2024, 118652.

Voutetaki, M.E.; Papadopoulos, N.A.; Angeli, G.M.; Providakis, C.P. Investigation of a New Experimental Method for Damage Assessment of RC Beams Failing in Shear Using Piezoelectric Transducers. Eng. Struct. 2016, 114, 226-240, doi:10.1016/j.engstruct.2016.02.014

Voutetaki, M.E.; Naoum, M.C.; Papadopoulos, N.A.; Chalioris, C.E. Cracking Diagnosis in Fiber-Reinforced Concrete with Synthetic Fibers Using Piezoelectric Transducers. Fibers 2022, 10, 5. https://doi.org/10.3390/fib10010005.

Yuksel E, Ilki A, Erol G, Demir C, Karadogan HF. Seismic retrofit of infilled reinforced concrete frames with cfrp composites. In: Wasti ST, Ozcebe G, editors. Advances in Earthquake Engineering for Urban Risk Reduction, Dordrecht: Springer Netherlands; 2006.

Zapris, A.G.; Naoum, M.C.; Kytinou, V.K.; Sapidis, G.M.; Chalioris, C.E. Fiber Reinforced Polymer Debonding Failure Identification Using Smart Materials in Strengthened T-Shaped Reinforced Concrete Beams. Polymers 2023, 15, 278. https://doi.org/10.3390/ polym15020278.